Coupled MEMS resonator networks

Kari Iltanen

School of Electrical Engineering

Thesis submitted for examination for the degree of Licentiate of Science in Technology.

Espoo 14.8.2017

Thesis supervisor:

Prof. Ilkka Tittonen

Thesis advisor:

D.Sc. (Tech.) Mika Koskenvuori

Aalto University
School of Electrical
Engineering

AALTO UNIVERSITY
SCHOOL OF ELECTRICAL ENGINEERING

ABSTRACT OF THE
LICENTIATE'S THESIS

Author: Kari Iltanen

Title: Coupled MEMS resonator networks

Date: 14.8.2017 Language: English Number of pages: 7+80

Department of Micro and Nano Science

Professorship: Micro and quantum systems

Supervisor: Prof. Ilkka Tittonen

Advisor: D.Sc. (Tech.) Mika Koskenvuori

Micromechanical resonance frequencies are in a standard manner a few tens of MHz and can even cover the frequency range up to a few GHz. When using high quality material such as quartz or silicon, also internal losses are very low.
By physical coupling of resonators into a network, one can realize various mechanical signal processing, filtering or for example neural network type behavior. Since coupling between resonators is realized by some kind of bridge, which can be either rather linear or alternatively intentionally very nonlinear, the overall behavior of the whole network is very complex.
Of general interest are effects that originate from multiple inputs and outputs and which could lead to a rather unexpected spectral or transient behavior of the signals, which can be found by computer modelling.

Keywords: Micromechanical resonators, Network, Mechanical signal processing, Electrical equivalent circuits, Simulations

AALTO-YLIOPISTO
SÄHKÖTEKNIIKAN KORKEAKOULU

LISENSIAATINTUTKIMUKSEN
TIIVISTELMÄ

Tekijä: Kari Iltanen

Työn nimi: Kytketyt MEMS-resonaattoriverkot

Päivämäärä: 14.8.2017 Kieli: Englanti Sivumäärä: 7+80

Mikro- ja nanotekniikan laitos

Professuuri: Mikro- ja kvanttisysteemit

Työn valvoja: Prof. Ilkka Tittonen

Työn ohjaaja: Prof. Ilkka Tittonen

Mikromekaaniset resonanssitaajuudet ovat tyypillisesti muutamia kymmeniä megahertsejä, mutta voivat kattaa taajuuskaistan aina muutamiin gigahertseihin asti. Käytettäessä korkealaatuisia materiaaleja kuten kvartsia tai piitä, myös signaalin häviöt ovat erittäin pieniä.
Kytkemällä resonaattoreita fyysiseksi verkoksi, voidaan mekaanisilla rakenteilla suorittaa signaalinkäsittelyä, realisoida suodattimia ja jopa neuroverkkoja. Koska yksittäisten resonaattorien välinen kytkentä on jonkinlainen silta, joka voi olla joko melko lineaarinen tai vaihtoehtoisesti tarkoituksellisesti erittäin epälineaarinen, on koko verkon käyttäytyminen erittäin monimutkaista.
Yleisesti kiinnostavia ovat useista sisäänmenoista ja ulostuloista johtuvat ilmiöt, jotka voivat johtaa signaalien spektrin tai transienttivasteen melko odottamattomaan tai epäintuitiiviseen käyttäytymiseen, jonka voi löytää ja tulkita tietokonesimulaatioilla.

Avainsanat: Mikromekaaniset resonaattorit, Verkko, Mekaaninen signaalinkäsittely, Sähköiset vastinpiirit, Simulaatiot

Preface

I want to thank Professor Ilkka Tittonen and my advisor Mika Koskenvuori for their guidance and patience during the writing process.

Halikko, 14.8.2017

Kari Iltanen

Contents

Symbols and abbreviations

Symbols

Abbreviations

AC	alternating current
APLAC	an object-oriented analog circuit simulator and design tool (originally Analysis Program for Linear Active Circuits)
DC	direct current
FWHM	full width half maximum
MEMS	microelectromechanical system
Q	quality factor

1 Introduction

Microelectromechanical systems (MEMS) consists of electrical and mechanical components integrated together. Their feature sizes can vary from nanometers to even millimeters but most of them are in size between micrometers and hundreds of micrometers. Nanoelectromechanical systems (NEMS) have many features less than hundred nanometers thus operating at lower energies than MEMS.

The use of MEMS has a long development history starting from the late 1950s but commercialization had to wait to the 1980s when fabrication technology was matured enough. Micromechanical solutions have enabled many applications by making components small, cheap, sensitive and energy efficient enough. Often they are also less sensitive to external disturbances. Most micromechanical components operate in analog mode with low associated noise. In many applications, MEMS can replace electronic and macroscale mechanical components while having better performance and energy efficiency.

Especially with mechanical components aging becomes a problem since for commercial devices at least 5-10 years durability is required. Aging stability is also extremely important. In addition, the temperature stability is important as it removes the need for a separate temperature control system or in a less severe case a circuit to compensate for heating or cooling.

The components can be either fabricated of thin films using surface micromachining or of the substrate material using bulk micromachining. Fabrication technologies required have been developed by semiconductor industry for integrated circuits (IC), but might require some adjustments to take account the differences between MEMS and ICs, such as larger etch depths and released structures.

One major problem can be the coupling of MEMS to an external circuit and possible losses from that. Therefore, more and more MEMS devices are integrated together showing a similar trend as in microelectronics reducing the amount of discrete components, power consumption, losses and costs. It is also possible to integrate electronics and MEMS together as fabrication processes and especially materials are usually compatible. Judge et al and Yang Lin et al report that integration can also ease some restrictions on individual components used as building blocks and relax fabrication tolerances somewhat compared to the use of a single MEMS [28, 34].

Sensors and actuators are one of the main target areas for MEMS but their use RF-technology steadily increases as more and more functions of discrete components such as filters, oscillators and mixers are integrated together. Sensors have been described for physical, chemical or biological quantities. Cantilevers for example can be used identify objects by measuring their mass. Some systems are nothing more than miniaturized versions of their macroscopic counterparts. MEMS based position and motion sensors were at first adopted by the automotive industry and then as the technology improved they have enabled motion based game controllers and position/motion detection systems for mobile devices.

Young et al state that MEMS switches have also been built and under gigahertz they are more energy efficient than transistors. Mechanical motion can be only so fast and delays rise also from time until voltage is high enough move the switch.

Small scale integrated circuits using MEMS relay have been developed and realized, but commercialization waits until the lifetime has been increased enough and circuit sizes have increased at least to the medium scale integration (MSI) or preferably to large scale integration (LSI) level. [45]

MEMS have found also use in laboratory chips, scanning probe microscopy and optical devices such as mirrors or switches. In digital micromirror devices (DMD) MEMS micromirros are used to generate the image by reflecting light from a lamp. Bright and dark pixels are generated by rotating the mirrors between on and off states. Grey scales appear when the rotation happens very quickly with the shade determined by the ratio of on and off times. DMDs are used in digital light processing (DLP) technology, which is used in projectors, displays and some 3D printers. Some other MEMS based display technologies also exist but are still in development.

According to Statsoft Inc. and Stergiou and Stiganos an artificial neural network (ANN) is inspired by nervous systems, the idea being to take advantage from the way interconnected neurons process information, which happens by learning from examples. ANNs have excellent ability to analyze complex or imprecise data and find trends or patterns from it that are too complex for either humans or computers to detect. Hoppensteadt and Izhikevich state that it is known that coupled MEMS-resonator network can be used as ANN as they have autocorrelative oscillatory memory [15].[17, 40]

Transceivers currently consists of several discrete components such as filters for RF and IF, voltage controlled oscillators (VCO), quartz crystal oscillators, solid-state switches, etc. Integrated high performance variable capacitors are not realizable with MOS or pn-junction silicon on-chip technology, but with MEMS technology monolithic capacitors have been made meeting linearity, high Q and large tuning factor requirements.

The capacitors are critical for low noise VCOs, antenna tuning, tunable matching networks, etc. They are realized with electrostatic actuation. High quality inductors are also essential and are achievable though micromachining technologies, but typically adjustable ones with moving parts are not required. Integrable switches are next necessary part and the main actuation method for them is electrostatic. Filters are used as part of channel selection. Adjustable antennas have also been realized. [45]

The integrability allows one to build a system on chip (SoC) that has the necessary receiver, transceiver and signal processing components with possible addition of the electronics for the system. As building a single high performance component is quite difficult to reach desired performance multiple components are connected together.

As coupled MEMS resonators will increasingly replace individual components understanding how they behave and what they can be used for becomes increasingly important. The behavior of a coupled MEMS resonator network depends on components used and how they are coupled together.

1.1 Research questions and scope

This work seeks to answer following questions:

1. How the response of coupled MEMS resonator network changes with network size?
2. How signal delay depends from network size?
3. Impact of coupling strength
4. Impact of randomized resonance frequencies
5. Impact of multiple inputs and outputs

This work is limited to simulations with mass-spring model for the network and considerations about how these systems could be realized are ignored.

2 Background

To understand the behavior of coupled microelectromechanical resonators, one must look at first into properties, behavior and modeling of resonators themselves. The next step is to understand how the input quantity is converted into mechanical motion and what limitations these micromechanical components have. Then the possible coupling methods and network topologies are reviewed before looking how coupling multiple resonators affects the response. After these I discuss some possible applications for these networks.

2.1 Microelectromechanical resonators

Nguyen reports that the new ultra wide band wireless systems operate on the frequencies of many tens of gigahertz, where MEMS can no longer be used requiring nanomechanical systems. Currently majority of wireless communication happens on frequencies below 6 GHz, where micromechanical systems can offer the required performance. [34]

Quality factor (Q) describes energy efficiency of the component and is defined with a following equation

$$Q = 2\pi \frac{\text{Energy strored}}{\text{Energy dissipated per cycle}}, \tag{1}$$

which becomes

$$Q = \frac{\sqrt{kM}}{D} \tag{2}$$

for a MEMS resonator modeled as a mass-spring system with D being the damping coefficient. The total quality factor can be acquired by combining individual quality factors for each source of energy loss. In bandpass filters Q is the ratio between the resonant frequency and bandwidth, which is defined as the width of the frequency range where power is at least half of the maximum. [34]

According to Younis, the behavior of dynamic system depends on nonlinearities and damping, which determine also stability. For analysis one has to first build a model describing the system. The nonlinearities are often extremely significant in MEMS due their small dimensions compared with motion and they can even enable wanted features. [46]

Three main sources of nonlinearities in MEMS are forcing, damping and stiffness. Forcing contains actuation/detection and forces that affect during operation such as capillary due humidity and van der Waals on surfaces close to each other. Stiffness has geometric and material nonlinearities. [46]

Quadratic nonlinearities come from electrostatic forces and piezoelectric materials, cubic nonlinearities on other hand rise from the geometry of microstructures. These two are the common and dominant nonlinearity types in the MEMS in most cases. Some nonlinearities are caused by actuation technique and can effect on the resonance frequency, stability, accuracy and calibration of the resonator. More about nonlinear dynamics and methods used in it in Chapters 2.1.5-2.1.6. [46]

2.1.1 Resonator types

Nguyen and Basu *et al.* report that RF-technology places strict demands on resonators regarding impedance, operating frequency, stability and Q. Multiple MEMS-resonator types exist but the most studied ones are beams, hollow disk ring, wine-class and contour-mode resonators (Figure 1). [34, 6]

The resonator types can also be divided by the type of vibration mode: flexural, torsional and bulk acoustic. Only bulk modes have high enough stiffness to be usable beyond the middle of VHF band. Some of unwanted modes can be avoided with electrode and resonator design while others have to be blocked or they are far enough from wanted modes to matter. [34, 6]

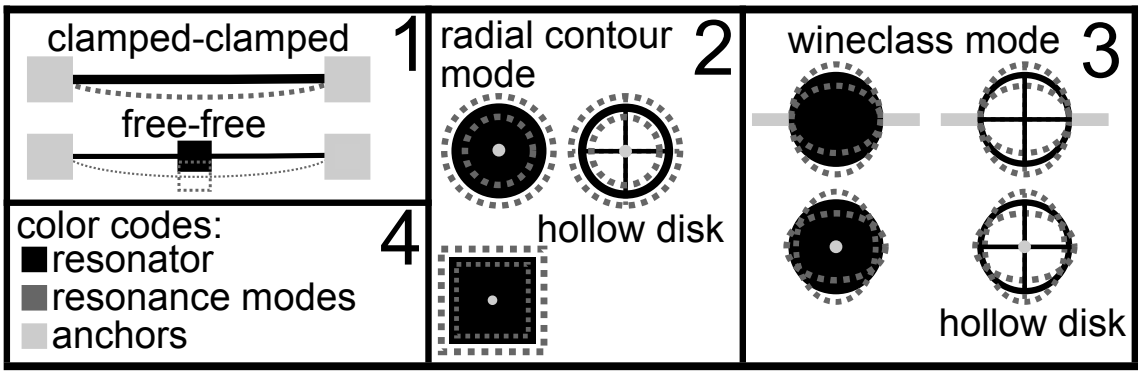

Figure 1: Profiles of some resonator types containing their resonance modes and anchoring methods. In the wine-class type resonator the anchoring can be realized either with center stump or from sides. For radial contour mode only center stump can be used. Two different resonance modes are portrayed for the disk resonators.

Nguyen states that beams can be clamped in multiple ways and are easy to fabricate but they are limited to the VHF band and below. They vibrate at a flexural mode. A system with quarter wavelength supports attached to the nodal points of the beam is known as Free-Free clamping and can reach 100 MHz with $Q > 10000$ in a vacuum, see an article by Kun Wang et al. [43]]. However, in air Q drops order of magnitude. With sufficient scaling and use of higher-order modes frequencies at 1 GHz range are attainable but have low Q. Ultimately with scaling multiple issues regarding especially noise, losses, power handling and impedance come up. [33, 34]

In wine-glass and contour-mode resonators, circular resonator structure is used which deforms as it vibrates in a bulk acoustic mode. Therefore their best anchor point is at the center of the disk which can be problematic to achieve but self-alignment has been proposed as solution. In the wine-glass resonator the deformation changes the resonator shape from circle to ellipse. Therefore, it also has four nodal points on edge. [34]

Nguyen and Clark *et al.* report that in contour-mode shape stays as a circle but radius changes in fundamental mode, in higher order modes nodal circumferences start to appear and divide the disk into n vibration zones, where n is the number of the order. They also have large scaling potential as frequency is approximately

inversely proportional to the radius. Contour-modes make resonators less susceptible to viscous gas damping due the large total kinetic energy of the high stiffness vibration mode. [34, 8]

Their resonance frequency depends on radius and material parameters though following approximate equation

$$f_0 = \frac{\kappa\alpha}{R}\sqrt{\frac{\rho}{E}}, \tag{3}$$

where κ is a parameter depending on Poisson's ratio, E is Young's modulus, ρ is density and α describes the order of the mode, which increases with the mode number. Thus the use of higher order modes enables bigger disks easing possible power handling issues. Lithographic constraints are not an issue when multigigahertz frequencies at the fundamental mode are achievable with the disk diameters of couple micrometers. Effects due anchoring and disk thickness were ignored. [34, 8]

According to Li *et al.* and Baghelani and Ghavifekr, hollow-disk resonators are disks where part of the disk is removed, but might require anchoring from sides as well in addition to support beams connected to the center. They also vibrate at contour-mode. Frequency of the hollow-disk resonator scales with the width of the ring. Impedance is also significantly lower than that of solid disks. Major loss sources for the hollow-disk resonator are support beams for the ring and design of their attaching points. By notching, the ring supports can be attached closer to the nodal points lessening losses, also using quarter wavelength supports reduces losses due acoustic impedance mismatch. One variant uses an anchoring ring instead of support beams. [26, 5]

Nguyen states that both contour-mode and hollow-disk resonators have been reported having $Q > 10000$ on frequencies over 1 GHz even in the air [34]. Naing *et al.* have demonstrated a hollow-disk with diamond ring $Q = 42000$@3GHz [31].

2.1.2 Damping

According to Younis and Ayazi *et al.* damping can be divided into extrinsic and intrinsic parts. Extrinsic losses from design nonidealities, such as losses due the surrounding fluid, non-smooth surfaces, acoustic radiation and structure mounts, usually dominate in MEMS. Intrinsic losses from the material itself, such as surface losses, phonon scattering and relaxation that contains thermoelastic, grain-boundary and defect damping become significant when reaching for a high quality factor by either minimizing or eliminating the extrinsic damping sources. [46, 3]

Some loss mechanism become significant only in micro-scale or below, the more important ones in this category are squeeze-film damping, thermoelastic damping, pull-in instability and stiction due the capillary forces. [46, 3]

Magnitude of damping from grain boundaries and defects depends on grain size and defect density. Significance of both can be reduced by using high quality single crystal material. In addition, the impact of surface and interface scattering can be greatly reduced by adjusting fabrication methods to create the smoothest surfaces possible. [46, 3]

Thermoelastic damping is a process where mechanical energy is lost when irreversible heat flow caused compression and decompression due the oscillation. The heat flow is caused by a thermal gradient because the side under compression has higher temperature than the other side. [46, 3]

Younis and Ayazi *et al.* state that phonons can scatter either from other phonons or electrons. In the previous case, there is a small difference in attenuation between the longitudinal and shear polarizations of acoustic waves when propagation direction, the temperature and frequency are the same. However, qualitative temperature dependence on both is similar. This means that both flexural and bulk acoustic wave (BAW) devices have similar qualitative temperature and frequency characteristics of phonon-phonon dissipation mechanism. Acoustic attenuation also has strong temperature dependence. These phonon-phonon interactions dominate in semiconductors and insulators. [46, 3]

Phonon-electron scattering, where phonons interact with mobile charges, can cause attenuation or amplify the acoustic wave. Strength of this interaction depends on the number of mobile charge carriers, which has a weak temperature dependence. Acoustic waves cause energy changes in conduction band electrons resulting in the undesired flow of charge carriers dissipating acoustic energy due ohmic loss. Importance of these effects on semiconductors depend on doping level becoming significant only at very high doping levels. In piezoelectric semiconductors, the coupling is caused by the piezoelectric material characteristics. [46, 3]

Support (anchor) losses are caused by uncanceled shear forces and moments at the ends of supports transferring energy from the vibrating structure to the substrate though propagating waves. These losses can be minimized with symmetric structures whose center of mass does not move as it vibrates or mechanical isolating mechanism used to isolate the vibrating part from its supports and proper design of the vibrating element and its mounting mechanism. Symmetries can also be used to reduce losses. Phononic bandgap is one possible isolation method. [46, 3]

According to Younis and Ayazi *et al.*, movement of mechanical element in a direction normal to its surface generates sound waves resulting in acoustic radiation, which can be significant if the acoustic wavelength is equal or smaller than the typical dimension of mechanical element, uncommon in the MEMS. Losses due the fluid are usually from drag, sliding and squeezed film. In squeeze-film damping fluid between plates of parallel plate capacitor resists movement of actuating plate. [46, 3]

As real insulators are imperfect, a shunt parasitic path to ground is created in the device equivalent circuit model. The dielectric loss tangent of material determines parasitic resistance and causes electric loading between input and output terminals impacting to the overall Q, if significant mismatch between the motional resistance and the sustaining amplifier exist. [46, 3]

2.1.3 Modeling

Younis and Kempe state that the goal of modeling is to gain better understanding about the properties of the device. This reduces costs and time required for the design process also the end result will be much better than with a trial and error

method. Modeling also enables novel devices. [46, 20]

The main challenges in modeling are accounting nonlinearities, physical field couplings and micro-scale phenomena present in MEMS, because ignoring them can lead to very large errors. The physical field couplings are connections between various energy domains and physical forces. For example, in moving structure material behavior and force used to move the structure have to be taken into account simultaneously. Due the small scale of MEMS, electromechanical interactions are considered quasistatic meaning that its behavior at any time can be determined by solving electrostatic field equations. [46, 20]

The modeling methods are divided into qualitative and quantitative ones. The former is used to investigate the stability of solution in the neighborhood of known solution of the differential equations without solving it. Quantitative methods are based on numerically solving the differential equations and choosing an correct one depends on what kind of solution one is interested and the strength of nonlinearities. [46, 20]

Younis reports that approximate analytical techniques often have convergence issues and are also limited to linearized cases thus limiting their effectiveness. The main method for modeling is currently different finite element (FE) and computer-aided-design (CAD) software packages meant specifically for MEMS problems which allow nonlinear and multiphysics analysis. However despite their usability and importance these softwares are not enough alone but need to be complemented with other analytical and numerical tools. Basic mass-spring models known as lumped element models are also extremely popular. [46]

The FE software itself does not provide any deep insight and understanding regarding various physical aspects of MEMS devices if used as black blocks. With numerous degrees of freedom advanced nonlinear dynamic analysis becomes hard to conduct with FE models and the same goes to many analytical and numerical tools. Analytical techniques can be used to gain qualitative understanding about the system with FE software used for quantitative results. RF design tools and circuit simulators also have some possible use especially when investigating systems containing MEMS. [46]

2.1.4 Lumped parameters models

Younis states that lumped element models, where the structure is modeled as a mass-spring system consisting of rigid bodies and lumped elements. They aim to describe the both static and undamped dynamic behavior of the system in the vicinity of natural frequency of interest. These models are useful approximations as first-cut but lack of accuracy and ability predict dynamic behavior such as higher order modes. This means that more accurate models have to take to account the continuous distribution of mass and stiffness. [46]

After the model is built one has to determine its parameters, especially stiffness, which can be done experimentally, numerically or analytically. The stiffness coefficient depends on the kind of force or moment affecting the microstructure. Experimental measurements are mostly based on static measurements, such as measuring force-

displacement curve and calculating the slope of its linear region or using stress-strain curves to determine Young's modulus. Dynamic measurements require prior knowledge of other system parameters, such as inertia, and are more complicated. [46]

Analytical methods for stiffness determination are useful when the geometry of microstructure is simple or can be approximated as one or be breakable to multiple simple parts. Necessary formulas are derived by solving the differential equation governing the displacement under specific force. Many structures can be considered compromising multiple springs connected in series and/or parallel. Some other methods also exist. [46]

According to Younis, with computational methods, such as finite difference and finite element methods, stiffness determination starts with building a model to describe the microstructure. Next, for a linear response a small force is applied as either a point or distributed load and deflection at desired location is obtained. Then the slope of the deflection-force curve is determined as represents the stiffness coefficient. Another approach is to determine natural frequency of the structure and if its mass is known linear stiffness constant can be evaluated. [46]

Several methods of constructing spring-mass models, which are the backbone of the lumped-parameter modeling, exist, such as the Galerkin's method where dynamics of the structure are expressed by using the product of the dominant or excited modeshapes and the modal coordinate or generalized variable. The modeshapes are for undamped-unforced microstructure but also corresponding natural frequencies are needed. These can be determined either analytically for simple structures or with finite element methods. [46]

Spring-mass model can also be constructed by using the known stiffness coefficient and the natural frequency near the mode of interest to calculate effective mass which is then used in models describing the behavior of the system. [46]

2.1.5 Methods in nonlinear dynamics

Younis states that nonlinear dynamics of MEMS can studied with multiple different methods, of which the following is a brief overview. In nondimensionalization and normalization, the differential equation is transformed an equation into a nondimensional one with normalized nondimensional variables, which leaves various variables of the system lumped together in a few nondimensional parameters. Purpose of this operation is to ease efforts to understand the behavior of the system. [46]

The first advantage is that by comparing various variables of the system against each other and basic elements of the system, their influence and strength can be determined. This allows choosing an appropriate analysis method including possible approximations. [46]

The second advantage comes from characterizing the system with universal parameters applicable to the generic system. These parameters, such as quality factor, allows one understand the characteristics of different systems and compare them with each other. [46]

The third advantage is computational. Small numbers can cause problems

with computational methods as their precision is limited but can be avoided with nondimensionalization. [46]

Younis reports that in linearization the behavior of the system is investigated near the equilibrium point using a small dynamic disturbance superimposed to the equilibrium solution whose behavior is monitored. The system is assumed not to have a direct time dependence. It is then substituted to the system of original first order differential equations that is expanded to Taylor series and then higher order terms are dropped. As a result, a linear system of first order constant coefficient differential equations is acquired, whose solutions are exponential form. By substituting it to the system we get an eigenvalue problem. The final solution is the superposition of exponent functions with eigenvector as the linear coefficient and eigenvalue in the exponent. [46]

Real part of eigenvalues determines whether the equilibrium point is stable as for it all of them have to be negative. If all eigenvalues are purely imaginary, then the equilibrium point is known as "center" and is marginally (neutrally) stable. In this case linearization method is not enough to determine the stability. [46]

In the long-time integration simulation method, a nonlinear single-degree-of-freedom model is integrated numerically with a Runge-Kutta method for long-time until steady-state is reached. The easy implementation of this approach is countered by convergence problems near bifurcation points, pull-in and where the domain of attraction of the periodic solution is too small. When integration schemes diverge in these problematic areas, it is difficult to tell whether it is caused the instabilities of the system or issues with the numerical methods. Other methods are then needed to find periodic solutions and analyze their stability, such as a finite difference method or shooting techniques. [46]

Younis states that the shooting method is used to discover periodic motion and analyze their stability for nonlinear systems, both stable and unstable solution can be predicted. The idea is to find an appropriate set of initial conditions that can result in a periodic motion for the system. This is achieved by using a Newton-Raphson method to correct initial conditions starting from the initial guess until difference between values from consecutive iterations is very small and thus convergence has been reached. [46]

Another useful tool for analyzing the dynamic response of an oscillator is a basin of attraction analysis, where the idea is investigated whether various sets of initial conditions lead stable or unstable solutions by integrating the equation of motion in time. Depending on their stability, these points are represented in the phase space (velocity-displacement plane) with different colors, points with stable solutions form a basing of attraction (safe basin), accordingly the ones with unstable solutions form an unsafe zone. [46]

As the system may have many attractors that may or may not coexist it is more efficient to study basins of attraction for each separately as excitation frequency changes. An integrity factor, which is defined as the normalized radius of the largest circle fitting within the safe basin, is an efficient tool used to study and track the erosion. [46]

2.1.6 Nonlinear dynamics

According to Younis, nonlinearities affect the response in multiple ways such as nonmonotonous frequency response, secondary resonances, energy transfers between modes and dynamic pull-in. [46]

The static and dynamic behavior of MEMS undergoes dramatic qualitative changes if one of its control parameters, such as biasing voltage or the damping coefficient, is adjusted. This phenomenon is known as bifurcation. In saddle-node (tangent, a fold) bifurcation stable and unstable solutions meet each other in the bifurcation point destroying each other. Therefore, no solution exists beyond the bifurcation point forcing the system to escape to a remote, potentially unsafe solution or state. Pull-in instability in parallel plate capacitor, where the plates are pulled together when electrostatic force between them exceeds the ability of mechanical restoring force to resist, is a good example for this case (Figure 2). It is also possible that stability of two different solutions switches around. [46]

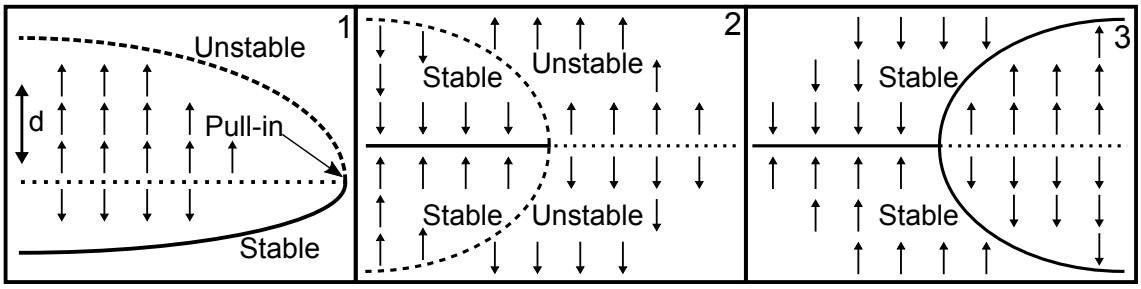

Figure 2: Bifurcation diagrams for saddle-node (1), subcritical (2) and supercritical (3) pitchfork bifurcations. The arrows indicate which direction the solutions develop. The dotted lines reperesent unstable equilibrium points and solid stable ones.

In pitchfork bifurcation, the solution splits into two solutions (Figure 2). It has two forms subcritical and supercritical from which the latter is considered unsafe from the viewpoint of the stability. One example is an movable electrode between two stationary electrodes with bias voltage sources on both sides, which becomes saddle-node bifurcation when the central electrode is moved closer to either side. Hopf bifurcation is dynamic bifurcation where periodic solution instead of equilibrium one is created. The solutions can be either stable or coexist with unstable ones. [46]

The dynamic response to harmonic excitation is classified either as primary or secondary resonance depending on excitation frequency. If excitation frequency is close to the one of the natural frequencies of the structure it is referred to primary resonance, otherwise it is known as secondary resonance. [46]

Younis reports that in the primary response, the frequency-response curve can be tilted and the maximum of the amplitude response can move from natural frequency (ω_n) to nonlinear resonance frequency. Also the response on certain frequencies might not be longer unique, which enables sudden jumps in different value. These phenomena can appear when reducing damping or increasing forcing as they lead to a amplified response. To trigger secondary responses in the system with quadratic nonlinearities, the excitation frequency (Ω) has to be close to twice or half of natural

frequency, and with cubic nonlinearities corresponding values are three and one third. It is possible to trigger all the previous resonances if the system has both quadratic and cubic nonlinearities. [46]

The response in superharmonic resonance has two components in frequencies Ω and $m\Omega$, where m is the degree of nonlinearity. In subharmonic resonance, the component $m\Omega$ is replaced with Ω/m. This means that response has a component close to the ω_n. The qualitative behavior of superharmonic resonance is similar to the primary response, it is also considered large but below of primary. Subharmonic resonance is larger than superharmonic but typically below that of primary. Typically considered safely of low amplitude and occurring much larger frequency than ω_n, thus sometimes completely overlooked in the design. Therefore, it is considered more dangerous in regard to stability than superharmonic. Dramatic and distinctive jumps in the response are another typical feature for subharmonic responses. [46]

In parametric excitation, forces appear though time varying parameters or coefficients in the differential equations. Many excitation methods can induce it naturally. Influence of the parametric excitation is stimulated and further amplified by the low-damping environment used to drive many microstructures. It can be used to significantly alter the response. [46]

Younis states that transfer of energy from one vibration mode into another due nonlinearity when the natural frequencies of modes are related by a constant is referred to intermodal (autoparametric) resonance. It is possible that energy from excited higher order mode transfers with low amplitude into a nonexcited lower order mode with large amplitude which might be order of magnitude larger than expected of a directly excited higher order mode. This can cause serious problems with the stability and reliability of MEMS. [46]

When excitation frequency is close to primary resonance, the basin of attraction is very small as instability 'fingers' rode increasing amount of space from the stable region. Thus borders between different areas become unclear or unsmooth and are known as fractal boundaries. Unpredictability from fractal behavior causes stability issues as practically at the certain frequency band the system is unstable though some stable solutions exist in this area. After transients die out time history approaches toward a set of points in phase space known as attractor. [46]

Many mechanisms described previously can cause the dynamic pull-in. In some applications, the need for the highest possible amplitude with stable resonance means operating in a region with the risk of the dynamic pull-in thus requiring active control mechanism to prevent it. The idea is to use feedback control techniques to improve stability and help to reject external disturbances, also possibility exist stabilizing the resonator even at the unstable region. [46]

A chaotic system is deterministic with sensitivity to initial conditions that has aperiodic long term behavior. Of many signs of chaos one of the most common is continuous broadband frequency spectrum. Chaos is usually undesirable in all other MEMS applications than encryption. [46]

2.2 Transducers

Transducer converts one signal type to another. Lenk *et al.* report that active transducers have an internal auxiliary power source and the power flow between the internal source and output is controlled by mechanical quantities. The control is realized by varying parameters of passive components, especially of resistive, inductive and capacitive components. Conversion is only possible from mechanical to electric and their usability is therefore limited to sensors. [23]

Passive transducers, which do not have an internal auxiliary power source, are components capable converting an electrical signal to mechanical and vice versa. Electrical energy is extracted entirely from the mechanical subsystem and vice versa. Some transduction mechanism work only in one direction. [23]

Two main transducers classes are electric and magnetic, which are further divided into subclasses. Magnetic ones are rarely used in resonator networks as magnetic materials and coils complicate the fabrication process and large currents required lead to issues with waste heat. The electric transducers are usually electrostatic or piezoelectric, but a few others exists such as capacitive-piezo, piezoresistive and electrothermal. [23]

Important factors in the selection of transduction mechanism are motional impedance, insertion loss, linearity, speed, Q-factor, the ease of fabrication, power consumption, required voltage/current levels, the length of motion and amount of force. Insertion loss is an issue for low Q values and high motional impedance causes problems in impedance matching for RF-circuits but both can be compensated by coupling resonators together. Fabrication processes place limits to the transducer design that can limit Q. Transducers are described as two-port networks in the electrical domain. [23]

2.2.1 Electrostatic

Lenk *et al.* state that an electrostatic/capacitive transducer is the most common transducer and the simplest realization consist of plate capacitor where the other plate deflects due the Coulomb force generated by the charge applied. The other plate can also be clamped from one or even multiple sides, then it has to be thinner than moving plate as its shape changes and it will be called a diaphragm. The plates can also slide perpendicular to each other as the gap remains constant. Figure 3 shows profiles of some of previously mentioned cases. [23]

Often the gap is filled with air or vacuum but there could also be an isometric insulator. Some possible applications for the diaphragm type are electrostatic microphones and speakers. Plate and diaphragm transducers are described differently, diaphragms behave as transformer and plates as gyrator. Electrically the transducer is an adjustable capacitor. [23]

Forouzanfar *et al.* and Lenk *et al.* report that electrostatic transducers are known to operate at gigahertz frequencies with high Q-factors. Their high motional resistance causes problems when used as part RF-circuits with standard $50\,\Omega$ impedance that can be compensated by reducing the gap or increasing bias voltage. In the closing gap variant, range of motion, maximum voltage and level of force can not be independently

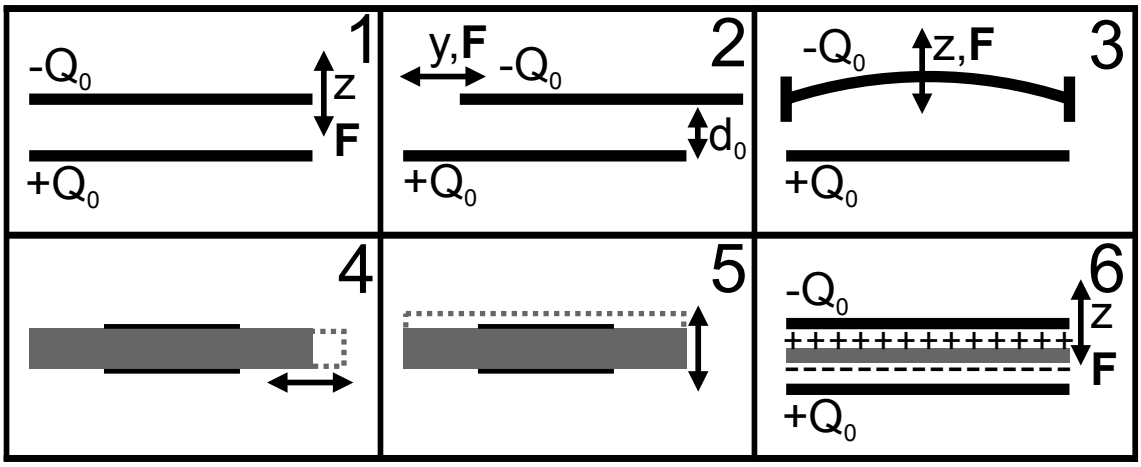

Figure 3: Frames 1-3 have profiles of three capacitive transducer types. The movement is indicated with line that has arrows on both ends. Profiles of longnitudal and thickness piezoelectric transducers are in frames 4-5, the deformation is demonstrated with grey dotted line and electrodes with black lines. Frame six has profile of piezo-capacitive transducer.

improved as there is a tradeoff between them. Maximum bias voltage is limited by pull-down where plates touch each other. [11, 23]

Li-Wen Hung *et al.* state that when the gap becomes extremely narrow (<50 nm) the significance of nonlinearities increases [16]. The gap is much narrower than the rest of dimensions in the component and can cause some issues in fabrication which raise production costs as more sophisticated techniques are needed. The component can be linearized with bias voltage that has to be much higher than the amplitude of the AC voltage. [11, 23]

Power handling is limited by the breakdown voltage or pull-in, whichever comes first, and nonlinearities. Safe maximum displacement assuming linear spring countering electrostatic force is one third of the gap size, after this pull-in happens. External disturbances and switching bias voltage on may cause the plate move into an unstable region even if the voltage is below the limit. Bigger displacements are possible by using a limiter to prevent contact, capacitor in series as voltage divider providing negative feedback or high speed electronics. The last two are especially problematic to realize in cost effective manner. [11, 23]

According to Lenk *et al.*, the electromechanical coupling is described with equilibrium force (F) at mechanical reference point, charge (q), voltage and position. The force is divided in to mechanical (F_{mech}) and electric parts (F_{el}) that have following equations $F_{mech} = \phi(z),\ F_{el} = \psi(q, x),\ F = f_1(q, z)$. Voltage u is also dependent from charge and position $u = f_2(q, z)$. Following equations are used to determine charge, current (i) and both mechanical and electric forces (F_{mech}, F_{el})

$$i = \frac{\mathrm{d}q}{\mathrm{d}t},\ z = z_0 + \Delta z,\ q = \frac{\varepsilon_0 A}{z} u,\ F_{mech} = \frac{1}{n}\Delta z + m\frac{\mathrm{d}^2 z}{\mathrm{d}t^2},\ F_{el} = \frac{q^2}{2\varepsilon_0 A} \qquad (4)$$

and $F = F_{el} - F_{mech}$, where ε_0 is the vacuum permittivity, A is the plate area, n is

the spring between the plates, z is the plate separation, m is the plate mass and u is the voltage. F_{el} is derived energy change caused by moving the capacitor plate distance Δz. [23]

Applied AC voltage $u(t) = \hat{u}\sin(\omega t)$ causes force progression at frequency 2ω, with addition DC bias U_0 electric force component can be written as $F_{el} = F_0 + F_{el}(t)$ and

$$F_{el}(t) = \frac{C^2}{2\varepsilon_0 A}(2U_0\hat{u}\sin(\omega t) + \hat{u}^2\sin^2(\omega t)),\ F_0 = \frac{C^2(z_0^*)U_0^2}{2\varepsilon_0 A}, \tag{5}$$

where C is the capacitance and z_0^* is the plate separation after application of the bias voltage. If $U_0 \gg \hat{u}$ then the squared sine part of $F_{el}(t)$ can be dropped as good approximation linearizing the component. The biasing causes operating point adjustment by moving the plates closer to each other. [23]

2.2.2 Piezoelectric

Lenk *et al.* report that a piezoelectric transducer utilizes piezoelectric effect where voltage is used to induce mechanical stresses to the component or vice verse. The internal mechanism for this is the elastic deformation of electric dipoles in the crystal lattice. They have yet to reach high Q-factors of electrostatic transducers but their motional resistance is lower, the length of motion is also short. High linear power handling capacity is another useful aspect. Integrating needed materials into the fabrication process can cause problems. In many piezoelectric materials, piezoelectric coefficients depend on stress, operating frequency and mechanical prehistory. The component can be linearized with DC polarization. [23]

Some piezoelectric transducers can operate at the frequencies of hundreds of megahertz. Depending on boundary conditions the resonator operates in many frequency ranges with some of them being partially overlapping. [23]

Fedder and Judy state that theoretical maximum operating frequency is limited by the time required to change the strain within the piezoelectric material, which is related to acoustic velocity in the material (typically several millimeters per microsecond). The design provides another limiting factor for the frequency. [22]

A linear actuator is the simplest piezoelectric transducer, where the cantilever contracts or expands linearly proportional to electric field depending on the polarity of the applied voltage. Length of the deflection is small, but generated forces are large. [22]

Bimorphs are composite structures with at least two layers and can be used to achieve large displacements. With multiple possibly parallel piezoelectric layers/strips and different polarities for them in addition to different clamping solutions usability is very high. [22]

Lenk *et al.* report that in longitudinal oscillators, the electric field and mechanical vibration are perpendicular to each other, in thickness oscillators on other hand their directions coincide, both can be described with networked finite elements. Profiles of these oscillator types are shown in Figure 3. [23]

The piezoelectric transducers can be modeled at low frequencies as the concentrated components of mass and compliance but at higher frequencies that approach

no longer works and a model of a one-dimensional waveguide has to be used. In the one-dimensional waveguide model for high frequency operation extensional waves travel along the rod axis and cause position-dependent inertial forces. The model is simplified by assuming that lateral dimensions are very small allowing inertial forces due the transverse strain to be ignored. [23]

Wave velocity c_D, wave admittance h_D and wave number β are used to describe the waveguide. They depend on density (ρ), Young's modulus (E), frequency (f,ω) and area of lateral cross-section (A) as can be seen from following equations $c_D = \sqrt{\frac{E}{\rho}},\ \beta = \frac{\omega}{c_D} = \omega\sqrt{\frac{\rho}{E}} = \omega\sqrt{m'n'},\ h_D = \sqrt{\frac{n'}{m'}} = \frac{1}{A\sqrt{\rho E}},\ \lambda_D = \frac{2\pi}{\beta} = \frac{c_D}{f}$, where λ_D is wavelength, n' and m' are length related compliances and masses respectively. [23]

In a quasi-static model, which is limited to cases where $\beta l \ll 1$, it is assumed that material is virtually massless. Therefore, field quantities have the same value at each point inside the piezoelectric material and are integrable. They are passed on to the description with integral quantities and concentrated components. [23]

Jaakkola *et al.* have demonstrated different piezoelectrically transduced bulk acoustic wave square plate resonators built from single crystal silicon with Q values of 18000@26MHz and 55000@22MHz. The transduction is achieved with aluminum nitride film on top of the resonator, available resonance modes depend from the film geometry and the anchoring method of the resonator. Available resonance frequencies depend from the plate size and crystal orientation. [18]

2.2.3 Capacitive-piezo

According to Li-Wen Hung *et al.* capacitive-piezo transducer (Figure 3), where piezoelectric material is placed between two electrodes with gaps on both sides, was developed to bridge the gap in Q-factors of electrostatic and piezoelectric transducers while offering lower motional resistance than in the electrostatic transducer. [16]

This is achieved by trying to eliminate some of the bigger sources of loss in piezoelectric transducers, such as resonator-to-electrode strain, thermoelastic effect and defects at the resonator-electrode interface. Linearity and low impedance are maintained though strong electromechanical coupling. Other advantages are reducing electrode losses by allowing thicker electrodes as thickness limitations due the mechanical losses are no longer an issue. [16]

Capacitive-piezo transducer with $Q > 12000$ at 50 MHz has been reported. Typical gap size is about 100 nm due the need to maintain strong electric fields though the piezoelectric material and keep the losses in strength of electromechanical coupling small compared with the rise of Q. [16]

2.2.4 Others

Kempe reports that piezoresistive transducer converts mechanical motion to the electrical signal by measuring changes on resistance due the mechanical stresses in the component. Resistance changes due to the temperature variations can mask

the stress induced changes. Two main approaches to compensate for this issue use either multiple resistors in Wheatstone Bridge configuration or measure both lateral and longitudinal voltages to analyze their ratio, which depends only on piezoelectric coefficients. Used mainly in sensor applications. [20]

An electrothermal transducer is based on thermal expansion caused by Joule heating and works only from electrical to mechanical. The process is quite slow, has high power consumption and generates much waste heat but bias voltage is lower than in the electrostatic transducer. Simple system, used at least in some switches and relays.

2.3 Coupling methods

Multiple methods of connecting the resonators to each other exist but main ones are mechanical and electric. Resonators can also be arranged to nearly limitless amount of topologies. The coupling can also be classified as strong or weak and often both are used in the array but in different directions. The coupling is usually nonlinear to some degree, which is necessary for many applications.

One indicator for system complexity is the degree of freedom, which is determined by the number of resonators. The network can be one-dimensional (1D, chains) or two-dimensional (2D), which are needed for most applications. Three dimensional network is theoretically possible but in practice not realizable with current technology. Another issue is possible coupling losses and in case of electric coupling parasitic capacitances.

It is also possible to combine multiple coupling methods. This provides one possible way to realize significantly different coupling strengths in the system. Some realizations have been reported.

2.3.1 Mechanical coupling

Kempe reports that mechanical coupling is realized by connecting the resonators in question to each other mechanically. The connection is usually realized with a spring, whose strength is determined by dimensions, geometry, material used and coupling location. Length is especially important. This is the simplest method with the strongest connection but the springs are not adjustable and may be problematic to fabricate. Also springs can usually be connected only to the nearest neighbors and are not crossable. Transfer functions are limited to “all-pole” ones. [20]

Usually, springs are build from beams as they are easiest to fabricate and by connecting them together it is possible to reduce unwanted movements. The points where the spring is connected to the resonator are an important loss source due to the non-zero width of the spring. [20]

One limiting factor for the length are electrostatic forces bending the spring toward the substrate. Fabrication technologies provide ultimate limits for both minimum width and height of the spring. Beam cross-section is assumed to be rectangular although in reality the sidewall profile has a slight angle, which has to be taken into account. Aspect ratio limitations and small widths necessary for in-plane

bending beams mean sensitivity to moments about the beam axis and forces in the out-of-plane direction. [20]

Wang *et al.* state that two important length classes for coupling beams are; below one eighth of wavelength and quarter wavelength with the wavelength corresponding to the filter center frequency. The first case is modeled with two half-static masses around the spring and as the resonators on edge get only half of extra mass compared with inner ones passband distortions emerge due mismatched resonator frequencies unless compensated out. The effects from added mass and adjusted stiffness compared with the massless coupler do not completely cancel each other requiring changes to the values of electrical equivalent circuit components leading to the use of nonidentical resonators. The second case allows the use of identical resonators if other dimensions are chosen so that the series and shunt arm impedances have equal and opposite values thus eliminating the influence of coupler reactance. [42]

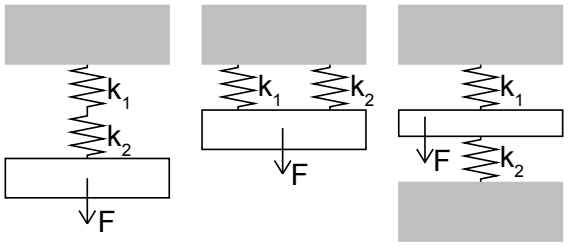

Figure 4: On left a diagram of springs in series, parallel and anti-parallel, where the gray areas are anchors and black lined boxes represent the moving mass.

According to Kempe, linear variant of Hooke's law links stress and strain (z) with following equation $\sigma(z) = \textit{constant} \times z$. In a serial connection (Figure 4) equal forces $F_1 = F_2 = F$ act on the two springs thus the partial displacements (z) add up to $\Delta z_\Sigma = \Delta z_1 + \Delta z_2 = \frac{F}{k_1} + \frac{F}{k_2}$ from where one gets $\frac{1}{k_\Sigma} = \frac{1}{k_1} + \frac{1}{k_2}$ for spring constant. In parallel and anti-parallel connection (Figure 4) the deflection is the same for both springs and thus forces add up to $F = F_1 + F_2 = k_1 \Delta z_\Sigma + k_2 \Delta y_\Sigma$ resulting $k_\Sigma = k_1 + k_2$. These formulas are valid only in a small region where the spring can be considered to be linear. [20]

By combining springs together compliance, which is inverse of spring constant for either deflection on specific axis or torsional motion, in desired directions can be increased while the same happens to stiffness for all other motions. Beam chains can be used to implement comparable compliances in two directions or reduce the effects of compressive stress and axial loads. Due the complexity of beam chains their spring constants have to be determined with computer algebra systems or possibly with finite element methods. [20]

Analytical estimation of beam chain stiffness starts from the following theorems $\frac{\partial U_F}{\partial F_i} = \Delta_i$ and $\frac{\partial U_\Delta}{\partial \Delta_i} = F_i$, where U_F and U_Δ are the elastic energy as function of generalized force, F_i, and generalized deflection, Δ_i, respectively. [20]

Galayko *et al.* state that often spring is assumed to be massless but it can cause some problems as in the real case the mass is distributed along the spring. On certain

frequency inertia starts dominate over elastic forces rendering the spring useless. Springs have the same loss mechanisms as MEMS (Chapter 2.1.2). [12]

According to Wang *et al.*, as the real coupling beams have finite mass and stiffness they can function as acoustic transmission lines. Reactances used to describe mass and stiffness are dependent on coupler dimensions and operating frequency. A T-network with series mechanical impedances and shunt impedance is used to model general wavelength fractions. [42]

2.3.2 Electric coupling

Pourkamali *et al.* report that electric coupling can be realized as electrostatic, with coupling capacitors or with active components. Main advantage of electric coupling is the tunability of the coupling strength though bias voltage. However, it requires wiring for each resonator and corresponding control electronics, which become quite fast complex as the number of resonators increases. It is also used to try to get around fabrication limitations that limit usability of the mechanical coupling elements in high frequencies although different resonator types and multipart spring geometries are also used as solution. A mechanical model is used when analyzing the coupling. [37]

According to Galayko *et al.*, one realization uses two electrostatic transducers with a common electrode between the resonators. The idea is that total charge of the common electrode is constant and capacitance change in one transducer forces charge redistribution among two transducers. This causes force variation though voltage change on both transducers, meaning that when the displacement of other changes the same happens in another. Thus mechanical coupling has been achieved. High impedance required by this coupler at operating frequency is realized with either an inductor or a resistor connected to the common electrode. The splitting of the common electrode removes geometry limitation from the system as resonators to be coupled do not have to be adjacent ones. Controlling the charge of the common node requires the use of a biasing technique to keep constant charge. [13]

Galayko *et al.* state that in the common node design described above a high value choke inductor or resistor connecting the DC source to the common node would prevent DC or AC current circulation keeping the charge of the node constant. However, high-value inductors or resistors are difficult to integrate and off-chip ones are extremely undesirable due high parasitic capacitances. One proposed solution to keeping the constant charge is to use a micromechanical switch that is closed only for time required by DC source to charge the node and parasitic capacitance. An input signal is brought in only after charging and as the node is isolated the charge remains constant. [14]

Pourkamali and Ayazi report that another coupling method uses grounded shunt capacitors, which can be either off-chip or integrated, between the resonators. The required transducer bias voltage is applied by polarizing the connected resonators with opposite polarities. Integrated capacitors are favored for many reasons such as reducing overall complexity and eliminating the large parasitic capacitances. In active cascading, active electric components, usually buffers or amplifiers, are used

as coupling elements to eliminate loading effects. This improves the response but complicates the system significantly. [38]

According to both Pourkamali and Ayazi and Pourkamali *et al.*, electrostatic coupling is also realizable without coupling elements by applying different polarization voltages to the adjacent resonators. Therefore, an attracting force dependent on the size of the coupling gap exists between the resonators. The size variation of the gap due the resonating resonators leads to force variations. The force is divided into the static DC contribution and to displacement dependent part that can be modeled with a spring between the resonators. The mechanical model for a system coupled this way has a large number of springs with different stiffness distributed along the resonator. Main advantage of this approach is its extreme simplicity but as always wiring can become complex and applicability to other resonator geometries than beams is problematic due the need for close proximity. [39, 37]

2.4 Coupled resonators behavior and properties

Yu-Wei Lin *et al.* report that coupling multiple resonators together (arraying) has many advantages, such as performance improvements and easing of the fabrication requirements. In filters, passband flattening is major advantage from arraying. Some applications are not possible with single resonators. [29]

Arraying also compensates for slight differences between individual resonators caused by fabrication tolerances. This happens though averaging assuming that variations are small, also standard deviation is reduced. Power handling is also improved as it is spread among multiple resonators that have sifted into single vibration frequency. Impedance reduction is also achieved. [29]

Agrawal *et al.* state that collective behavior of coupled resonators means that individual components work together, synchronization, which can be considered as phase locking and frequency entrainment, being example of this. [1]

The network, especially a large one, is in many ways analogous to a crystal lattice and the same techniques are useful especially tight binding approximation. The passbands of individual resonators form frequency bands that have much sharper borders, dispersion relation can also be determined. MEMS modeling techniques described in Chapter 2.1.3 are also useful here.

2.4.1 1D network

Choybey *et al.* report that chain of N linear resonators coupled together linearly have N equations of motion that have the following form

$$\begin{aligned} &m_1 x_1'' + b_1 x_1' + k_{s1} x_1 + k_{c1}(x_2 - x_1) = F, \\ &m_i x_i'' + b_i x_i' + k_{si} x_i + k_{ci-1}(x_i - x_{i-1}) + k_{ci}(x_i - x_{i+1}) = 0,, \\ &m_n x_n'' + b_n x_n' + k_{sn} x_n + k_{cn-1}(x_n - x_{n-1}) = 0 \end{aligned} \tag{6}$$

where F is a external force driving the system, b_i is a damping coefficient, m_i is the mass of the resonator, k_{si} is a spring constant, k_{ci} is a coupling spring constant. After mass normalization one acquires damping and stiffness matrices and force vector.

Eigenvalues of the stiffness matrix (λ_i) are related to the resonant frequencies (f_i) of the system $f_i = \sqrt{\lambda_i}/(2\pi)$. By performing Laplace transform to the equations, transfer function can be determined. [7]

According to Alastalo *et al.* by generalizing the dispersion relation for a periodic unanchored chain one for a resonator chain is acquired

$$\omega(\kappa) = \sqrt{\frac{2k}{M}}\sqrt{1 - \cos(\kappa a) + K}, \tag{7}$$

where M is the mass of the resonator, k is the resonator spring constant, κ is the wave vector, a is the period of the chain and

$$K \equiv k'/k = \frac{2}{(\omega_a/\omega_s)^2 - 1}. \tag{8}$$

The wave vector is limited to $[-\pi/a,\, \pi/a]$ and k' is the coupling spring constant, subscripts a and s indicate the resonator and coupling spring respectively. [2]

Judge *et al.* have investigated the wave propagation in a chain of linearly coupled undamped linear oscillators. By assuming that their vibration can be described as $u_n e^{i\omega t}$, the equation of motion for a single oscillator can be written as following

$$-\omega^2 m u_n + (k_0 + k_c)u_n - k_c u_{n-1} - k_c u_{n+1} = 0. \tag{9}$$

The oscillator has a mass m, nominal stiffness k_0, stiffness of coupling between neighbors k_c, natural frequency $\omega_0 = \sqrt{k_0/m}$, non-dimensional coupling ratio $R = k_c/k_0$ and vibration amplitude u_n. By rewriting the equation to matrix form one gets following

$$\begin{Bmatrix} u_{n+1} \\ u_n \end{Bmatrix} = T \begin{Bmatrix} u_n \\ u_{n-1} \end{Bmatrix},\ T = \begin{bmatrix} \left(\frac{1+2R-\omega^2/\omega_0^2}{R}\right) & 1 \\ -1 & 0 \end{bmatrix} \tag{10}$$

with eigenvalues being $\lambda_{1,2} = \frac{1}{2}(T_{1,1} \pm \sqrt{T_{1,1}^2 - 4})$. [19]

By using corresponding eigenvectors T can be transformed into a wave matrix

$$\begin{Bmatrix} L_{n+1} \\ R_{n+1} \end{Bmatrix} = W_0 \begin{Bmatrix} L_n \\ R_n \end{Bmatrix},\ W_0 = \begin{bmatrix} \lambda_1 & 0 \\ 0 & \lambda_2 \end{bmatrix}, \tag{11}$$

which describes relationship between the amplitudes of left- and right-going waves (L and R) on either side of the oscillator n. The eigenvalues determine how much the waves attenuate as they pass the oscillator, which is the same for each resonator leading to exponential decay of the spatial amplitude with rate $\gamma = \ln(|\lambda_1|)$. The equation of motion can be rewritten as $a^2\nabla^{(2)}u = [(\omega^2 m - k_0)/k_c]u$, where a is the spacing between resonators and $\nabla^{(2)} = 1/a^2(u_{n-1} + u_{n+1} - 2u_n)$. [19]

The discrete nature of the system limits the minimum wavelength to $2a$, meaning that the maximum wavenumber (k) is π/a. Therefore, the eigenvalues of the 1D discrete Laplacian are given by

$$e(k) = 2/a^2(1 - \cos(ka)),\ e(k) \in [0,\, 4/a^2] \text{ for } k \in [0,\, \pi/a]. \tag{12}$$

If $\nabla^{(2)}$ is replaced with $e(k)u$ and ω^2 solved, one gets following

$$\omega^2 = \frac{k_0 + k_c a^2 e(k)}{m} = \omega_0^2(1 + 2(1 - \cos(ka))R) \tag{13}$$

and thus the propagating frequencies have to be between ω_0 and $\omega_0\sqrt{1+4R}$. [19]

The width of the passband is approximately $2R\omega_0$, if R is small which is the case in weakly coupled systems. The filter quality factor (Q_{filter}) is the ratio of filter center frequency to filter bandwidth and for small R it is $1/2R$. [19]

Judge *et al.* also state that damping means adding imaginary term proportional to the damping coefficient δ to the equation of motion and $j\delta/R$ term to $T_{1,1}$. This means that the eigenvalues of T no longer have a unit magnitude within the passband and have non-zero spatial decay constant γ at all frequencies. If the damping is small compared to R, then $\gamma_d \approx \frac{1}{\sqrt{\alpha(4-\alpha)}}\left(\frac{\delta}{R}\right)$ where α is the passband position defined as $(\omega/\omega_0)^2 = 1 + \alpha R$ for $\alpha \in [0, 4]$. [19]

If the resonators are not fully identical, wave amplitude decay also appears in the passband of an undamped system. The disorder is described though varying oscillator stiffness and the variations of coupling stiffness are ignored. The stiffness k_n of oscillator n varies from the nominal (k_0) by $\Delta k_n = (k_n - k_0)/k_0$, which adds term $\Delta k_n/R$ to $T_{1,1}$. The wave transfer matrix is

$$W_n = \begin{bmatrix} 1/t_n & -r_n/t_n \\ r_n/t_n & t_n - r_n^2/t_n \end{bmatrix}, t_n = \frac{\lambda_2}{(1+\beta)}, r_n = \frac{-\lambda_2\beta}{(1+\beta)}, \beta = \frac{\Delta k_n}{(R(\lambda_1 - \lambda_2))}, \tag{14}$$

where t_n and r_n are transmission and reflection coefficients respectively. Increasing the stiffness difference between oscillator n and a nominal one means a greater reflectance. [19]

The global wave transfer matrix $Wg = \prod_{n=1}^{N} W_n$ tells the total transmission and reflection for the network. As t_n varies between individual resonators the amplitude decay along the chain is not smooth, but as N approaches infinity the decay becomes asymptotically exponential. [19]

The approximate exponential decay constant for a system with both damping and disorder is

$$\gamma_{md} = \frac{1}{\sqrt{\alpha(4-\alpha)}}\frac{\delta}{R} + \frac{1}{2\alpha(4-\alpha)}\left(\frac{\sigma}{R}\right)^2, \tag{15}$$

which is valid when the ratios δ/R and σ/R are small. At the passband center ($\alpha = 2$) the ratio $\delta R/\sigma^2$ determines significance of disorder as source of the decay. The decay caused by disorder prevents the use as low insertion loss filter before the coupling variations become too large and the approximation breaks down. [19]

According to Judge *et al.*, the lower limit of achievable bandwidth without insertion loss and distortion is limited by the fabrication tolerances regardless of dissipation minimization. This means that increasing Q is not enough and disorder induced localization has to be reduced by better fabrication tolerances, post-fabrication

"tuning" or the use of less sensitive filter designs. As average quantity γ_{md} is not accurate for individual resonators although it provides insight to relative effects of disorder and damping. Accurate prediction of signal amplitude at the end of the chain is not possible with γ_{md}. [19]

2.4.2 2D network

In an 2D-array consisting of single-degree-of-freedom resonators with strong coupling in one direction and a weak one on another has the following equation of motion

$$\begin{aligned} &-\omega^2 m u_{n,m} + (k_0 + 2k_c^{weak} + 2k_c^{strong})u_{n,m} - k_c^{weak}u_{n-1,m} - k_c^{weak}u_{n+1,m} \\ &- k_c^{strong}u_{n,m-1} - k_c^{strong}u_{n,m+1} = 0 \end{aligned} \tag{16}$$

with indices in the vertical and horizontal directions being n and m respectively. [19]

With following substitutions

$$u_{n,m} = e^{-i\omega t}\ u_{n-1,m} = e^{-i\omega t - ik_w a_w}\ u_{n,m-1} = e^{-i\omega t - ik_s a_s}, \tag{17}$$

where k_w, k_s, a_w and a_s are corresponding wavenumbers and distances between the oscillators, for the ideal array the passband frequencies are then the following

$$\omega_2 = \omega_0(1 + 2(1 - \cos(k_s a_s))R_s + 2(1 - \cos(k_w a_w))R_w), \tag{18}$$

where $R_w = \dfrac{k_c^{weak}}{k_0}$ and $R_s = \dfrac{k_c^{strong}}{k_0}$. The R_s and R_w are the coupling ratios for strong and weak coupling respectively. From the previous equation one can determine that in the vertical direction a wide frequency band exists while only a narrow band exists in the horizontal direction.[19]

Judge *et al.* also report that as in the 1D network disorder is modeled as stiffness variations and characterized by the standard deviation of those variations (σ). Even though σ/R_w is non-negligible, strength of the weak coupling is determined by desired passband. For strong coupling the requirement is that $(\sigma/R_s)^2$ is negligible small. This allows low attenuation propagation along the rows and as many propagation paths exist part of energy in each oscillator is transferred though the weak coupling to another row along which part of energy can propagate while another part is transferred though the next weak coupling. This happens with each oscillator in each row and reduces amount reflection due disorder. Now, each row can be considered effectively as a single oscillator, and the average of the transmission at each coupling location between the two rows is the total fraction of energy transmitted from one row to the next. [19]

As the disorder is described as a random variable with standard deviation σ, this means that the average stiffness of any N oscillators varies randomly with standard deviation $\sigma/\sqrt{N}$. The 2D array with oscillator counts N_w and N_s is effectively the 1D array whose length is N_w and effective disorder $\sigma_{eff} = \sigma/\sqrt{N_s}$. [19]

Just as with the 1D array, the number of wavelengths in each of the array directions can be used to characterize the modes of the 2D array. The amplitudes can vary within a given row at resonance as standing wave shapes will occur in each direction.

Near antinodes of the standing waves in the strong coupling direction transmission from one row to the next occurs most readily. [19]

The passband is in standard case from ω_0 to $\omega_0\sqrt{1+4R_s+4R_w}$ and contains N_s subbands that include N_w resonances each, whose width is determined by R_w. With different excitation methods the passband can be manipulated as only certain resonance modes are excited, usually the goal is narrower band. As with 1D case the ripple due resonance modes in the passband can be smoothed by selecting input and output impedances correctly. [19]

Judge *et al.* state that in an array with identical oscillators, the selection of a narrow passband is possible by exciting a single wavenumber in the strong coupling direction due to the orthogonality of the mode shapes. Disorder means altered the modes of the system and that orthogonality between modes in other groups and the excitation is no longer perfect. As the variations among the oscillators are small, the desired modes will be the most strongly driven ones and a near orthogonality exists between the excitation and the other modes. [19]

With the increasing N_s the number of extraneous passbands increases and their spacing reduces unless the overall frequency band is widened though R_s. Exciting the central passband, where all oscillators have the same amplitude, is favored due its the greatest separation from extraneous bands and straightforwardness. [19]

In the central mode group, the extra damping can suppress extraneous passbands, while having only a minor effect to the desired band. In a given row and in the strongly coupled direction, all odd oscillators are at antinodes vibrating at equal amplitude and even ones are at nodes of a standing wave thus not vibrating. However, all even oscillators are not at nodes for the other mode groups, where vibration can be suppressed though damping, with the different wavenumber in the strongly coupled direction. In a ideal situation this would not be necessary as in any other groups no forcing of modes exist, but in a real case, where disorder is present and all other mode groups excited, significant benefit can be achieved. [19]

According to Judge *et al.* each strongly coupled row acts effectively as a single oscillator, whose properties are a weighted average of individual oscillators in the row. If the central mode group is excited, then by taking a simple average across odd resonators the required result is acquired. The effective disorder is smaller than the actual disorder. With use of 2D array the passband distortion can be mitigated as increasing N_s reduces the effective disorder leading to the passband more closely resembling that of an ideal filter. [19]

Increasing N_s is beneficial only for negligible spatial decay in the strong coupling direction. The localization can be problematic for large N_s and the transition point becomes higher as the strong/weak coupling ratio increases. Dissipation can limit N_s similarly than disorder and the final limits for the array size are set by fabrication technology. [19]

2.5 Applications

Nguyen and Young *et al.* report that for some applications usage of coupled MEMS-resonator networks over individual MEMS or electronics is preferred or even necessary.

Many useful signal processing functions such as mixing, amplification and limiting are only possible due the nonlinearities . Usage of RF-technology especially in mobile devices is growing rapidly and with it need for low power integrable filters, mixers and other transceiver components. MEMS networks respond to these demands and those of many other applications with some waiting to be discovered. Commercialization of these systems is just beginning but in time massive systems at VLSI level and beyond will appear as systems with over hundred resonators has been demonstrated almost a decade ago. [45, 34]

Nguyen states that for RF-technology, the ultimate goal is software defined radio (SDR), which uses narrow band filters adjustable over wide frequency range to avoid the need complex switching systems with large amount of individual filters, multiple transceivers for different frequency bands or an extremely high performance analog to digital converter (ADC) with extremely wide frequency range. Further advancement of the SDR concept is an addition of a cognitive feature to automatically find an unused frequency band. Extremely narrow band filters are required for this to achieve low power consumption. [35, 36]

Superheterodyne transceiver is a widely used system that uses intermediate frequency for signal processing and amplification with mixer converting the signal to/from radio frequency for/from the antenna. Oscillators, mixers, filters and possibly even amplifiers are can be realized with MEMS networks and individual MEMS components allowing most of the system to be integrated together ensuring high performance. Examples of some possible realizations of components based on coupled MEMS resonators found in literature are given in the following chapters.

According to Nguyen, one possible design of MEMS amplifier consists of two mechanically coupled resonators with structural design used enable displacement amplification on the input resonator and the output one impacts the output electrode as it vibrates on the orthogonal axis to the input. Both resonators have slots, which increase displacements by reducing stiffness, but they are orthogonal to each other. Resonant mechanical switches (“resoswitches”) as these components are known also act as filters. [36]

In addition, there are different computing applications and cryptography, where MEMS networks can be used as a seed for generating encryption keys.

2.5.1 Integration

Nguyen reports that possibility to integrate MEMS based components in to a single chip is a major advantage as necessary components for frequency or timing control could be placed close together forming micromechanical circuits. The extra space or cost penalty from integrating at least hundreds or even thousands components is negligible. To increase the limited functionality of individual components combining them into more complex circuits to better fit specific tasks is necessary. The combining is enabled by the low loss of individual MEMS components. A system created by arraying can offer a better performance than a single component thus allowing one to meet the required standards easier. Also overall losses decrease when all necessary components are integrated to single chip the losses from coupling discrete components

to each other are no longer an issues. [34]

Low capacitance single-chip integration with transistors is important due the need for control electronics. At the same time this solves the high impedance issues as the allowed on-chip parasitic capacitors have impedances in the kΩ range. [34]

Performance advantages from integrated micromechanical circuits are maximized by utilizing them in a massive scale as has been achieved in electronics with ICs. One possible LSI circuit is a RF channel selector for transceivers, which would enable reducing performance requirements for other parts. [34]

Nguyen states that one approach to simplify the design of integrated MEMS networks is to start with resonators, filters and mixer-filters as building blocks. Design of these systems relies largely CAD layout tools with lateral dimensions defining system characteristics. The entire structure could be automatically generated from lateral dimensions by a CAD program leading to the automatic generation of the layout from the filter specifications, a comparable process for electronics exists. There are many similarities between electronic and micromechanical circuit design principles and methods. [34]

Frequency of some resonator types is determined by thickness, which is not specifiable via layout tools limiting available choices somewhat. The use of the lateral dimensions to determine frequencies allows components with different frequencies on a single chip and layer. Other demands for integrability include Q values of at least 1000, preferably over 10 000, in frequencies up to 6 GHz to prevent high losses and allow a channel selecting. Geometric flexibility means attaining necessary frequency with many different resonator types and modes. [34]

2.5.2 Delay lines

As their name implies delay lines delay the signal and can be used for time-inversion, Fourier-transformation, convolution and noise reduction. In MEMS the signal propagates as an acoustic wave with low losses enabling high Q components. All MEMS realizations act also as bandpass filters, which has advantages for RF applications. They could be used in extremely wideband receivers. Delay lines are often realized as the line of coupled MEMS resonators though networks can also be used.

Alastalo *et al.* have investigated and realized a narrow band delay line for HF from MEMS resonators and capacitive transducers. The system was modeled with a chain consisting of elementary resonators coupled together. The resonators consists of two moving masses m coupled with spring k and anchored to stationary with springs k' supports. This model does not take the losses into account. The chain is periodic except for the ends with period a. The resonators are connected to each other with a beam that has mass m_0. [2]

The resonator has two eigenmodes: symmetric and antisymmetric. In the symmetric mode the masses move in the same phase while in antisymmetric mode they have 180° phase difference. The resonance frequencies are for symmetric mode $\omega_s = \sqrt{k'/m}$ and for antisymmetric $\omega_a = \sqrt{(2k + k')/m}$. The ratio of the anchoring to coupling spring is following

$$K \equiv k'/k = 2/((\omega_a/\omega_s)^2 - 1) \tag{19}$$

as determined by the resonance frequencies. [2]

The dispersion relation $\omega(\kappa)$, where $\kappa = 2\pi/\lambda$ is the wavevector, determines the frequencies that the periodic chain can vibrate and carry signals. For anchored chain $\omega(\kappa) = \sqrt{2k/M}\sqrt{1-\cos(\kappa a)+K}$, where $M \equiv 2m + m_0$ is the total mass of coupled resonator and $\kappa \in [-\pi/a, \pi/a]$. The chain has a passband response due the nonzero k'. [2]

According to Alastalo *et al.*, the group velocity is acquired from the dispersion relation and is following

$$v_g = \frac{\partial\omega}{\partial\kappa} = \frac{a}{2}\sqrt{\frac{2k\sin^2(\kappa a)}{M(1-\cos(\kappa a)+K)}} \tag{20}$$

and the phase velocity is then following $v_{ph} = \omega/\kappa$. The center frequency $\omega_0 = 2\pi f_0$ and bandwidth $\Delta\omega = 2\pi\Delta f$ are then following

$$\omega_0 = \omega(pi/(2a)) = \sqrt{\frac{2k(K+1)}{M}} \text{ and } \Delta\omega = \omega(\pi/a) - \omega(0) = \sqrt{\frac{2k}{M}}\,(\sqrt{K+2} - \sqrt{K}). \tag{21}$$

The group and phase velocities for the center frequency are

$$v_{ph}^0 \equiv \frac{\omega}{\kappa}\Big|_{\omega_0} = \frac{2\pi}{a}\sqrt{\frac{2k(K+1)}{M}} \text{ and } v_g^0 \equiv \frac{\partial\omega}{\partial\kappa}\Big|_{\omega_0} = \frac{a}{2}\sqrt{\frac{2k}{M(K+1)}}. \tag{22}$$

[2]

A single capacitively transduced resonator, which is characterized by parameters k, m and Q, can be modeled with a series RLC circuit (Figure 5). The transducers are capacitive parallel-plate ones with length B, thickness H, gap size d and rest capacitance $C_0 = \epsilon_0 BH/d$. The components have following values $R = \sqrt{km}/(Q\eta^2)$, $L = m/\eta^2$, $C = \eta^2/k$, where $\eta = C_0 V/d$ with V being the bias voltage. [2]

Similar representation to for spring-mass-chain transmission line can be found by solving the propagation constant κa from the dispersion relation in regards to ω. The square $(\kappa a)^2 = Z_s Y_p$ is then expanded as a power series with respect to ω^2 around the passband center, Z_s is the series impedance and Y_p is the shunt admittance of the waveguide per unit length. One can then write

$$(\kappa a)^2 = \left(\frac{j\omega M}{\eta^2} + \frac{2k}{j\omega\pi\eta^2}\left[\pi(1+K) - \left(\frac{\pi}{2}\right)^2\right]\right)\frac{j\omega\pi\eta^2}{2k} \text{ and } Z_s = j\omega L_s + 1/(j\omega C_s),$$
$$Y_p = j\omega C_p, \text{ where } L_s = \frac{M}{\eta^2},\ C_s = \frac{\pi\eta^2}{2k\left[\pi(1+K) - (\pi/2)^2\right]},\ C_p = \frac{\pi\eta^2}{2k}. \tag{23}$$

The characteristic impedance of the line is then based on previous expressions following $Z_c = \sqrt{Z_s/Y_p} = \sqrt{kM}/(\eta^2\sqrt{2(K+1)})$. [2]

Alastalo *et al.* state that the center frequency and phase velocity increase while bandwidth, group velocity and the characteristic impedance decrease as K increases.

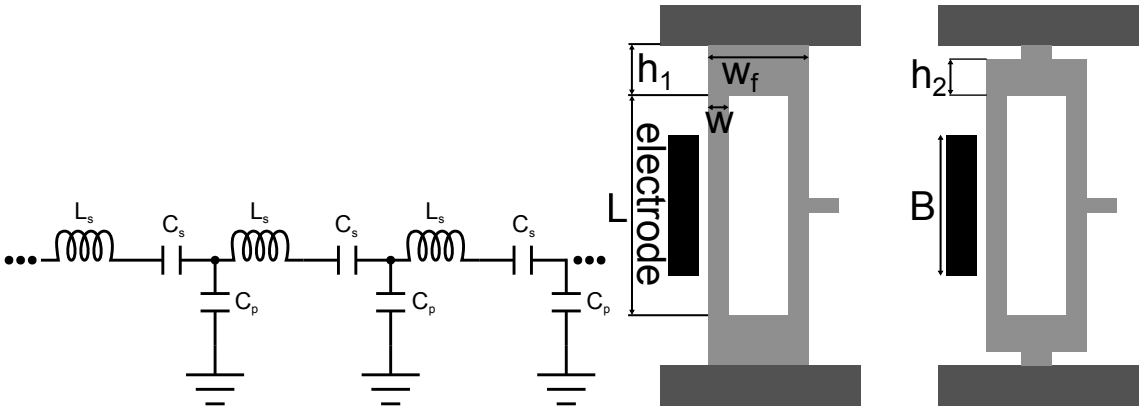

Figure 5: On left electrical equivalent circuit for the resonator chain based series RLC model. On right the design of tuning fork resonators for different K values, the one on right has smaller K than the resonator on left. The sizes of different parts are also marked to the diagram.

For electrostatic transducers Z_c is typically much higher than $50\,\Omega$. Higher K values also reduce the variation of the group velocity as a function of frequency at band center. As high K as possible is therefore desirable for good signal coupling and delays. [2]

One possible realization uses a double-supported tuning-fork design. The impact of K value was tested with two different anchoring structures, while all other size parameters remained constant. The strength of the anchoring can be reduced by decreasing the anchor length so that a narrower area connects the anchor to the support as shown in the Figure 5. [2]

2.5.3 Filters

Judge *et al.* report that filters can be realized either as line or MEMS network and their order is usually the same as the number of resonators used. The most important filter parameters are center frequency, bandwidth, stopband rejection, insertion loss, ripple, shape factor and the quality factor. Lines as bandpass filter can provide better characteristics, such as lower impedance, ripple and larger rejection, than individual MEMS for reasons shown in Chapter 2.4. With networks, multiple band filters can be realized. The main purpose of filters is to reduce the performance requirements of amplifiers, tuning circuits and ADCs. [19]

In filter applications, odd-order nonlinearities causing signal intermodulation are problematic as they can generate unwanted frequency components within passband. Communications demand sharp roll-off and large stopband rejection achievable with higher order filters. Filter type is determined by coupling characteristics such as strength and topology. Weak coupling required for narrow band filters means arrays prone to localization when disorders are present. [19]

Transfer function contains all necessary information about the behavior of the filter in the frequency domain. Filters can be classified by the type of transfer function. With higher-order filters, one can get sharper transition between pass and

stop bands. Poles are roots of the denominator polynomial of the transfer function.

Sheng-Shian Li *et al.* state that by replacing individual resonators in parallel coupled filters with series-coupled sub-filter structures possessing higher order frequency transfer functions the roll-offs from passband to stopband sharpen and stopband rejections increase. They also fabricated and tested these systems. [24]

Sheng-Shian Li *et al.* report that unwanted modes can be suppressed in a composite-array consisting of disk resonators by electrode design and choosing the dimensions of couplings correctly. The "wine-glass" mode is blocked by surrounding the disk fully symmetrically with electrode that has openings only for couplings, see Figure 6 for an diagram of the system. The other modes are shifted away by springs with infinite stiffness. For frequencies close to the filter center frequency effectively infinite stiffness is achievable, if coupling dimensions correspond to an effective half-wavelength at the center frequency or their array coupling beam lengths satisfy $L_a = n\sqrt{\frac{E}{4f_0^2\rho}}$, $n = 1, 2, 3\ldots$, where E is Young's modulus and ρ is density of the structural material and f_0 is the center frequency. They also demonstrated a small system of this type. [25]

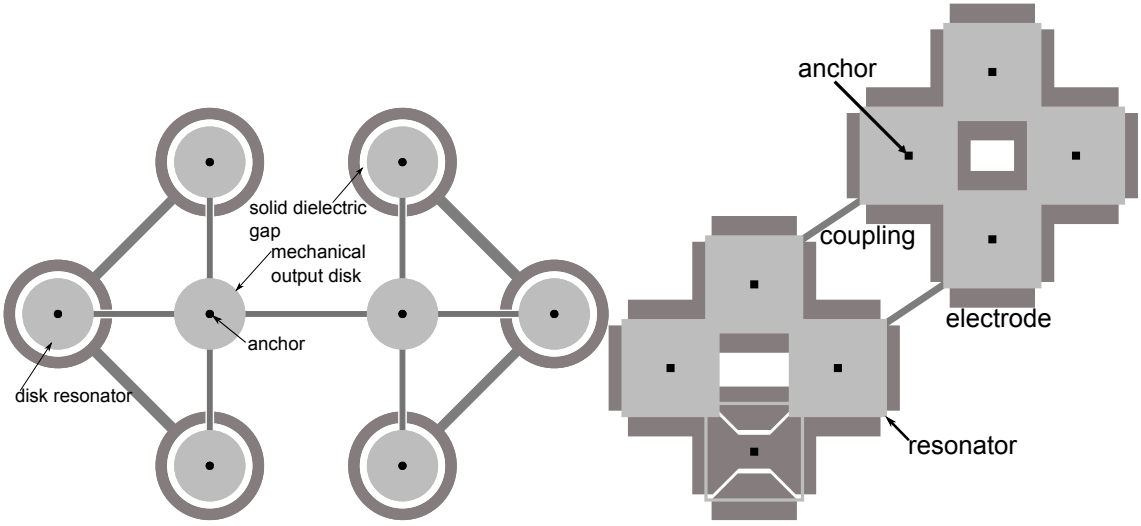

Figure 6: Diagram of disk resonator array (on left) and coupled square resonators (on right) showing placement of couplings, anchors, resonators and electrodes. On bottom one can see the electrode placement under the resonator. On left the length of the shorter couplings are $\lambda/2$ and large one in center is $3\lambda/4$.

The composite arrays are linked to each other with $n\lambda/4$ couplings, with n being odd integer, so that the mass and stiffness contributions of the coupler cancel each other at the attachment location to the adjacent resonators, allowing the use of identical resonators. [25]

According to Clark *et al.* resonator arrays consisting square resonators hard-coupled together at overlapping corners shown in Figure 6 act as single resonator that are then coupled to each other mechanically can be used to improve power handling and reduce impedance levels. The resonance frequencies of component

resonators are locked by the hard-coupling. As each resonator has electrode below, the transducer area increases with resonator count reducing the motional impedance. This particular resonator type suffers from parasitic effects and voltage limits preventing full termination of these filters. [9]

Resonator geometry and material determine the filter center frequency and characteristics of the coupling spring sets placement and separation of poles. The relative bandwidth of two-pole filter is following $BW = \frac{k_s}{k_r\, k_{12}}$, where k_s is the equivalent stiffness of the coupling beam, k_r is the equivalent stiffness of the resonator at the coupling point and k_{12} is a tabulated filter parameter for the desired filter type. If there are multiple resonator behind the coupling spring then one has to add n_c term, which is the number of resonators stacked up behind the couplings, to the denominator of the earlier bandwidth formula while k_r remains as stiffness of single resonator. [9]

Motiee *et al.* report two different filter types based on either cantilevers and flexural coupling beams or clamped-clamped beams coupled together with V-shape spring build from beams. The first type is the transverse filter (TF) and the second is the lateral filter (LF). Diagrams of these systems are shown in Figure 7. [30]

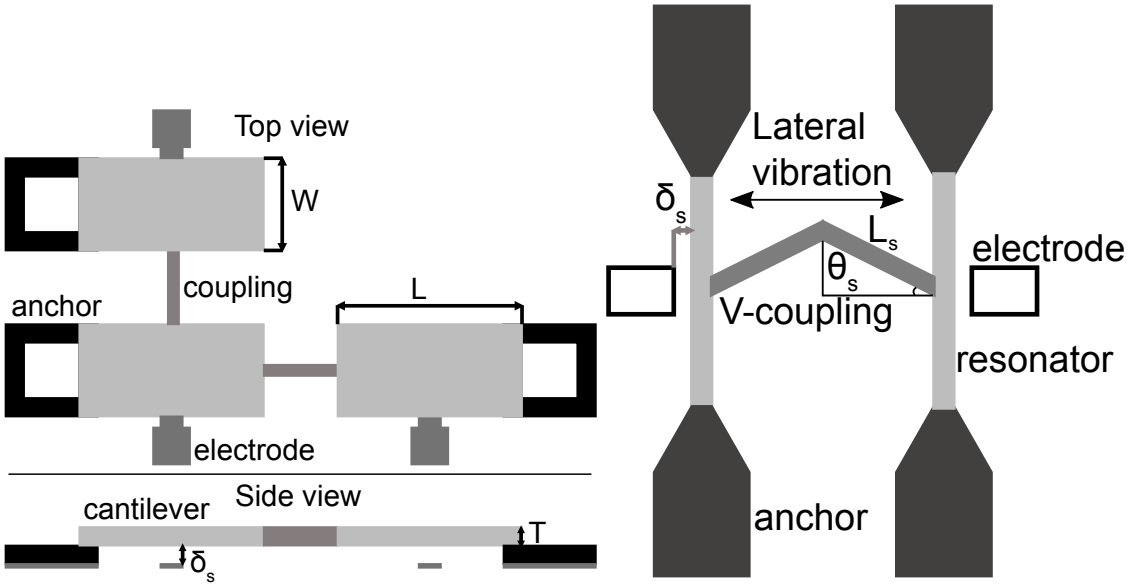

Figure 7: Diagrams of TF (on left) and LF (on right) systems showing resonator dimensions and placement of couplings, anchors, resonators and electrodes.

The coupler consists of two beams for which $L_s < \lambda/8$ connected at angle θ_s. The mass of coupling beam is divided between the resonators leading to shifted resonance frequencies. Passband shape distortions due the mass additions of different resonators not being identical have to be taken into account in the design, which can be difficult for systems more than two resonators. The main advantage of this coupling mechanism is the ability to adjust the coupling stiffness by changing the angle. [30]

Galayko *et al.* have designed and tested filters based on electrostatic coupling between the resonators. By attaching the signal electrode coupled to anchor with mechanical spring to a rigid bar it can be moved with additional electrostatic transducer closer the resonator to reduce the transducer gap to submicron levels. The coupling can be modeled as mechanical lumped-parameter system with two mobile nodes connected to each other and fixed reference with springs k_{112}, k_{12} and k_{122}, where the subscripts of side springs between nodes and references have twice the number of node. These parameters depend from bias voltages, transducer gaps, parasitic capacitance and transducer capacitances at zero displacement. The resonance frequencies of individual resonators have to be matched to the filter center frequency by taking into account the impact of coupling. [14]

2.5.4 Mixer

Knoll *et al.* have investigated the use of linearly coupled oscillators vibrating orthogonally to each other for mixing, modulation and amplification. The structure consists of two parallel input oscillators coupled linearly by springs, and resulting vibration is then coupled nonlinearly to third oscillator vibrating perpendicularly to the input (Figure 8). They have also demonstrated these functions with MEMS resonators. [21]

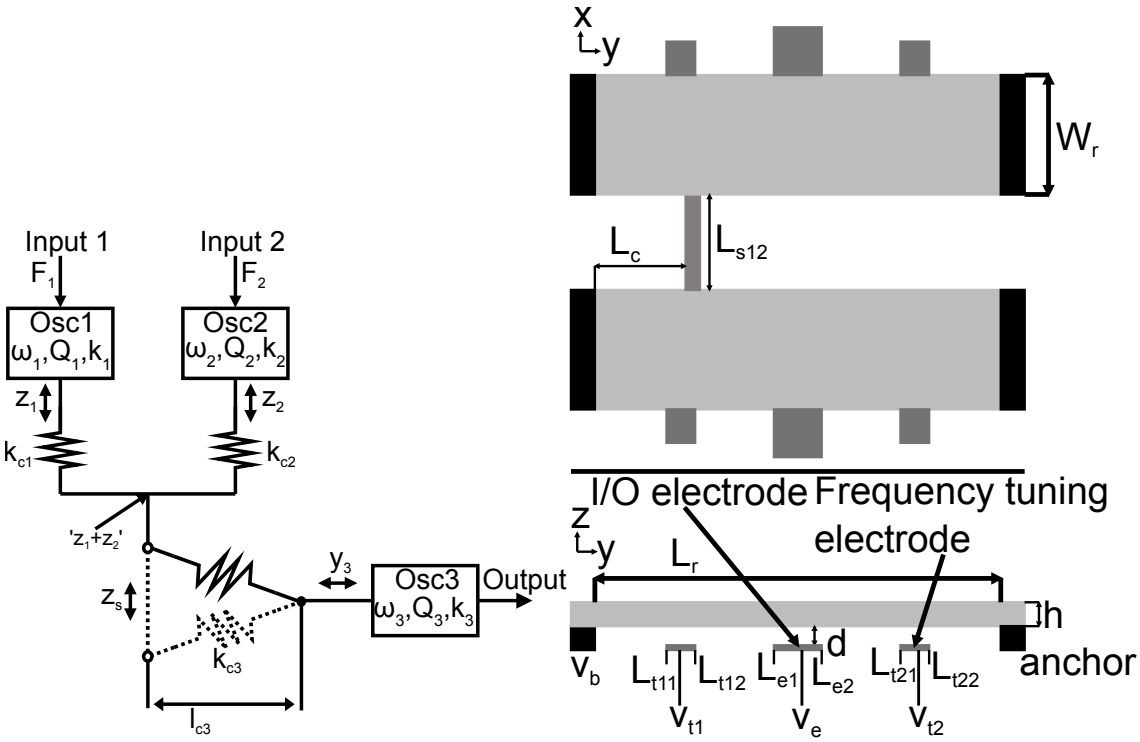

Figure 8: Diagram of the proposed mixer consisting of oscillators and nonlinear coupling (on left) and a mixer-filter combination (on right). Amplitudes and directions of the movement are also marked to the figure. On right placement and dimensions of the system are visible along with some other important notations.

If two oscillators vibrating orthogonally to each other are coupled with spring that has stiffness k_c and length l_c, then the coupling potential is

$$U_c(z,y) = \frac{1}{2}\, k_c((z^2 + (l_c + y)^2)^{1/2} - l_c)^2. \tag{24}$$

The force in y-direction is then following

$$F_y = \frac{\partial U_c}{\partial y} = k_c\,(l_c + y)\,(l_c/(z^2 + (l_c + y)^2)^{1/2}) \approx k_c\,(y + \frac{z^2}{2l_c}). \tag{25}$$

This means if the input oscillator vibrate sinusoidally at frequency ω that the output has to vibrate at frequency 2ω if one wants large output amplitude.

The inputs Osc1 and Osc2 have vibration amplitudes z_1 and z_2 respectively. They are coupled to a common point $z_s = z_1 + z_2$ with springs k_{c1} and k_{c2}, which describe the mechanical compliance of the coupling structure. The output oscillator Osc3 is excited by the motion z_s though the nonlinear coupling generated by spring with axis perpendicular to the z-direction. At rest the coupling spring has length l_{c3} and stiffness k_{c3}. [21]

The total coupling potential of the three oscillator system is

$$U_c(z_1, z_2, z_s, y_3) = 1/2\, k_{c1}\, (z_1 - z_s)^2 + 1/2\, k_{c2}\, (z_2 - z_s)^2 + 1/2\, k_{c3}\, ((z_s^2 + (l_c + y_3)^2)^{1/2} - l_c).$$

The constraint of zero total force in equilibrium ($\partial U_c/\partial z_s = 0$) is used to determine z_s, which is for small z_1, z_2 and y_3 approximately

$$z_s = (k_{c1}\, z_1 + k_{c2}\, z_2)/(k_{c1} + k_{c2}).$$

[21]

If $k_{c1} = k_{c2}$, then $z_s = 1/2\,(z_1 + z_2)$. By inputting it to the formula for F_y one gets following expression $F_{y,z1,z2} = \dfrac{k_{c3}}{l_{c3}\, z_1\, z_2}$, which proportional to the product $z_1\, z_2$. If

$$z_1 = A_1\, \cos(\omega_1\, t) \text{ and } z_2 = A_2\, \cos(\omega_2\, t), \tag{26}$$

then the expression for the force becomes

$$F_{y,\omega_1,\omega_2} = 1/2\, k_{c3}\, A - 1\, A_2\, \cos((\omega_1 + \omega_2)\, t) \tag{27}$$

vibrating with the frequency $\omega_1 + \omega_2$. If one chooses the resonance frequency of the output $\omega_3 = \omega_1 + \omega_2$, then $y_3 = A_1\, A_2$. The output vibrates only if both inputs have nonzero amplitude. Mixer function with logical AND function are identifiable mechanical vibrations encoding the logical states. [21]

Knoll *et al.* state that the mixer can act as an amplitude modulator, where one input is high-frequency carrier (ω_c) and the other is the low-frequency modulator (ω_1). The system generates force at frequencies $\omega_c - \omega_1$ (lower sideband) and $\omega_c + \omega_1$ (upper sideband). [21]

The upper sideband gain is then linearly dependent from ω_c. The negative gain of lower sideband means that power flows from carrier input via output to the modulator

input allowing it to be excited without any external signal. This enables extremely high gain figures, but the system is potentially unstable due its regenerative nature. [21]

Knoll *et al.* show also a more realistic model that takes into account the finite mass (m_s) of coupling springs with differential equation describing the motion of the mass. If the resonance frequencies of coupling springs are much higher than those of oscillators, then no or infinite frequencies can be used as good approximation. [21]

Stringent design and operational constraints are imposed on the system due the instabilities. High coupling efficiency of the output requires that the stiffness of the spring is high, order of magnitude of the oscillator spring constants. This is achieved with bulkier geometries that have larger mass causing the internal resonance frequencies of the coupling drop leading to a critical dependency between the output amplitude and the actual internal resonance frequency at vibration amplitudes that stay below critical values for chaotic behavior. The output amplitude does not reach stable value at high input amplitudes. [21]

2.5.5 Filter-mixer combination

According to Ark-Chew Wong and Nguyen, mixer and a filter can be combined as one device with the use of capacitive mixing transducers, which downconvert RF-signal to IF, and coupled MEMS resonators performing the filtering reducing losses compared with separate devices,. The structure consists of clamped-clamped beam resonators and a flexural beam at low velocity location. Figure 8 on page 31 shows a diagram of this system. [44]

Tunability and functionality of each resonator is increased with additional electrodes and to reduce local oscillator-to-output coupling a highly resistive coupling beam is used. Of three electrodes under the resonator, the central one is for input/output and the ones placed symmetrically around it are for frequency tuning. Localized annealing across the resonator enhances filter performance in contaminated environments and is realized with electrodes at anchors. [44]

The transducer has a square law transfer function meaning that

$$F_z = \frac{\partial E}{\partial z} = \frac{\partial}{\partial z}\left[\frac{1}{2}\,C_1\,(v_e - v_b)^2\right] = \frac{1}{2}\,(v_e^2 - 2v_e\,v_b + v_b^2)\,\frac{\partial C_1}{\partial z} \tag{28}$$

assuming that tuning electrodes have the same DC potential as the beam. Now v_e and v_b are voltages at electrode and conductive beam respectively, C_1 is input electrode to resonator capacitance, which is function of displacement (z) and time (t). The voltage product term represents mixing and equation for C_1 contains total resonator stiffness (both mechanical and electrical components) $k_r(y)$ at location y, $k_{re} = k_r\,L_r/2$, $Z_{mode}(y)$ describes the resonance mode shapes of the beam. Sum or difference of RF input signal v_{RF} and local oscillator v_{LO} is contained in the difference voltage $v_e - v_b$ in addition of DC bias V_P for filter termination. [44]

Ark-Chew Wong and Nguyen also state if $f_{RF} = f_{IF} + f_{LO}$ the force equation

can be rewritten as

$$\begin{aligned} F_z = &\tfrac{\partial E}{\partial z} = \frac{1}{2}\,(v_{RF} - V_{P1} - v_{LO})^2\,\tfrac{\partial C_1}{\partial z} = \\ &\left(\frac{1}{2}\,V_{P1}^2 + \frac{1}{2}\,v_{RF}^2 + \frac{1}{2}\,v_{LO}^2 + V_{P1}\,v_{LO} - V_{P1}\,v_{RF} - v_{LO}\,v_{RF}\right)\,\tfrac{\partial C_1}{\partial z}, \end{aligned} \tag{29}$$

where the last three are mixing terms, if v_{RF} and v_{LO} are purely sinusoidal then the last term will expand to

$$-\frac{1}{2}\,v_{LO}\,v_{RF}\,\frac{\partial C_1}{\partial z}\,\cos((\omega_{RF} - \omega_{LO})\,t). \tag{30}$$

As can be seen the transducer output has component at IF band, which is then filtered and fed in to output transducer generating current $i_{z2} = V_{P2}\,\dfrac{\partial C_2}{\partial z}\,\dfrac{\partial z}{\partial t}$. Terms two to five of force equation can cause interferences in mixer applications if either v_{RF} or v_{LO} have components with frequencies near $1/2\,\omega_{IF}$ or ω_{IF}, which are usually removed with filters before the mixer. [44]

Reducing large voltage levels demands setting the electrode-to-resonator gap to about 20 nm, however if larger impedances are allowed the gap does not have to be so small and a larger gap might be preferred for dynamic range reasons. This would be the case when MEMS and electronics are integrated together to reduce node capacitances also bringing other performance improvements. [44]

3 Model and methods

The electrical equivalent circuits enable the use of circuit simulators to investigate coupled MEMS resonators. With circuit simulators, it is easy to take into account the external circuit used to drive, bias and read the output of the MEMS system. Qualitative result about the MEMS system are acquirable even in a complex non-linear system without simulators. Circuit simulators are optimized solving and especially providing quantitative results for the complex electromechanical systems in question here. This work was done using mainly Aplac, but the multi-output part and chains with Q values 400-1000 were done with ngspice-26 using translated Aplac models.

3.1 Electrical equivalent circuits

Zhu *et al.* and Liwei Lin *et al.* report that the main part of the system consists of micromechanical resonators, which can be modeled with series RLC-resonator circuits analogous to the lumped element mechanical model. The electrical equivalent is possible due the formal similarities between the differential equations for mechanical and electrical systems. Analogies exists between electrical and mechanical quantities. [47, 27]

In the RLC circuit, displacement is modeled with capacitor charge, restoring force with capacitor voltage, mass with inductance and damping with resistance. Nonlinearities are taken into account though charge controlled capacitance. The coupling between resonators is realized with capacitor C_{sij} and transducers are modeled with transformers. [47, 27]

The values of components are determined with following formulas

$$L_i = M_i\eta^2, C_i = \frac{1}{k_i\eta^2},\ R_i = D_i\eta^2,\ C_{sij} = \frac{1}{k_{sij}\eta^2},\ \eta = \frac{1}{V_{Pi}\left(\frac{\partial C}{\partial x}\right)_i},$$

where V_{Pi} is the bias voltage and the nonlinear coupling terms use the same formula than the linear term. These formulas are not important for qualitative investigation of the circuit. [47, 27]

Zhu *et al.* and Veijola state that in Aplac, MEMS component modeling is based on voltage controlled current sources as force is equivalent current and both displacement and velocity to voltage. Damping is again linked to conductance, but mass is now described with capacitance. The resonator is modeled as four noded device with two separate parts. The model of capacitive transducer has six nodes, a variable capacitor for the gap and current source for forces generated by the device. Generally the RLC-model is considered preferable over the current source variant. [47, 41]

3.1.1 NormalTransducer

The Aplac model named as NormalTransducer describes a plate capacitor with movable rectangular plates, which have dimensions w and l, the gap height (h) is divided into a static component d and the dynamic part z depending on voltage.

The equation for capacitance is the following $C = \dfrac{\varepsilon_r \varepsilon_0 lw}{h}$, $h = d + z$ and for the electrostatic force

$$F_{el} = -a_F \frac{u_c^2}{2} \frac{\partial C}{\partial h} = a_F \frac{u_c^2}{2} \frac{\varepsilon_r \varepsilon_0 lw}{h^2}, \tag{31}$$

where a_F is a force scaling coefficient with default value 1, which good for gap dimensions in order of micrometers.

According the Aplac manual, in the practical implementation, the gap height relation is divided into three zones depending whether the height is above the force and capacitance saturation starting point (h_{min}), between zero and h_{min} or negative, the corresponding equations are

$$h,\ h = \frac{(h')^2 + h_{min}^2}{2h_{min}},\ h = \frac{h_{min}}{2}, \tag{32}$$

where $h' = d + au_z, h_{min} = dMGAP$, a is a scaling coefficient with default value of $1\,\mu\mathrm{m\,V^{-1}}$ and $MGAP$ is a gap height specifier with default value of 0.05. However, pull-in likely becomes issues before h_{min} is reached. The capacitance and force equations are following

$$\begin{aligned} &q = Cu_c,\ \frac{\partial q}{\partial u_z} = u_c \frac{\partial C}{\partial h} \frac{\partial h}{\partial u_z},\ i_{el} = -a_F \frac{u_c^2}{2} \frac{\partial C}{\partial h},\ \frac{\partial i_{el}}{\partial u_c} = -a_F u_c \frac{\partial C}{\partial h}, \\ &\frac{\partial i_{el}}{\partial u_z} = -a_F \frac{u_c^2}{2} \frac{\partial^2 C}{\partial h^2} \frac{\partial h}{\partial u_z},\ \frac{\partial^2 C}{\partial h^2} = \frac{2\varepsilon_r \varepsilon_0 lw}{h^3} \text{ and } \frac{\partial h}{\partial u_z} \end{aligned} \tag{33}$$

is also piecewise defined with three zones that have following values a, $a\dfrac{h'}{h_{min}}$, 0. The electrical equivalent circuit is shown in Figure 9. [10]

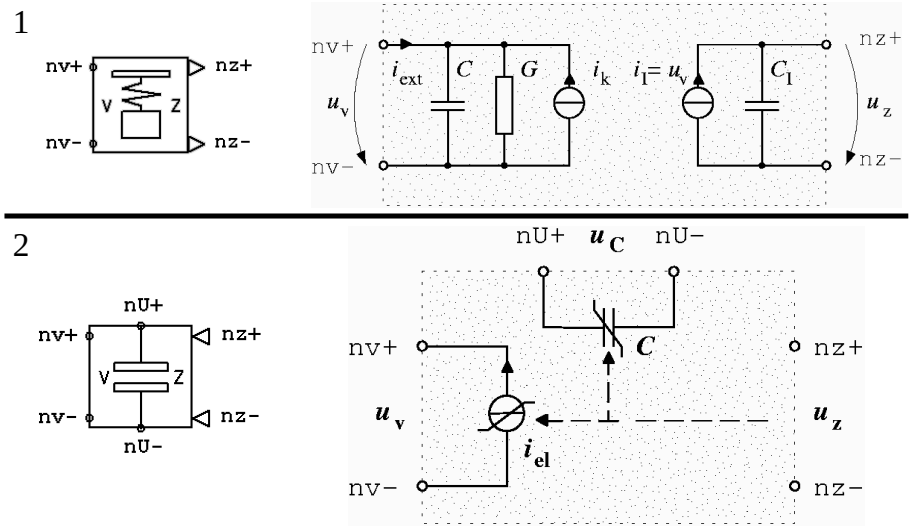

Figure 9: The electrical equivalent circuits of Aplac models LinearResonator (1) and NormalTransducer (2). The figure contains also the circuit symbols for both models. Source: Aplac manual.[10]

The manual also states that effects due the fringe capacitances can be ignored if h is much smaller than l or w. Perforation holes would reduce gas damping but reduce the capacitance and the electrostatic force. An additional isolating layer in the gap on electrode is described as capacitor in series with the variable one, the gap is between surface of the isolating layer and the plain electrode.

If the surface of the isolating layer is rough, then the surface height distribution has to be taken into account and three different regions with different expressions for capacitance exist. The regions are no contact, partial contact and full contact. In no contact and partial contact regions the expressions contain logarithms of terms dependent on the range of height distribution, layer thickness, height and the ratio of relative permittivities of the isolating layer to the gap.

3.1.2 LinearResonator

LinearResonator is an Aplac model describing one-dimensional mass-spring system with damping and possible quadratic and cubic nonlinearities. If the system is not inductively or capacitively loaded, then resonance frequency (f_r), spring constant (k_r) and mass (m) are tied together with following equation $f_r = \sqrt{k_r/m}/(2\pi)$, which means that two of them have to be given as parameters, and the quality factor (Q) is following $Q = \sqrt{k_r m}/\zeta$, where ζ is the loss coefficient. The electrical equivalent circuit is shown in Figure 9, where

$$i_k = aku_z + k_2a^2u_z^2 + k_3a^3u_z^3, G = \zeta \tag{34}$$

and $C_I = 1\,\mu\text{F}$ as default. [10]

3.2 Model

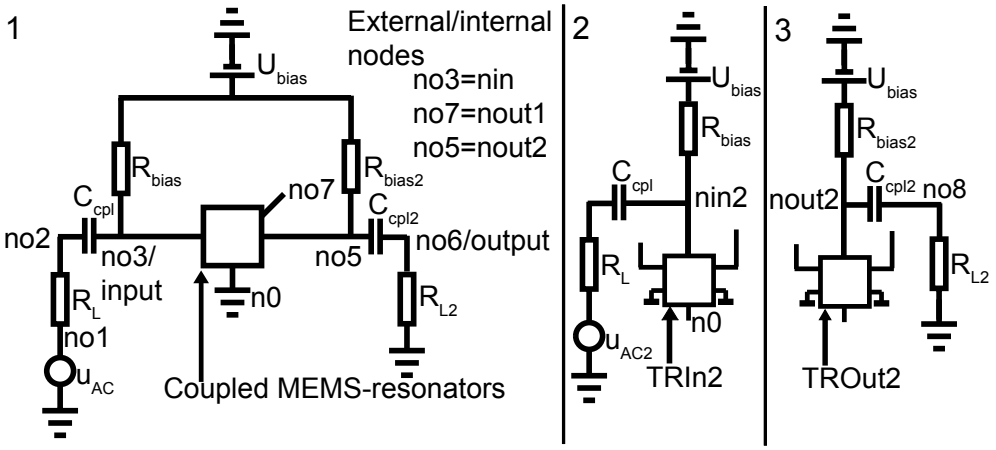

Figure 10: The circuit diagrams of the external circuit (1), the extra input block (2) and the extra output block (3). The nodes are also marked into the diagrams.

The model consists of AC source as input signal, DC bias source with bias resistors, DC separation capacitors (C_{cpl}), output impedance and the resonator network. R_L

is the internal resistance of the AC source. Circuit diagram of the system with its nodes is shown in Figure 10.

The location of the input(s) is on left side and the outputs on right side of the network. Both input and output require a transducer for conversion between mechanical and electrical domains. The possible extra inputs are each a block containing transducer, resistors, capacitor, AC and DC source (Figure 10). The extra output block contains transducer, resistors, capacitor and DC source. The position(s) of these block(s) is(are) important. The nU- node of each transducer is connected to n0 node, which is then subsequently grounded.

The resonator network consisting of the resonators and springs is inserted into the external circuit as a custom component, which also contains the transducers and the possible extra inputs. This component is defined with the DefModel−EndModel structure where the network is generated and then used as any other component.

3.2.1 Topologies

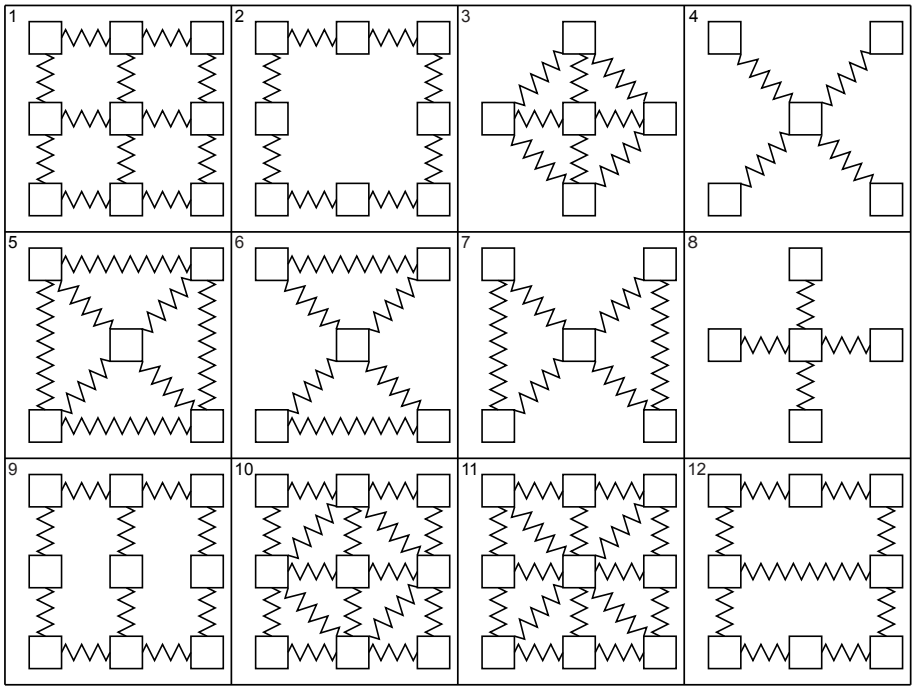

Figure 11: Examples of possible topologies, which are numbered for later referencing.

Here topology means how resonators are positioned and connected in the array, the possibilities being nearly limitless. If the first and last resonator are directly connected to each other and all other others are contained within this loop the topology is known as closed, otherwise it is open.

In addition of connections to any direction, bridging connecting non-adjacent resonators can be used. Only limiting factors for topology are used resonator type and practical considerations regarding what can be implemented. In mechanical

coupling, the springs can not cross each other unless they are stacked with large enough horizontal gap, which is extremely problematic to realize. Topology also determines the length of the shortest path from input to output. Figure 11 shows twelve examples of possible topologies.

3.2.2 Resonator network

The nv- and nz- nodes of LinearResonator components, which are arranged as a square grid with vertical and horizontal coupling springs as shown in Figure 12, modeling the resonators are grounded. Springs are modeled with LinearResonator components whose mass is set to zero, which also leads to loss coefficient value of zero.

The resonators and springs that connect them are generated with nested for loops requiring the use of COMPONENTVECTOR and NODEVECTOR structures to store them. If statements can be used to prevent generation of couplings that can not exist in the system, disable some of the connections altering the topology or allowing randomization. If one wants each resonator or spring have different parameters, the parameters in question must be in in a vector from where the value is read when needed. Parameters kv and kp are used to change horizontal and vertical coupling strengths respectively by multiplying the spring constants.

The topologies were discussed in Chapter 3.2.1, which also contains Figure 11 on page 38 from where one can check what topology the numbers used to refer them correspond.

The optional randomization is implemented though a randomization factor $(1+st)$, where st is a random number meeting condition $|st| < 2.5sigma$ from normal distribution with zero mean and standard deviation $sigma$. A repeat-until-loop is used to generate st by using NRan(0,$sigma$) command until the previously mentioned stop criteria is met. The default resonance frequency is multiplied with $(1 + st)$ and saved to a vector for use. The for-loop generating the resonators reads the resonance frequency of each resonator from the vector where they were saved.

A diagram of the resonator network for topology one are shown in Figure 12. The network size parameters M and N are the number of resonators in the horizontal and vertical directions in the edges for rectangular topologies. By giving individual resonators matrix style coordinates (i,j), the location of input one is (1,1) and output (M,N) in the topology one networks.

In the topologies 4–7 the resonator and node numbering start with topology one network and the extra resonators and nodes in the topologies 4–7 get numbers after the main part and the coordinates of the output become $(2M - 1,2N - 1)$ (Figure 12). As these networks contain an extra resonator grid within the topology one grid, marking $MxN\_M - 1xN - 1$ is used to describe is arrangement.

3.3 Translation for ngspice

Ngspice is open source circuit simulator. Requirement for a DC path to ground from every node was handled with .option rshunt=value line, this value has to be

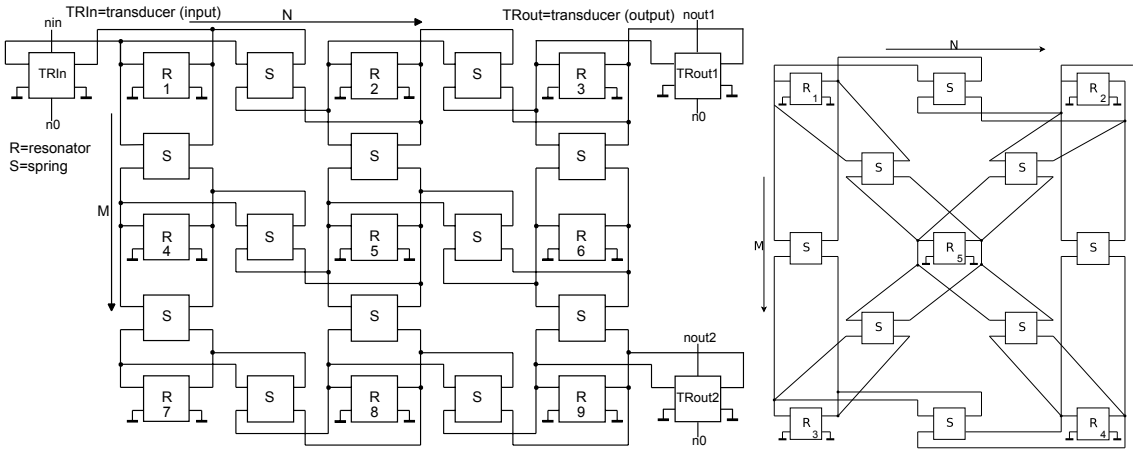

Figure 12: Electrical equivalent circuit diagram of the topology one resonator network (on left) and a block from topology five network (on right). The internal nodes of the resonator circuit are numbered with resonator numbers, which are also marked into the diagram. The nv+ and nz+ nodes of the transducer are connected to nv+ and nz+ nodes of the nearest resonator as shown above. The nv- and nz- nodes of resonators and transducers are grounded. The nv+/- and nz+/- nodes of springs are connected to different resonators as shown in here.

orders of magnitude larger than the largest resistor in the circuit and at least in the gigaohm range. As ngspice does not allow components and nodes placed in vectors a Perl script was used to generate the required netlists, run the simulation and then clean the resulting text file by using sed and awk. The translation was done from descriptions given in the Aplac manual. The resulting netlists can be used used with small modifications in other Spice variants.

The models were placed to parametrized subcircuits. The translated NormalTransducer model currently does not contain all features and limitations of original model, however lacking features were not used in the Aplac simulations and displacement stays within the first region specified in the model documentation. As ngspice does not have a conductance component, a resistor with $resistance = 1/conductance$ has to be used. The ngspice manual recommends replacing zero conductance with very large resistor.

The required subcircuits are given in the Attachment B and use non-linear behavioral source (B-source) as VCCS. Variable capacitor in NormalTransducer model was realized though variable change with dependent source and linear capacitor, the current though linear capacitance was then fed back into the circuit.

For transient simulation with specified pulse length both B-source and normal voltage source as sine wave are required, see Attachment B for the main simulation file containing the external circuit and simulation commands. The simulation was run in bulk mode so analysis type was specified with .tran or .ac lines followed with .print line for printing the results and specifying what values are saved.

3.4 Methods

The simulation file containing the model can be build based on diagrams in Figures 10-12, which show how the circuit elements are connected to each other and default values of the components. Sweep-command was used to define the simulation type by stating the variable (TIME,FREQ) to be swept along its range and division. In this work both time and frequency step were constant. Transient analysis mode 0 was used.

Due the extremely large number of simulations required batch files were used change desired variables before launching another simulation. The major changes such as topology, enabling the optional randomization, amount of extra inputs were done by manually chancing the required parameters. The results were saved into text files with automatically generated filenames based on the system parameters to ensure that it contained all information about the parameters.

The acquired data was then plotted and/or analyzed with Matlab using scripts that take into account the systematic file naming scheme and generate required titles, correct axis sizes, division and labeling, legends and saving low resolution bitmap version of the figure for viewing and visual analysis. To ease comparisons multiple graphs were drawn into same figure.

3.4.1 Circuit simulation

The circuit equations are usually differential-algebraic equations, where some unknowns have no derivatives in the equations. Circuit simulator uses nodal analysis method to solve voltages on the circuit and while some symbolic ones exist their usability is limited due the nonlinearities preventing closed form solutions or even if such solutions exists they are too complex forcing one to resort numerical methods.

In the nodal analysis voltages of each node relative to the reference node (ground) is determined by using Kirchoff's current laws, which state that the sum of currents at node is zero, to generate equations for the node voltages. After solving the equations the branch currents can be determined by using voltage-current relationships of the individual components.

Circuit simulators solve the resulting equation system by using Gaussian method for linear case. The nonlinear systems can have multiple solutions and generally combining known solutions into new ones is not possible. Matrices containing mostly non-zero elements represent cases where most of elements are coupled to each other instead of only to nearest neighbors, which results matrix with mostly zero elements. When most of elements in the matrices containing the circuit equations are zero solving them with appropriate algorithms takes less computational resources than using standard algorithms.

Both transient and AC analysis are preceded by DC analysis. In the AC analysis, which is performed in the frequency domain and uses complex voltages and impedances, only small signal behavior can be investigated and the system is linearized at the operating point before solving it. The output magnitude scales linearly with the input magnitude due the linearization. [10]

Transient analysis gives information about time domain behavior in response to fast changes in the input and requires solving the nonlinear differential equation system describing the circuit without any additional approximations used in AC analysis.

The time step in transient analysis has to be small enough to capture the dynamics of the circuit. Initial estimate can be made based on frequencies and nonlinearities, but in the end one has to try different values to see when decreasing the step causes only minimal changes to the response. The signal can also be lost if the analysis time is not long enough. Decreasing the size of frequency step in the AC analysis does not affect the response.

4 Results

At first, what can be learned about the system with analytical methods is shown before moving to the simulations. Unless stated otherwise the simulated systems consist of identical resonators and couplings and all circuit parameters have default values. Then we look into chains, which are a special case of networks. The networks are looked much more closely than chains.

4.1 Analytical approach

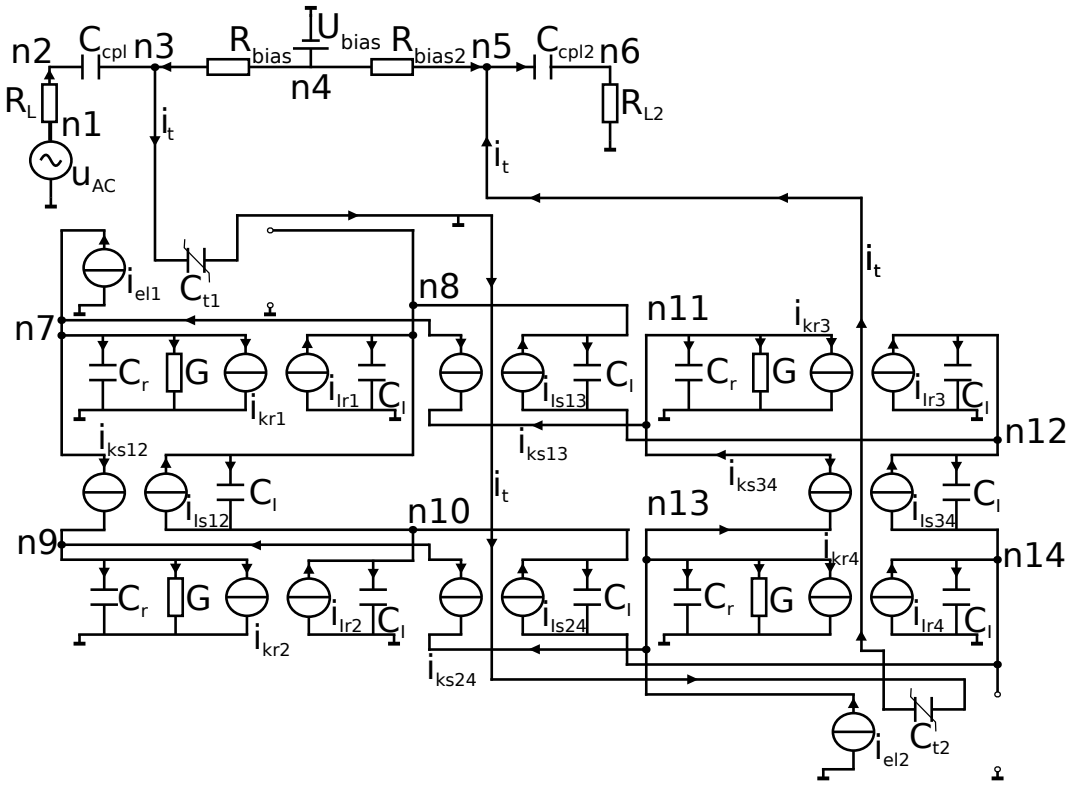

Figure 13: The circuit diagram of 2x2 resonator network by using electrical equivalent circuits. The node voltages are following: n1/u_{AC}, n2/V_2, n3/(U_{bias}+V_3), n4/U_{bias}, n5/(U_{bias}+V_5), n6/V_6, n7/u_{v1} , n8/u_{z1}, n9/u_{v2}, n10/u_{z2}, n11/u_{v3}, n12/u_{z3}, n13/u_{v4}, n14/u_{z4}.

By combining Figures 10, 9 and 12 one gets the circuit diagram for the electrical equivalent circuit of 2x2 network shown in Figure 13. Based on the diagram, the formulas of both capacitances C_t and currents of the current sources from Chapter 3, the current through capacitor $i = \frac{\mathrm{d}C(t)U(t)}{\mathrm{d}t}$ and Kirchoff's current law the circuit equations describing the behavior of 2x2 network can be generated. The current sources for the springs are following

$$i_{ksij} = (k_c\, a\, (U_{zj}(t) - U_{zi}(t)) + k_{c2}\, a^2\, (U_{zj}(t) - U_{zi}(t))^2 + k_{c3}\, a^3\, (U_{zj}(t) - U_{zi}(t))^3) \quad (35)$$

and $i_{Isij} = U_{vj}(t) - U_{vi}(t)$ for coupling between resonators i and j. This system can be solved only numerically. The nonlinearities arise from transducers and coupling springs.

Table 1 contains the default values of the components, transducer size parameters, spring constants, resonance frequencies and Q. The loss coefficient (ζ) and mass (m) are calculated with following formulas $\zeta = k_r/(2\pi f_r Q)$ and $m = k_r/(2\pi f_r)^2$. The level of input voltage was chosen so that the impact of the nonlinearities is minor. The previously generated circuit equations were verified by inserting the simulated response to them and checking at what precision the sum of currents on each node was zero. The answer as at least with a few parts of thousand.

Table 1: The default values of the circuit elements, the subscript c indicates coupling.

u_{AC}	1 V 0°	U_{bias}	30 V	w	10 µm	k_r	10 kN/m	Q	200
R_L	5 MΩ	R_{bias2}	5 MΩ	l	40 µm	k_c	800 N/m	ζ	7.9577 mg/s
C_{cpl}	100 nF	C_{cpl2}	100 nF	d	200 nm	k_{c2}	10 GN/m^2	m	255.30 ng
R_{bias}	5 MΩ	R_{L2}	5 MΩ	f_{res}	1 MHz	k_{c3}	2 EN/m^3		

The degree of nonlinearities can be reduced with following approximations

$$1/(d + au_z)^2 \approx (d - 2aU_z)/d^3,\ 1/(d + au_z) \approx (d - au_z)/d^2 \tag{36}$$

and

$$(U_{bias} + V_x(t))^2 \approx U_{bias}^2 + 2U_{bias}V_x(t)\ x = 3, 5, \tag{37}$$

which are valid when $u_z \ll d$ and $V_x(t) \ll U_{bias}$. If the second term in the previous approximations is small enough, then as a further approximation it can be also ignored. The linear approximation of the transducer capacitance differs from the true value at most a few percent when the displacement is below 20 nm as expected and is 160–195 fF. For at most 70 nm displacement the capacitance is within range 130–270 fF.

The formula given in Chapter 3.1.1 indicates the transducer current i_{el1} is the largest when V_3 is large and the displacement $z1$ negative with large absolute value. The areas where the current is large are small but on other hand on the small absolute values of V_3 the current is small and changes only a little in large areas.

The total amount of spring forces affecting resonator n consists of the couplings from resonator n to its neighboring resonators and the spring force of the resonator n. As the spring forces are at most third degree polynomials the total force can be expected to be well behaved.

As the system is linear in regards to the derivatives it can be easily transformed in to $\mathbf{f}' = \mathbf{f}(\mathbf{x}, t)$ format, which is required by numerical solvers and allows checking the dependencies of the derivatives. The direct dependencies, meaning that they appear in the formula of the derivative in question, from the system parameters and node voltages are limited though the effects of all others are accounted indirectly though the node voltages in the expression.

The only dependencies from the external circuit to the time derivatives of U_{zi} are U_{bias}, V_3 and V_5 though currents i_{el1} and i_{el2}, the rest of required parameters are spring constants, scaling coefficients, masses, losses and transducer dimensions. The currents from the transducer model affect directly only $U'_{z1}(t)$ and $U'_{z4}(t)$. On other hand $V'_i(t)$ depend on transducer dimensions, circuit parameters, node voltages V_i, scaling coefficients, the internal node voltages of the equivalent circuit and the AC source.

4.1.1 Coupling strength

As can be seen from Figure 14 the impact of the nonlinearities in the coupling becomes significant only after the displacement is large enough. The nonlinear spring force with both second and third degree nonlinearities is slightly smaller than linear if $-k_{c2}/k_{c3} < x < 0$ ($-5\,\mathrm{nm}$) and becomes 5 % larger when

$$x > \frac{\sqrt{25k_c k_{c3} + 125k_{c2}^2} - 5k_{c2}}{10k_{c3}},\ x < -\frac{\sqrt{25k_c k_{c3} + 125k_{c2}^2} + 5k_{c2}}{10k_{c3}} \tag{38}$$

($-7.6\,\mathrm{nm}$, $2.6\,\mathrm{nm}$). The spring force of the nonlinear coupling is stronger than the spring force of the resonator when

$$x < -\frac{\sqrt{\left(4k_r - 4k_c\right)k_{c3} + {k_{c2}}^2} + k_{c2}}{2k_{c3}} \text{ and } x > \frac{\sqrt{\left(4k_r - 4k_c\right)k_{c3} + {k_{c2}}^2} - k_{c2}}{2k_{c3}}, \tag{39}$$

whose numerical values are approximately $-70\,\mathrm{nm}$ and $65\,\mathrm{nm}$ respectively.

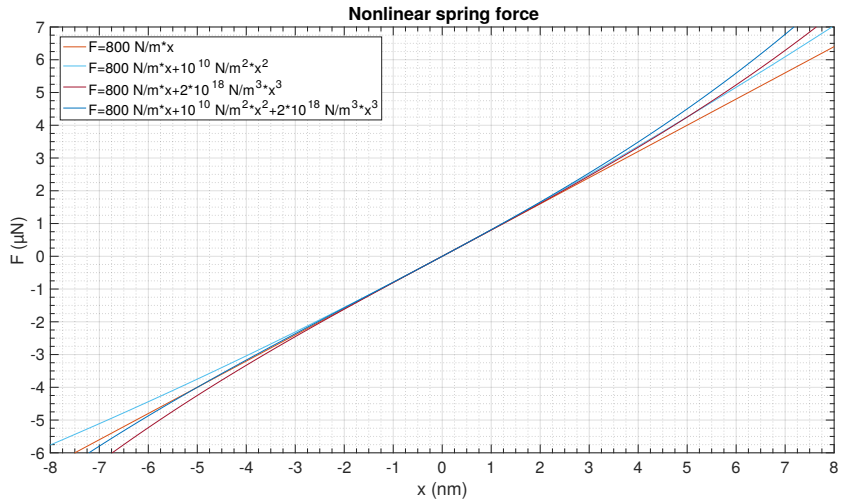

Figure 14: Impact of nonlinearities to the coupling strength. The differences in spring force become evident as the displacement increases. In the fully nonlinear case the spring force is close to linear spring force in much larger area than it would be if only either of nonlinear terms is taken into account.

4.1.2 Resonator chain

The solutions of equations of motion of one, two and three element resonator chains show how the response evolves as the resonator count increases, the equations are given below. Here amp is the forcing amplitude and ω is the angular frequency of the forcing. It is assumed that the system is at rest in the beginning. The full solutions are given in Attachment A.

One resonator:

$$m\,z1''(t) + \zeta\,z1'(t) + k_r\,z1(t) = amp\,\sin(\omega t). \tag{40}$$

Two resonator chain:

$$\begin{aligned} &m\,z1''(t) + \zeta\,z1'(t) + k_r\,z1(t) + k_c\,(z1(t) - z2(t)) = amp\,\sin(\omega t) \\ &m\,z2''(t) + \zeta\,z2'(t) + k_r\,z2(t) - k_c\,(z1(t) - z2(t)) = 0. \end{aligned} \tag{41}$$

Three resonator chain:

$$\begin{aligned} &m\,z1''(t) + \zeta\,z1'(t) + k_r\,z1(t) + k_c\,(z1(t) - z2(t)) = amp\,\sin(\omega t) \\ &m\,z2''(t) + \zeta\,z2'(t) + k_r\,z2(t) - k_c\,(z1(t) - z2(t)) + k_c\,(z2(t) - z3(t)) = 0 \\ &m\,z3''(t) + \zeta\,z3'(t) + k_r\,z3(t) - k_c\,(z2(t) - z3(t)) = 0. \end{aligned} \tag{42}$$

The steady state solution is following form $a1(\omega)\,\sin(\omega t) + a2(\omega)\,\cos(\omega t)$, which can be written as $c(\omega)\,\sin(\omega t + \varphi(\omega))$ where

$$c = \sqrt{a1^2 + a2^2} \text{ and } \varphi = \begin{cases} 2\arctan\left(\frac{a2}{\sqrt{a1^2+a2^2}+a1}\right) & \text{if } a1 > 0 \text{ or } a2 \neq 0, \\ \pi & \text{if } a1 < 0 \text{ and } a2 = 0, \\ \text{undefined} & \text{if } a1 = 0 \text{ and } a2 = 0. \end{cases} \tag{43}$$

The required parameter values are given in the Table 1 on page 44. In all three cases one eigenfrequency is

$$\frac{\sqrt{4k_r m - \zeta^2}}{2m\,2\pi} \approx 0.999\,997\,\text{MHz}.$$

. In two resonator chain the second eigenfrequency is

$$\frac{\sqrt{(4k_r + 8k_c)m - \zeta^2}}{2m\,2\pi} \approx 1.077\,030\,\text{MHz}$$

and in three resonator chain the additional eigenfrequencies are

$$\frac{\sqrt{(4k_r + 4k_c)m - \zeta^2}}{2m\,2\pi} \approx 1.039\,23\,\text{MHz and } \frac{\sqrt{(4k_r + 12k_c)m - \zeta^2}}{2m\,2\pi} \approx 1.113\,55\,\text{MHz}.$$

The local maximums are quite close eigenfrequencies. The initial transient solutions consists of sum of exponentially decaying sine waves with eigenfrequencies. Their amplitudes and phases are different.

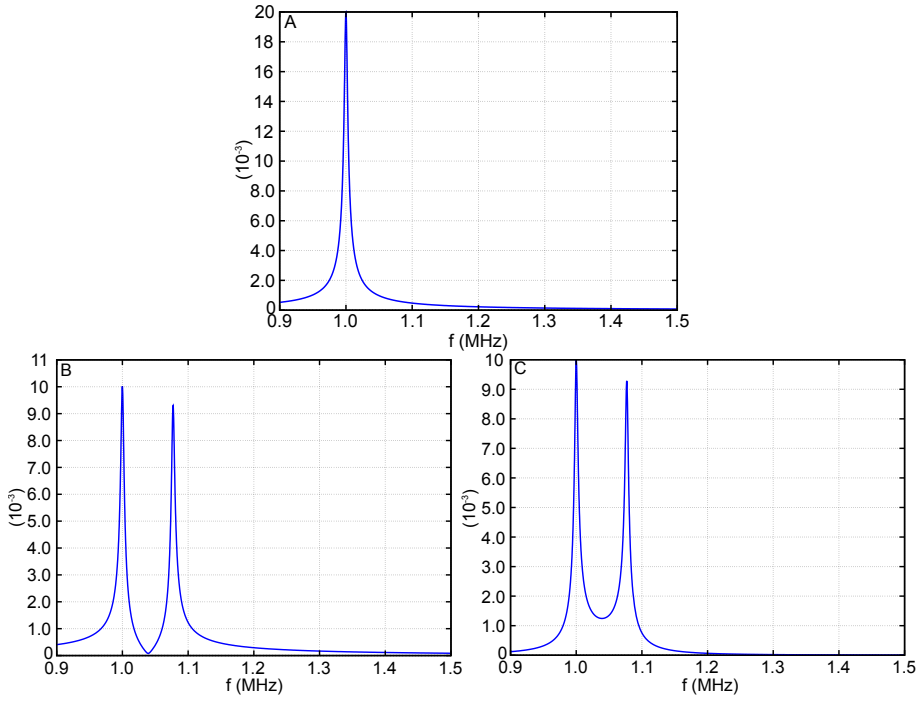

Figure 15: Steady state amplitude factors of single resonator (A) and resonators one (B) and two (C) of two element chain as function of the input frequency. The locations the extreme values in (B) and (C) differ from each other less than one hertz.

From Figures 15-16 one can see how the steady state frequency response develops as the length of chain increases from one to three resonators. In three resonator chain the phase difference between resonator one and three is about 180° at the position of the centermost resonance peak.

In two resonator chain the denominators of the steady state amplitudes are the same for both resonator eight degree polynomials of ω. The nominators are twelfth and eight degree polynomials of ω under square root. Only difference between in the initial transient responses of resonators one and two is the 180° phase shift in the second frequency component.

In three resonator chain the denominators of the steady state amplitudes are the same in resonators one and three, while the corresponding denominator for resonator two does not have the third component. The denominators are eight and twelfth degree polynomials of ω with mass, spring constant and loss coefficient as coefficients. The nominators are twentieth, eight and twelfth degree polynomials of ω under square root.

In initial transient response of three resonator chain the first frequency component is the same in all resonators, while resonator two does not have the second frequency component between resonators one and three the second components have 180° phase shift. In the first and third resonator the third frequency components is identical, wile in the second resonator its amplitude is half and it has 180° phase shift compared to the first and third resonator.

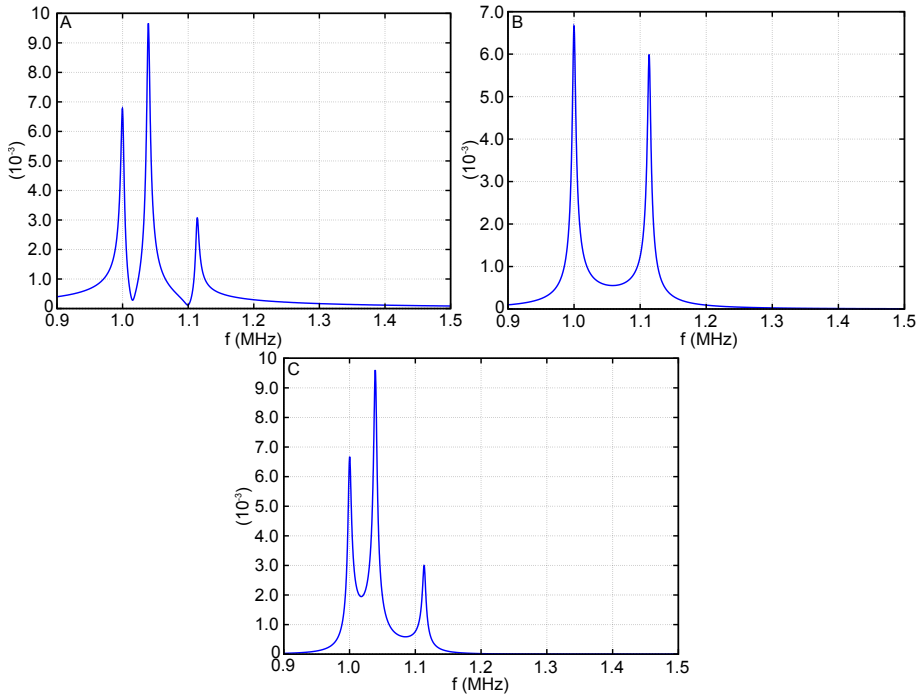

Figure 16: Steady state amplitude factors of resonators 1-3 (A to C) of three element chain as function of the input frequency. Note how the centermost resonator has only two resonance peaks due symmetries.

4.1.3 Two dimensional resonator network

$$\begin{array}{ccccc} & & r4 & & \\ & & | & & \\ r1 & — & r2 & — & r3 \\ & & | & & \\ & & r5 & & \end{array}$$

Equations of motion for two dimensional coupled resonators have the same format as in the one dimensional network though the functions for vibration are vectors. As an example, the function for resonator one written as the sum of x- and y-components: $\mathbf{z1} = x1\,\mathbf{i} + y1\,\mathbf{j}$. The equations for topology eight (Figure 11 on page 38) network with five resonators are following:

$$\begin{aligned} &m\,\mathbf{z1}''(t) + \zeta\,\mathbf{z1}'(t) + k_r\,\mathbf{z1}(t) + k_c\,(\mathbf{z1}(t) - \mathbf{z2}(t)) = \mathbf{amp}\,\sin(\omega t) \\ &m\,\mathbf{z2}''(t) + \zeta\,\mathbf{z2}'(t) + k_r\,\mathbf{z2}(t) - k_c\,(\mathbf{z1}(t) - \mathbf{z2}(t)) + k_c\,(\mathbf{z2}(t) - \mathbf{z3}(t)) + \\ &\qquad k_c\,(\mathbf{z2}(t) - \mathbf{z4}(t)) + k_c\,(\mathbf{z2}(t) - \mathbf{z5}(t)) = 0 \\ &m\,\mathbf{z3}''(t) + \zeta\,\mathbf{z3}'(t) + k_r\,\mathbf{z3}(t) - k_c\,(\mathbf{z2}(t) - \mathbf{z3}(t)) = 0 \\ &m\,\mathbf{z4}''(t) + \zeta\,\mathbf{z4}'(t) + k_r\,\mathbf{z4}(t) - k_c\,(\mathbf{z2}(t) - \mathbf{z4}(t)) = 0 \\ &m\,\mathbf{z5}''(t) + \zeta\,\mathbf{z5}'(t) + k_r\,\mathbf{z5}(t) - k_c\,(\mathbf{z2}(t) - \mathbf{z5}(t)) = 0, \end{aligned} \tag{44}$$

where ζ is the loss coefficient from Chapter 3. The resonators were numbered by following scheme: left (1), center (2), right (3), top (4) and bottom (5).

This system of equations is also valid for three dimensional network and is solved by forming separate equations for each direction. In two-dimensional network, the forcing happens in the angle θ in regard to x-axis and the amplitude components for x-(ax) and y-directions (ay) are following $ax = amp\,\sin(\theta)$ and $ay = amp\,\cos(\theta)$. The solutions consist of sum of transient and steady state solutions, which are given in Attachment A.

The equations of motion were solved symbolically and as initial condition it was assumed that the system is at rest when $t = 0$. It appears that resonators 3–5 vibrate completely identically due symmetries and resonator two has the simplest response as it contains only two transient frequencies. The vibration axis is determined by the direction of the forcing and is the same for all resonators.

The initial transient solution is a sum of three sine waves with different frequencies and phases decaying exponentially according following formula $e^{-\zeta\, t/(2\, m)}$. For parameter values given in the Table 1 on page 44 the transient has decayed below 50 %, 10 %, 5 % and 1 % of maximum at 45 µs, 147 µs, 191 µs and 294 µs respectively. If the forcing in the equation of motion is a pulse then second transient solution appears after the pulse again consisting exponentially decaying sum of sine waves with eigenfrequencies and the steady state solution dies.

The frequencies of the transient part are the eigenfrequencies of the system, which are following:

$$\frac{\sqrt{4k_r\, m - \zeta^2}}{2m\, 2\pi} \approx 0.999\,996\,\text{MHz},\ \frac{\sqrt{(k_c + k_r)\, 4\, m - \zeta^2}}{2m\, 2\pi} \approx 1.039\,227\,\text{MHz and}$$
$$\frac{\sqrt{(5\, k_c + k_r)\, 4\, m - \zeta^2}}{2m\, 2\pi} \approx 1.183\,213\,\text{MHz}.$$

The steady state solution is a phase shifted sine wave with frequency ω. Both the amplitude and phase have an explicit nonlinear dependency from the input frequency ω. The solutions for x- and y-directions differ from each other only by the linear amplitude scaling coefficient ax or ay respectively.

The steady state amplitude factors of resonators 1–3 as the function of input frequency are given in Figure 17 as resonators 3–5 behave identically due symmetry. The vibration amplitude is determined by multiplying the amplitude factor with the input amplitude. The nominator and denominator degrees are the same as for three resonator chain, but the response is about 100 kHz wider. Denominator is always positive.

The height of the first local maximum at slightly below 1.0 MHz in all three cases appears to be within 5 % of each other, the same applies to the third local maximums in the resonators one and three. Resonator two does not have a second local maximum but the other two maximums exist. The absence of the centermost resonance peak from resonator two is caused by the influence of other resonators canceling each other for the specific mode. The differences between the locations of the corresponding extreme values are at most a few hundred hertz. Figure 17 also demonstrates the bandpass behavior of the system with multiple passbands, whose width is about 10 kHz.

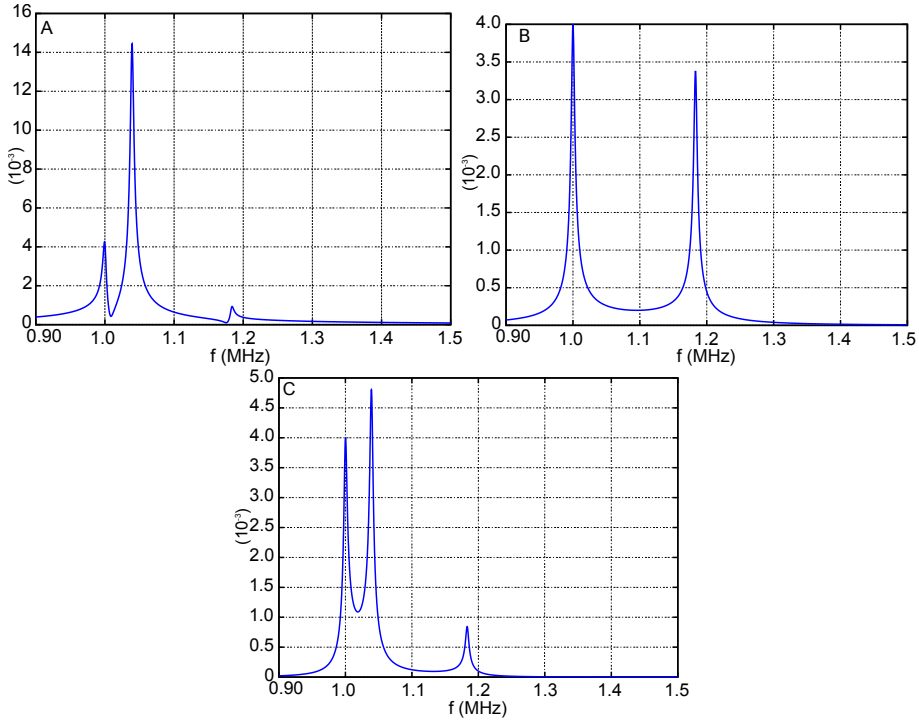

Figure 17: Steady state amplitude factors of resonators 1–3 (A to C) as function of the input frequency.

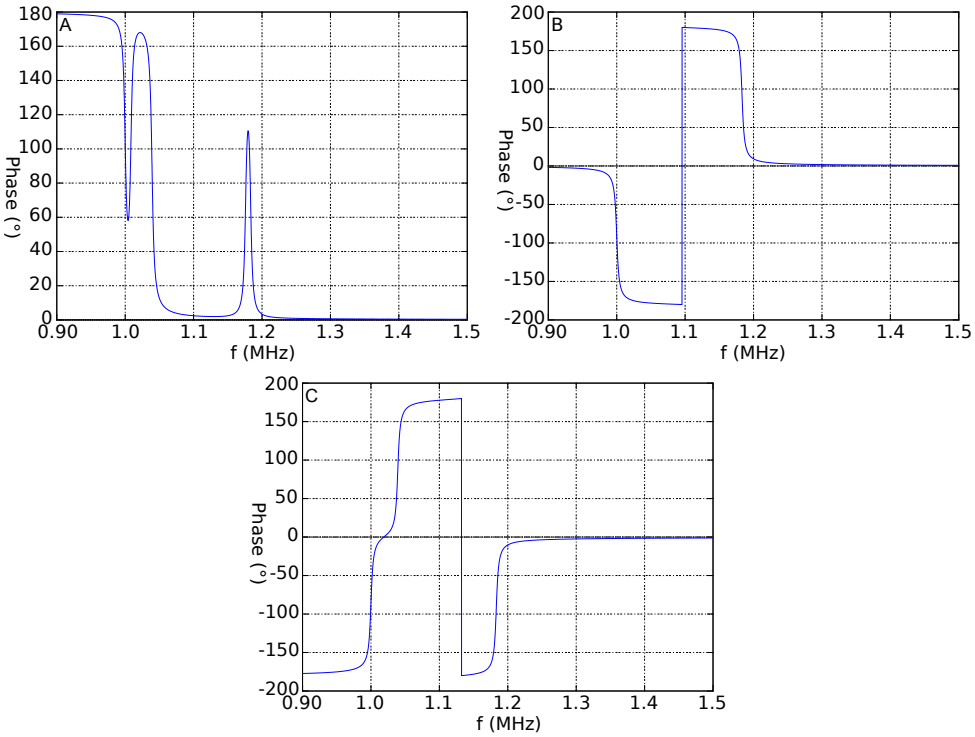

Figure 18: Steady state phases of resonators 1-3 (A to C) as function of the input frequency.

The Figure 18 shows the phases of the steady state frequency response. As with the amplitudes all features of the phases are limited about 250 kHz area beginning from slightly below one megahertz that consists of the passband. The rapid phase transitions correspond with the locations of the passbands and in the stopbands the changes are slow, usually only ten to twenty degrees.

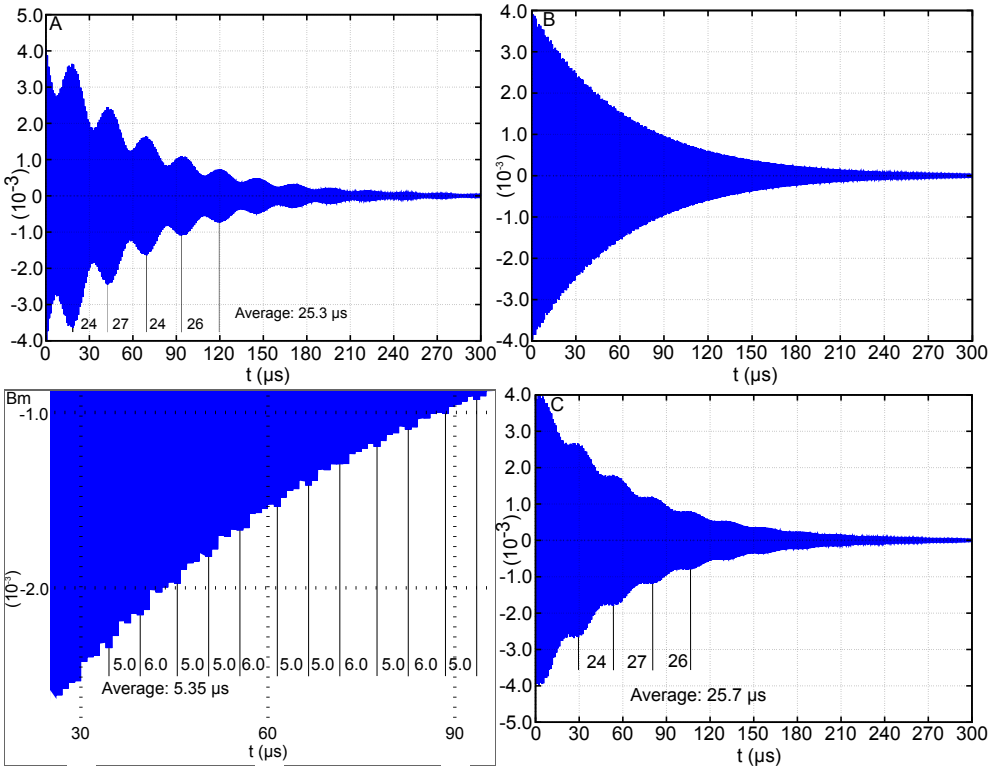

Figure 19: Initial transient response of resonators 1-3 (A to C) on the first eigenfrequency without the steady state component. The image marked with Bm is magnified area from the response of resonator two. The solid black horizontal lines within plots mark peaks of the envelopes and the numbers their distance in time. Average distance between peaks is also given.

The Figure 19 shows the transient response without the steady state component when the input frequency is the first eigenfrequency. The transient response of resonator two has only two frequency components as the centermost component is absent, while all other resonators have three. On some input frequencies at the beginning the amplitudes of the initial transient solution can exceed the steady state amplitude, but has dropped below it after at most tens of microseconds. The amplitudes of the intitial transient solutions also depend from input frequency.

The amplitudes of the first frequency component in different resonators are the same, while the amplitude of third frequency component of resonator two differs from all other resonators with a factor of four and 180° phase shift. The amplitude of the second frequency component of resonator three is one third of that of resonator one and has 180° phase shift. Differences between the transient responses are caused by the previously described differences in the amplitudes and the phases of the frequency

components.

In resonators one and three, the distance between the large peaks in the transient response correspond to the difference between the first and second eigenfrequency. In the transient response of resonator two, the difference between the first and third eigenfrequency corresponds with the distance between the large peaks visible in Figure 19. Table 2 lists the differences between eigenfrequencies and corresponding time values. In the response of resonator two only the second value is possible as it does not have the second frequency component. In responses of resonators one and three input frequency determines, which value is the most prominent.

Table 2: The difference between eigenfrequencies and corresponding time values, below them are locations of local maximums of frequency response and their differences for each resonator.

type/ frequencies	2nd-1st	3rd-1st	3rd-2nd
frequency difference	39.23 kHz	183.2 kHz	144.0 kHz
time value	25.49 µs	5.458 µs	6.945 µs

The response this particular network to 50 µs input pulse with frequency 1.08 MHz was calculated analytically for the resonator network and then simulated both without and with the external circuit. There is a difference of a few percent between amplitudes determined analytically and with simulator, which are caused by numerical methods used in the simulator. The responses with and without external circuit have significant differences due the reflections and electrostatic forces of transducers present in the full system. Figure 20 demonstrates this.

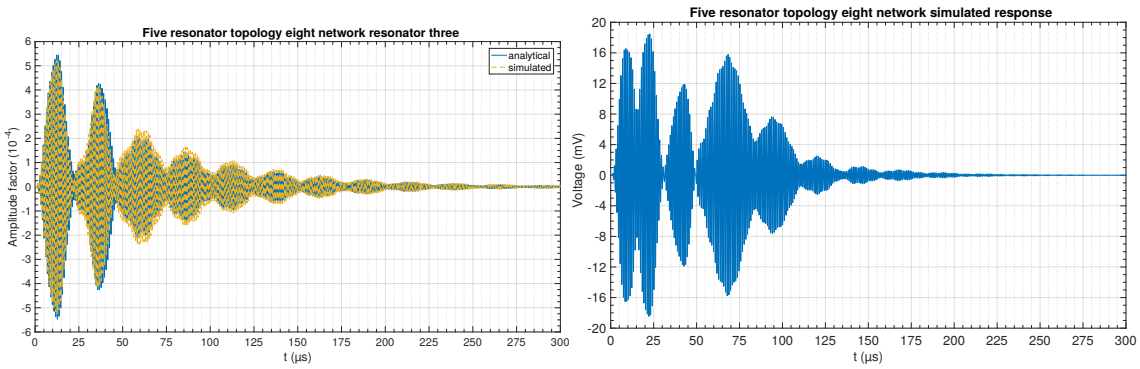

Figure 20: Response of resonator three in the bare resonator network (on left) and no6 node in full system with transducers and external circuit (on right). The response of resonator three was determined both analytically and with simulator, the difference in the amplitude is at most a few percent.

4.2 Chains

First $Mx1$ networks (chains) were investigated. For small M, the effects of individual resonators dominate Mag(Vac(f,no6)). Where Mag(Vac(f,no6)) means the magnitude

of AC voltage as a function of frequency at the no6 node. The number of resonances visible in Mag(Vac(f,no6)) is M for $M < 5$ after that they start to overlap each other (Figure 21).

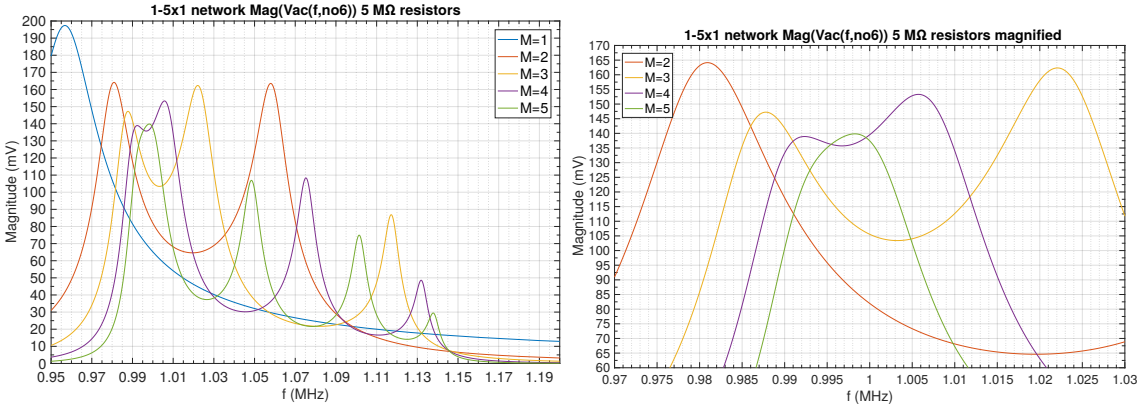

Figure 21: Mag(Vac(f,no6)) of the $1-5x1$ (on left) and magnified area of $1-5x1$ (on right) networks.

For chains, the shape of Mag(Vac(f,no6)) resembles a Gaussian skewed to the right but it contains rippling whose amplitude and width on frequency axis decreases as the chain is lengthened. The shape becomes fully developed only after $M = 50$. When $M = 50$ amplitude of this rippling is at maximum about ten percent of Mag(Vac(f,no6)) but in shorter chains there can be many tens of percent. Rippling is also visible on the input node but on much smaller scale. In Figure 22 Mag(Vac(f,no6)) of $16-20x1$ and $51-55x1$ networks is shown and both the rippling and its reduction as M increases can be clearly seen from the figure.

As M increases the beginning and the end of the band move towards the center. The decrease occurs in a zigzag pattern. This can be explained by assuming that the response of bandpass filters in series is a product of the responses of the individual filters.

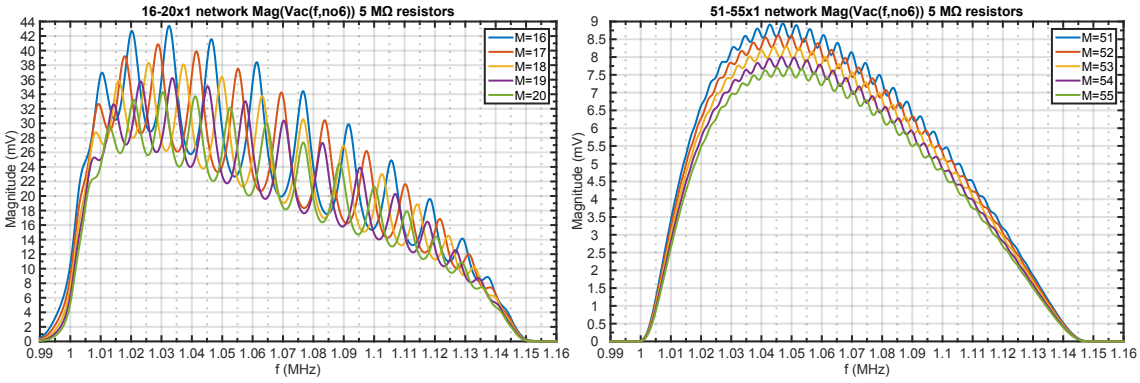

Figure 22: Rippling of Mag(Vac(f,no6)) in the $16-20x1$ (on left) and $51-55x1$ (on right) networks is clearly visible as is its decrease with increasing M.

The group delay function ripples around zero within the passband with the

amplitude of rippling decreasing and the end point moves to lower frequency as M increases. The non-constant group delay is problematic as it can cause distortions in the signal. Alastalo et al. state that this rippling is caused by impedance mismatch between the resonator network and the external circuit [2].

The amount of input signal that passes though the network can be increased with two different main approaches. The first is to modify network parameters to reduce the internal losses, increase the stiffness of coupling springs or improve transducers for better coupling. Increased stiffness causes Mag(Vac(f,no6)) to increase and widens the response from the end (Figure 23), these simulations were done with ngspice. Judge *et al.* state that the width of the passband is proportional to the coupling stiffness and the loss per resonator is inversely proportional to the coupling stiffness [19]. This means longer the chain is the increase of Mag(Vac(f,no6)) is larger for the same increase of coupling stiffness.

The second is to increase the amount of input entering the network by changing the values of the components of the external circuit and possibly adding some components. The values of the resistors R_{bias}, R_{bias2} and R_{L2} have significant impact on values and shape of the frequency response as currents though the bias resistors change chancing voltages across them.

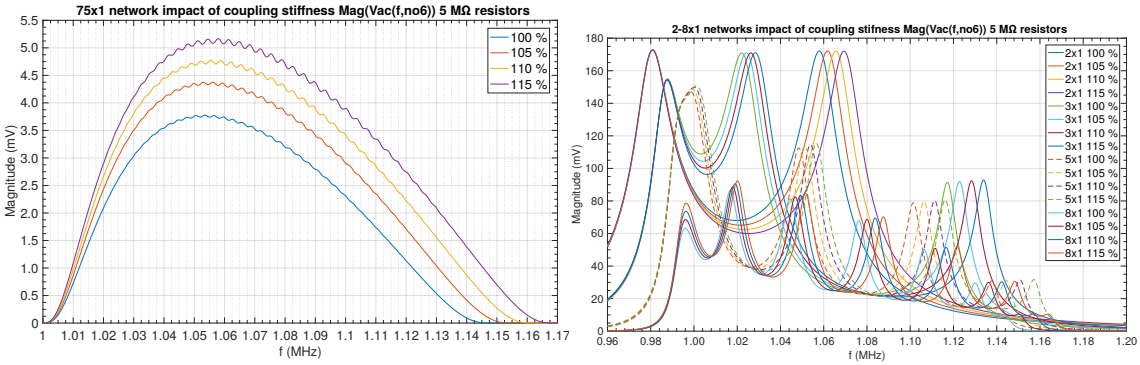

Figure 23: Impact of increasing coupling stiffness to Mag(Vac(f,no6)) of $75x1$ network (on left) and $2-8x1$ networks (on right) with 5 MΩ resistors. The legend tells the value of the new coupling stiffness compared to the original value.

4.2.1 Impact of Q

Also, losses of resonators can be reduced and thus increase magnitude at output by increasing Q but it causes more rippling to Mag(Vac(f,no6)). In longer networks, Q can be raised a few tens of percent without rippling becoming significant enough to make the system useless as filter as can be seen from Figure 24, where Mag(Vac(f,no6)) of $50x1$ network for Q values 200–500. The ripple and bandwidth increase with the Q and maximum of Mag(Vac(f,no6)) moves to lower frequency. As losses decrease bandwidth becomes closer to its ideal value determined by the coupling and anchoring stiffnesses of resonators. The losses decrease Mag(Vac(f,no6)) especially on the sides.

The group delay varies over larger area when resistances or Q are increased. The part after 1.01 MHz has nearly periodic oscillations with frequency dependent

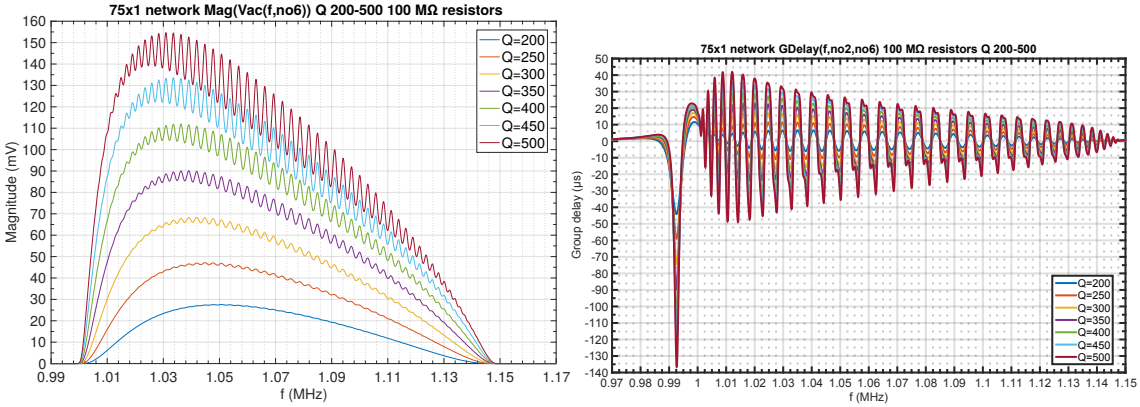

Figure 24: Impact of increasing Q to Mag(Vac(f,no6)) (on left) and GDelay(f,no2,no6) (on right, Group delay between no2 and n06 nodes as function of frequency) of $75x1$ network. The magnitude increase looks larger than it is in the beginning and the end of the passband due the low magnitude in there.

amplitude. The group delay has a strong dependence on Q. The average of the group delay is slightly below zero eventually going to zero after passband. As Alastalo *et al.* attribute the group delay ripple to the impedance mismatch the decrease of the resistive part of the impedance likely worsens the mismatch [2].

4.2.2 Transient responses

The output pulse can be divided in to multiple parts which are scaled down versions of each other and put together in descending order partially on top of each other. The maximum length of the chain is determined by the point when noise levels around the signal are approximately on the same level as the maximum within signal in transient analysis. The transient voltage is overall well behaved but in some places has local minimums that are much closer to the maximum than the expected location in negative side of U-axis. Vtran(t,no6) means the transient voltage on no6 node as function of time.

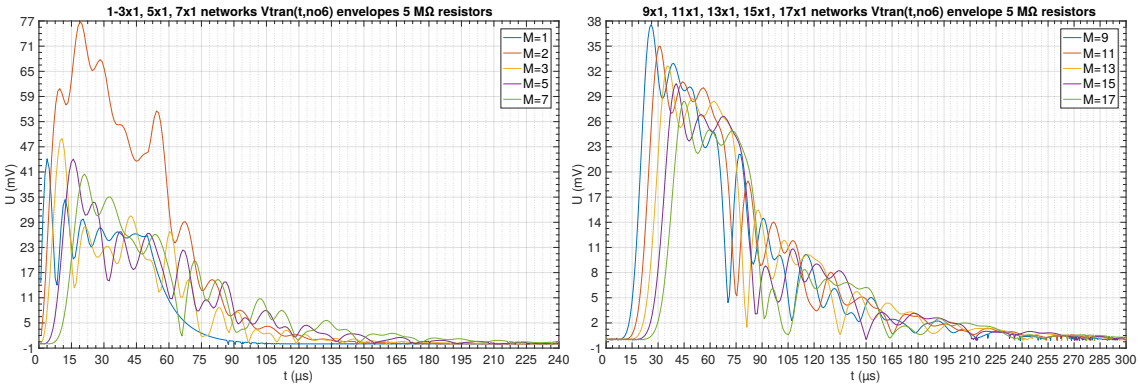

Figure 25: The envelopes of the transient responses of $1-3x1$, $5x1$, $7x1$ (on left) and $9x1$, $11x1$, $13x1$, $15x1$, $17x1$ (on right) networks on no6 node.

Singular peaks in the end of the pulse start to appear after $M = 142$ in increasing numbers and their size relative to the pulse increases with M. For smaller M, the amplitude of the pulse is large enough to mask these peaks, but on longer chains the distortion can be a severe problem. The non-distorted area of the signal is reduced mainly from the end as the low amplitude parts become masked by the noise. The size and location of peaks seem to be random and independent of network size. The fact these peaks do not exists in simulation results acquired with ngspice indicates that the issue is caused by Aplac's solvers. In Figure 25, the envelopes of the transient responses of ten networks between sizes $1 - 17x1$ are shown to demonstrate how the response develops as network size increases.

The location, where the amplitude of the pulse for the first time exceeds 50 % of the maximum, in the time axis is linearly dependent on M (Figure 26). This point is the beginning of the pulse. The delay per added resonator is about 2.15 µs, which is about 0.5 % larger than the value calculated for anchored chain at the center frequency. Increasing Q affects to delay per resonator only fraction of percent (Table 3).

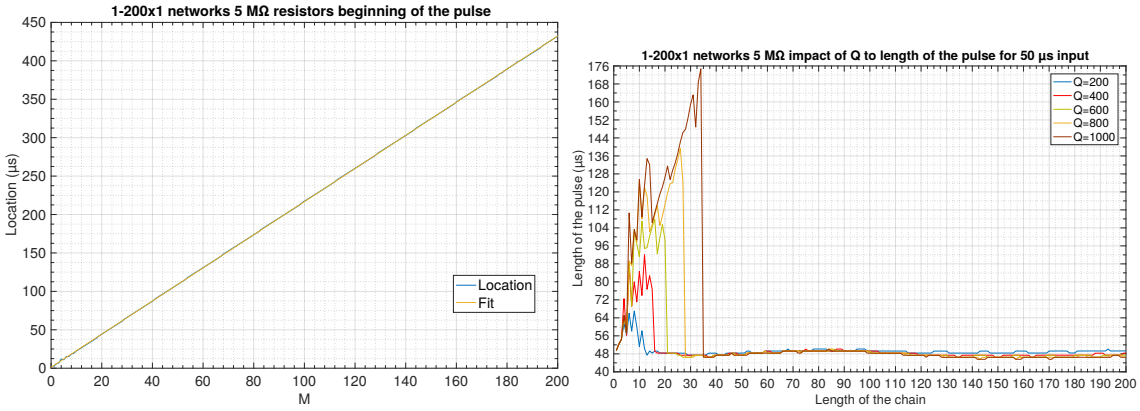

Figure 26: On left the beginning of the pulse as function of M and line fitted to the data in $1 - 200x1$ networks with $Q = 200$, the fit is excellent. On right the length of the pulse for Q values 200–1000, note the increasing pulse lengths as Q rises. Both are for 5 MΩ resistors.

The calculated value is acquired with formulas for group velocity given by Alastalo *et al.* in their article [2], when calculating the value one has to take into account the formulas are for resonator chain with two identical anchoring springs in parallel per resonator and therefore the value inserted into the formulas is only half of the true value. The formula takes only spring constants for coupling and anchoring springs and the resonator mass.

The rapid increase in the length of the pulse for small M as Q increases is caused by the fact the transient response decays slower for larger Q. The pulse reflects from transducers causing the secondary pulses after the main pulse, as the length of the chain increases these secondary pulses move further from the main pulse and their amplitude decreases faster than the main pulse due them going though the chain multiple times. The length of pulse is the difference between positions where the

amplitude of the pulse for the first and last time exceeds 50 % of the global maximum.

Table 3: The constants a and b for $a * M + b$ with different Q values. The values of a and b are in microseconds.

parameter/ Q	200	400	600	800	1000
a (5 MΩ)	2.1549	2.1598	2.1596	2.1602	2.1605
b (5 MΩ)	1.2917	1.4074	1.6394	1.6761	1.7022

4.2.3 Magnitude as function of M

There is a clear exponential dependency of form $a\,e^{b\,M}$ between the length of the chain and magnitude at each frequency due the same relative loss at each resonator in the chain, which multiplied with each other to reach the total loss of the chain. By adding more resonators to the chain the response approaches the rectangular shape of an ideal bandpass filter due the faster decrease of the magnitude outside passband than close to the maximum.

4.2.4 Full width half maximum

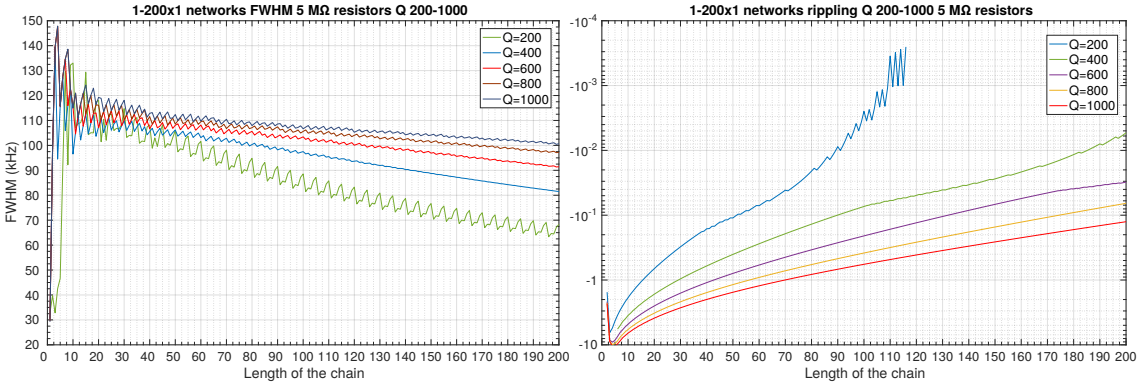

Figure 27: $FWHM$ (on left) and rippling (on right) of the chains as a function of M for five different Q values. Note the logarithmic scale on y-axis on right.

The full width half maximum ($FWHM$) of chains (Figure 27), which is the difference between points from right and left where the magnitude for the first time exceeds 50 % of the maximum, decreases non-linearly as M increases at decreasing rate. The impact of increasing Q to the $FWHM$ and rippling decreases as Q increases. The rippling is clearly visible when $M < 70$ and is zero for $M > 125$ for $Q = 200$, as Q increases the rippling never drops to zero. The size of ripple is determined by calculating ratio of every local maximum to the minimum next to it on right side and then selecting the largest of one. This number is then subtracted from one and the end result is used to characterize the strength of rippling.

$FWHM$ drops below 90 kHz at $M = 70$, 80 kHz at $M = 106$ and 70 kHz at $M = 153$ for $Q = 200$. The difference in the widths of passband for different Q values

increases with network size as expected. The dependency between M and $FWHM$ is very close to exponential as expected due the exponential dependence between magnitude and the length of the chain.

4.3 Networks

When topology one networks where $N > 1$ were investigated it was noted that Mag(Vac(f,no6)) chances significantly when N increases. Whereas Mag(Vac(f,no6)) of chains drops to close to zero at 1.15 MHz in networks the corresponding point can be somewhere closer to 1.3 MHz or at even higher frequency. Simulations were run for M values 9–13 and 20, N was between 2 and $M + 10$, also $2 - 201x2 - 7$ networks were looked at, but the investigation focused on the last two groups. The network size is marked as MxN, where M and N are the resonator counts in the lateral and horizontal directions respectively.

In Figure 28 frequency responses of $2x2$ and $3x1$ networks are compared to each other. The differences between chains and networks are caused by multiple different routes for the signal in the networks.

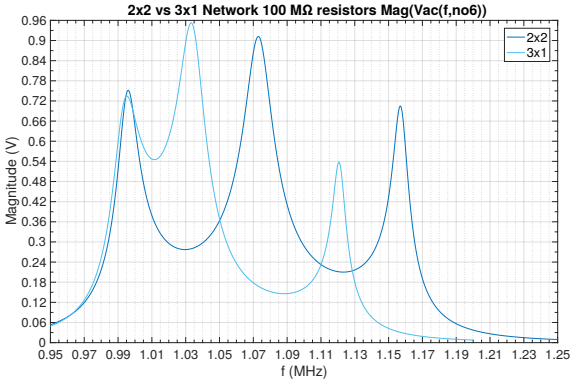

Figure 28: Mag(Vac(f,no6)) of $2x2$ and $3x1$ networks. The response of network is wider than the chain due the multiple routes for the signal.

Figure 29 shows the response develops as the network size increases from $2x2$ to $6x2$. The responses of the networks with identical weak couplings are complex because the bands overlap each other and therefore their usability is extremely limited (Figure 29). As is the case with $N = 1$ bandwidth decreases as the area where the magnitude is non-zero is narrowed from both ends as M increases.

If the resonator count remains constant and M decreases the magnitude levels rise due the shortened path for the signal. The change in the magnitude levels corresponds with exponential dependency from the length of the path. Group delay decreases somewhat.

The frequency where the magnitude becomes larger than 5 % of the global maximum increases with M nonlinearly. As N increases the frequency in question for $2xN$ network increases and the fast increasing part in the beginning diminishes. The beginning of the band also starts to move to higher frequencies in steps, which

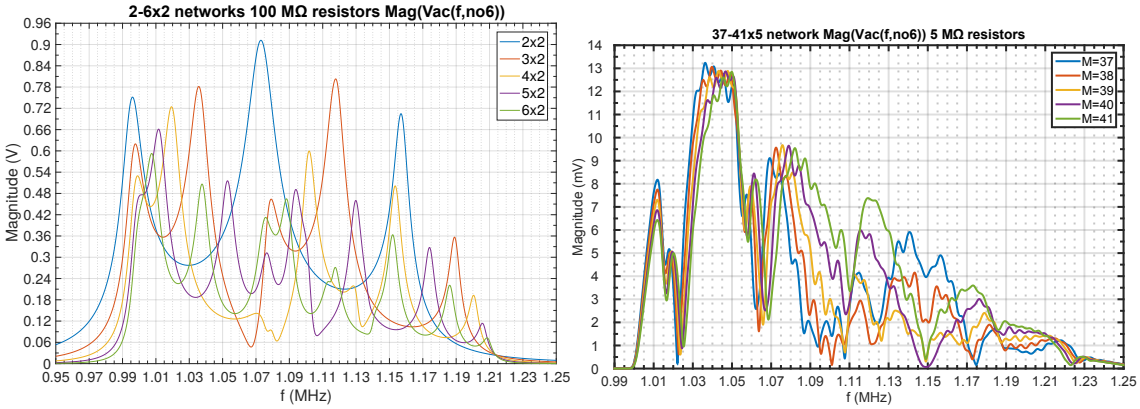

Figure 29: Mag(Vac(f,no6)) of $2-6x2$ (on left) and $37-45x5$ (on right) networks. The individual resonance peaks are clearly visible on left, though their number is smaller than the resonator count because some peaks overlap each other. On right the complexity of the response in larger network is visible.

consist of increasing part and a slight decrease from the local maximum with roughly the same widths.

4.3.1 Coupling strength

By increasing the coupling strength in horizontal direction leads to a response consisting of N bands with M subbands due the resonators in the strongly coupled direction acting effectively as a single resonator as stated in the Chapter 2.4.2, where an article by Judge *et al.* [19] is discussed. The subbands are visible as rippling, whose level decreases with increasing coupling strength. As the coupling strength increases eventually a point where the first band changes only minimally is reached. One application is to compensate for effects caused by nonidentical resonators.

The total passband width depends from coupling strength in both directions divided with the stiffness of the anchoring spring and increases if either or both are increased, the subband width is determined by the strength of the weak coupling. This means that if the strength of the weak coupling remains constant while increasing stiffness in strong coupling direction the subband separation increases.

Increasing strength of vertical or both coupling directions widens and raises the frequency response, but also leads to prominent subbands with varying height. In the former case the responses are higher than in the latter.

The bands move closer to each other as N increases as expected while coupling strength remains constant, eventually becoming partially overlapping, and increasing coupling strength has the opposite effect. The increase of separation of the bands becomes larger as one moves to higher frequencies and decreases as coupling strength is increased. The coupling strength required to fully separate the bands increases slightly faster than linear with N.

The rippling within the first band is at the same level than in the $Mx1$ networks and decreases as one moves to higher bands. Magnitude of higher bands increases

with N, and the maximum magnitude of the second band exceeds that of the first as N increases. As the amount of energy transmitted between the rows depends on how much each resonator in the row contributes to it it, the higher magnitude of the second band could be caused by the fact that oscillators with different phase do not contribute as much and cause the transmitted signals negate each other partially. Increased coupling strength decreases magnitudes of the higher bands and rippling in them, probably due the increase of the effective anchoring stiffness in the higher modes. The effect becomes larger as one moves to higher frequencies. The location of the maximum of the first band seems to be independent of N. Figure 30 demonstrates these claims.

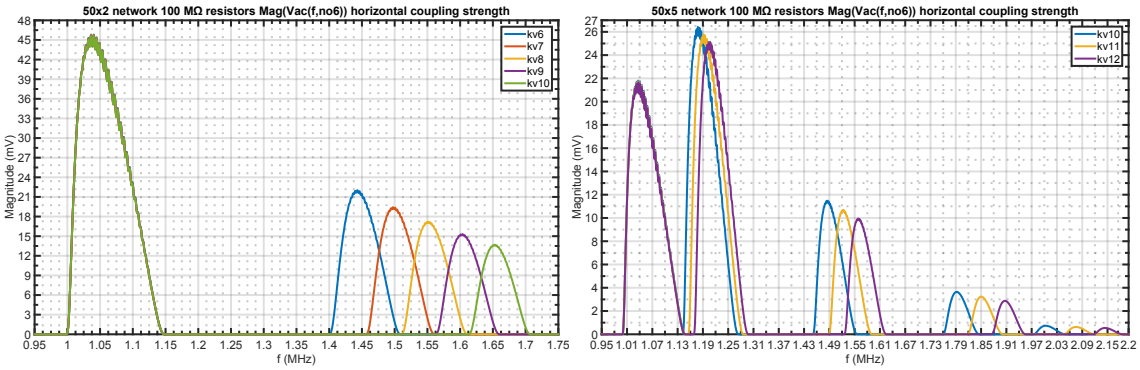

Figure 30: Impact of increased horizontal coupling strength to the magnitude on no6 node of $50x2$ (on left) and $50x5$ (on right) networks. The kvx marking in the legend means that coupling strength is x times the default value. Increased band separation and lower magnitude in the higher bands due higher coupling strength is clearly visible.

The magnitude decreases exponentially with M when the bands are clearly separate due the chain like behavior. The rate of decrease increases slightly with coupling strength when the N bands are separate. The minimum of the rate in the first band is the same than in the chains.

For $N > 2$ $FWHM$ of the first band seems to be independent of N and the higher bands widen as N increases. Increased coupling strength has only a minor impact to the width of the first band after its stabilization, but the higher bands become narrower with decreasing rate. The last band becomes narrower as N increases. The narrowing due the increased coupling strength happens from the end of the band. The bands shrink from both ends as M increases as expected due the chain like behavior.

4.3.2 Transient responses

In these simulations the input frequency for $2 - 201xN$ networks was changed only when N was changed. There is some rippling before and after the signal that can be considered as noise and its amplitude is independent of network size. The distortions become significant when their size is a significant fraction of the maximum amplitude

of the pulse. When signal levels are close to this noise the network has reached its maximum size. Even before the peaks within the signal become visible they start distorting edges of the pulse. As these distortions do not appear in data acquired with ngspice they are probably caused by somesort issues with Aplac's solvers.

Raising the three resistors to 100 MΩ increases the levels of distortions. The pulse itself becomes cleaner. In Figure 31, the first case of distortion within pulse ($92 - 96x2$ networks) and the transient response of $31x2$ network are shown.

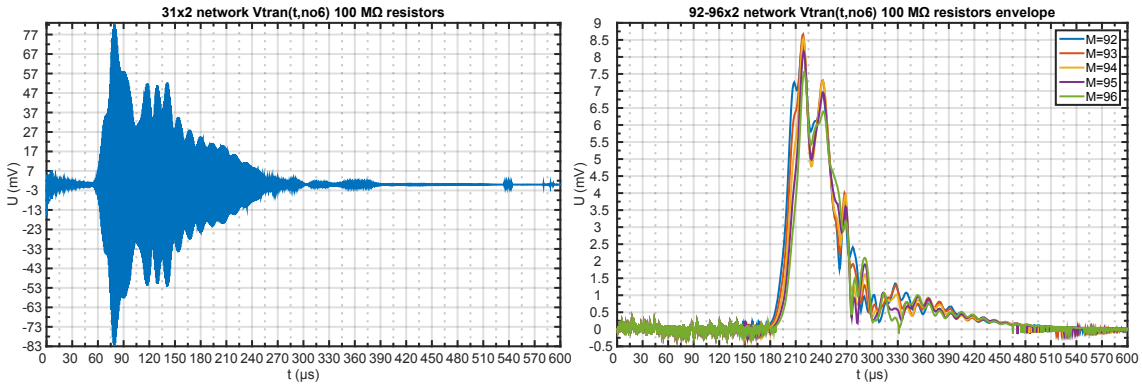

Figure 31: Transient responses of $31x2$ (on left) and $92 - 96x2$ (on right) networks. The noise before the pulse is clearly visible on the both graphs. In the larger network the amplitude of the pulse is lower and the distortions are visible in the edges of the pulse.

In some cases chancing M does not affect the response much but sometimes the amplitude of a network with $M + 1$ can be about fifteen percent lower than that of with M. For small M, the amplitude can sometimes significantly increase with M. These can be traced to changes in the frequency response, which determines the steady state amplitude.

The shape of the pulse is heavily frequency dependent and in some cases it can be multipart. In some cases, the output pulse has an area with approximately constant amplitude before the main part of the pulse, which is likely part of the initial transient solution. The amplitude of this region can be lower than 5 % of the maximum and in many cases practically indistinguishable from the background. Whether this is the case or not depends are the initial values large enough compared to the main the pulse to distinguishable.

The total pulse length at output can be over 60 % longer than the input. The end of the input pulse is visible as fast amplitude drop in the output in position $delay + (pulselength)$ in small networks. In some networks the beginning, end and length change only a little in certain input frequency ranges. The secondary pulses after the main pulse are caused by reflections from transducers. The initial transient response has significant impact to the shape of the pulse during the first tens of microseconds as it decays exponentially. How large this impact is depends from initial conditions, both steady state and transient amplitudes and the length of the input pulse. The end of the pulse after the input ends is dominated by the transients caused by switching off the input.

The point where the amplitude of the pulse exceeds for the first time 50 % of the the maximum increases linearly with M if N is not changed by following formula $(a\,x + b)$. The rate of increase varies only a few percent with N and the impact of using 100 MΩ resistors instead of 5 MΩ resistors is very small. Changing M by one adds or removes one resonator from the path of the signal leading to linear relationship between the delay and M. Table 4 list values of a and b.

Table 4: The constants a and b for $a*M+b$. The values of a and b are in microseconds. Note that the input frequency is not the same for all Ns.

parameter/ N	1	2	3	4	5	6	7
a (5 MΩ)	2.16	2.14	2.12	2.19	2.18	2.18	2.19
b (5 MΩ)	12.4	5.53	8.85	6.76	5.30	5.19	6.17
a (100 MΩ)	2.15	2.15	2.13	2.16	2.17	2.19	2.19
b (100 MΩ)	17.0	5.07	9.77	5.96	6.04	4.95	6.07

4.3.3 Impact of Q

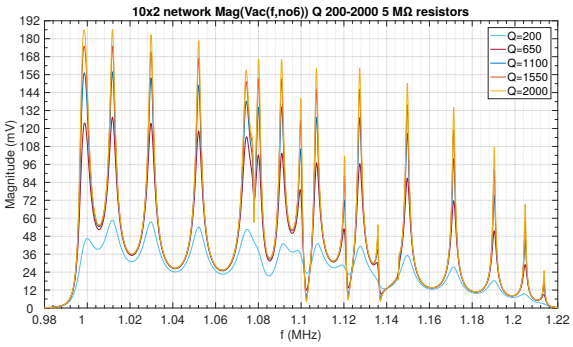

Figure 32: The magnitude (on left) on $10x2$ network for Q values 200–2000. The graph of magnitude demonstrates the increase of maximums with the minimums remaining at same level resulting extremely narrow passbands.

Increasing Q affects mainly the maximums of the magnitude by increasing them while minimums remain constant though some minimums decrease. The width of the resulting peaks becomes smaller as Q increases. In networks with strong coupling in the smaller dimension the locations of the band remain the same but the rippling due the individual resonators increases. Figure 32 shows the magnitude and in $10x2$ network for Q values 200–2000.

The amount and locations of peaks in the frequency response depend only from M and N if no other parameter is changed. Peaks represent subbands due individual resonators and their prominence increases with Q. Some peaks are not visible in small Q values.

On transient analysis the responses on some Q values differ significantly from others. In one case, the same or higher amplitude is not reached again until Q is about 80 % higher.

4.3.4 Nonidentical resonance frequencies

Nonidentical resonance frequencies cause extra resonances compared to the situation with identical resonance frequencies and lower magnitude due the disorder as Figure 33 demonstrates. The changes in resonance frequency caused proportional changes in resonator mass as the anchoring stiffness remains constant. The response is affected more if the difference between resonance frequencies of neighboring resonators is large as it leads to larger reflections and localizations, see Chapter 2.4.2 and Judge et al. [19]. This limited data also indicates that the response widens more into the direction that the distribution of the resonance frequencies is skewed. The frequencies used in networks are given in Table 5.

Table 5: The resonance frequencies used when analyzing nonidentical resonance frequencies. The frequency unit is megahertz.

network	frequencies (MHz)								
resonator	1	2	3	4	5	6	7	8	9
2x2	0.99	1.00	1.01	1.02					
3x2	0.98	0.99	1.00	1.01	1.02	1.03			
3x3	0.98	0.985	0.99	0.995	1.00	1.005	1.01	1.015	1.02

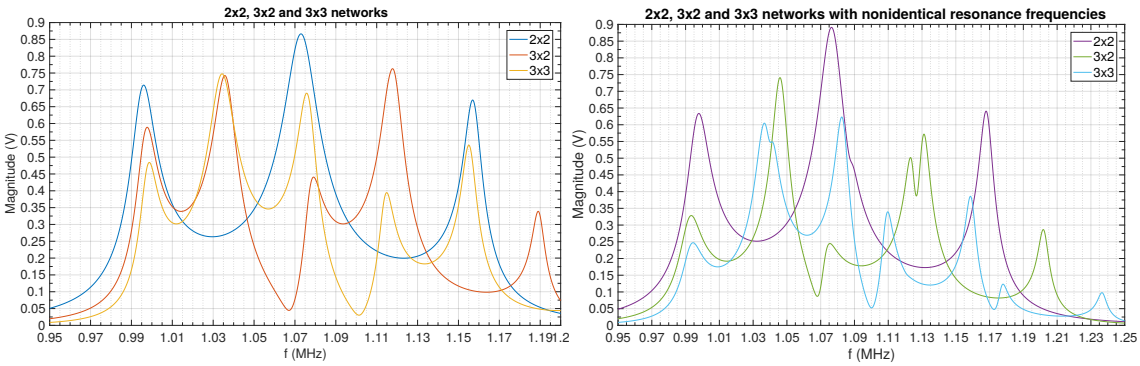

Figure 33: Frequency responses of 2x2, 3x2 and 3x3 networks with identical (on left) and nonidentical (on right) resonance frequencies.

When investigating normally distributed resonance frequencies maximum difference from mean was set at two and a half times standard deviation. The area contains about 98.7 % of possible frequencies.

From data gathered with hundred simulation runs for $20x15$ and $50x2-4$ networks, one can get a fairly reliable idea how the randomization affects the response. When investigating Mag(Vac(f,no6)) from multiple simulation runs with the same parameters it was noted that the impact to the width, starting and end points of the response is minor. There is minor differences in the location of the extreme values of the magnitude though their type may change. Changes in the magnitude itself are major as can be seen from Figure 34.

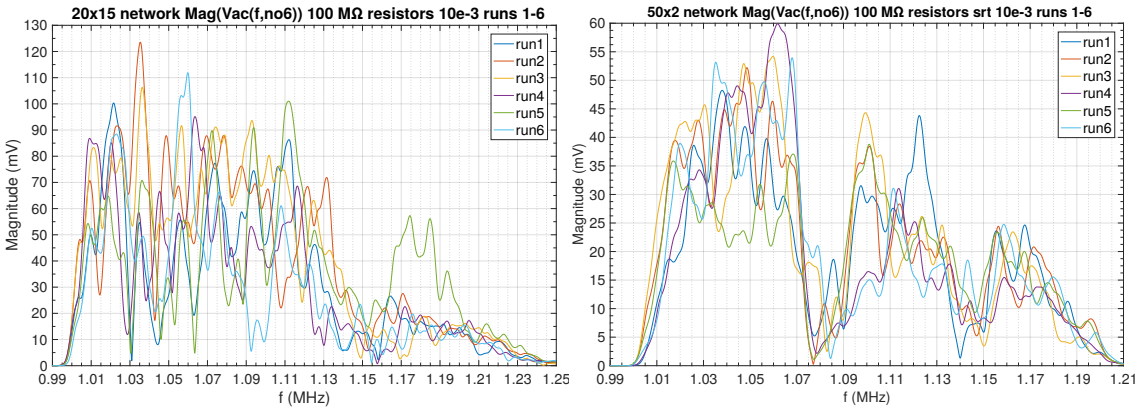

Figure 34: Mag(Vac(f,no6)) of $20x15$ (on left) and $50x2$ (on right) networks with randomized resonance frequencies with standard deviation of 0.01, six runs on each graph.

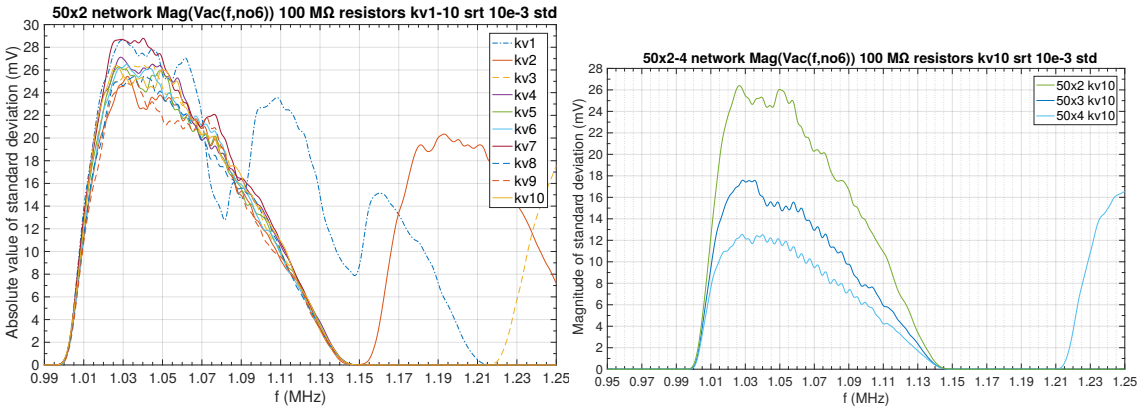

Figure 35: Standard deviation of Vac(f,no6) of $50x2$ network with multiple different vertical coupling coefficients (on left) and $50x2-4$ networks with vertical coupling coefficients being ten times of their default values (on right). The standard deviations are calculated from results of hundred simulation runs with frequency region 0.95–1.25 MHz and with standard deviation of frequencies 0.01 .

The impact of randomization can be reduced by increasing coupling strength in vertical direction and N as shown in Figure 35. The reduction is caused by averaging over the strong coupling direction discussed in Chapter 2.4.2, which causes larger reduction in the standard deviation of the responses for the same coupling strength as N increases due the decreased disorder.

4.3.5 Multiple outputs

All simulations in this chapter are done with 5 MΩ resistors, only one input is used. The extra output block is shown in Figure 10 on page 37. The final output voltage is the sum of voltages on the no6 node and the equivalent nodes in the extra output blocks. The summing is done with a controlled voltage source.

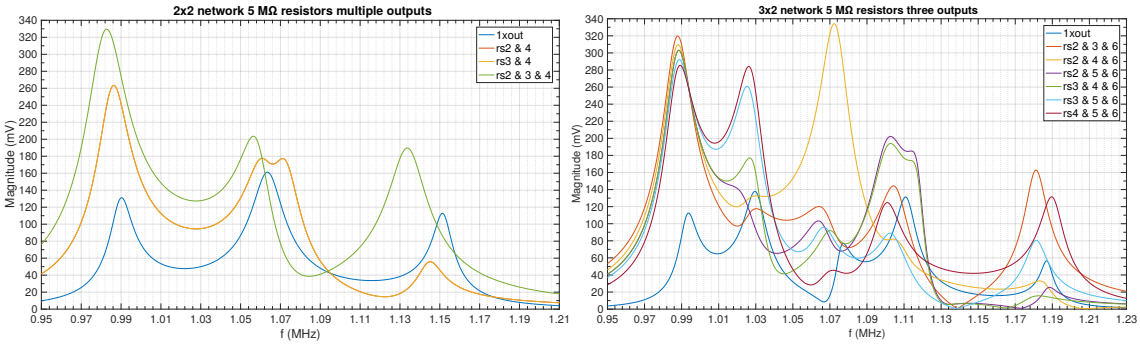

Figure 36: Impact multiple to the response of $2x2$ (on left) and $3x2$ (on right) networks. The rsx markings, where x is the resonator number, in the legend tell the location of the extra outputs. Both have the single output sitution for comparison with marking 1xout. On left symmetries mean that the responses for two inputs are identical

When multiple outputs are used the response increases significantly compared to single output as discussed in Chapter 2.4. The increase of response depends on the amount and positions of extra outputs (Figure 36). As expected response generally increases when the amount of outputs is increased. The extra outputs change the response of the entire network slightly due electrostatic forces of the additional transducers.

4.3.6 Multiple inputs

A stopband is area where Mag(Vac(f,no6)) is less than 10 % maximum of adjacent passbands. A passband ends when Mag(Vac(f,no6)) is less than half of band maximum. The extra input block is shown in Figure 10 on page 37. Extra inputs were used to complicate the response in order to get the network to behave strangely. The problem is the massive number of possible combinations with amplitudes, phases, frequencies and locations of the extra inputs. Each input causes specific response and the final response is a sum of of these responses, which explains why the impact of extra inputs is so significant.

The Mag(Vac(f,no6)) can change drastically just by changing the amplitudes of the extra inputs. The amplitude of certain individual resonators can be kept nearly constant for a specific time period for many different parameters of the extra inputs. The amplitude changes of the extra inputs have the strongest impact to local minimums and maximums of magnitude. With extra inputs, the number, shape, size and location of passbands can be modified.

If the amplitude of the input one is much larger than that of input two, then the local minimums of the response are much higher than the stopband limit, usually they are around half of the value of the corresponding local maximum. This is caused by the fact that the response caused by the extra input is so small that it cannot affect the response of input one enough. The impact of extra inputs increases as they move closer to the output.

Adding inputs with identical AC voltages and phases to subsequent lines from bottom results initial increase and then decreasing response as more inputs are added. Adding inputs from top results decreasing response until fifth or sixth input is added and the response starts increasing (Figure 37). The used AC voltage depends on the number of inputs (n_{in}) and is determined with following formula u_{ac}/n_{in}, where u_{ac} is the AC voltage when only single input is used. The additional inputs with identical voltages lead to higher response than with single input if they cause resonators near output vibrate with larger amplitude than would case with single input.

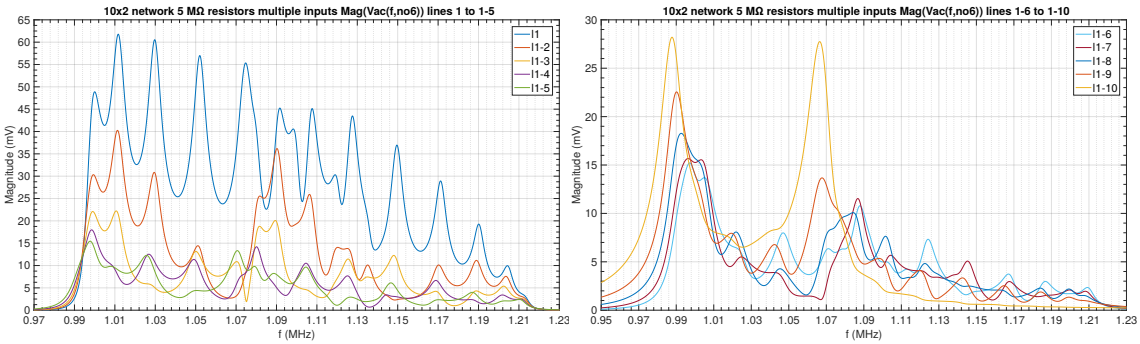

Figure 37: Mag(Vac(f,no6)) of $10x2$ network with 1–5 inputs (on left) and 6–10 inputs (on right). The legend gives the lines where the inputs are. On right emergence of two distinct peaks is clearly visible as the number of inputs increases.

In transient analysis,as expected the starting point of the output pulse and most of the pulse move earlier when the location is moved downwards. The reason for this is the shorter path that the pulse from the extra input has to to the output.

5 Summary

This work focused to investigating responses of coupled MEMS resonator networks in different conditions.

The resonators can be connected to each other with either mechanical or electric means. Springs, whose strength is determined by dimensions, geometry, material used and coupling location, are usually used to realize mechanical coupling and usually they are built from beams. Hooke's law can be used to determine spring forces. The assumption of massless spring breaks down when frequency increases enough. Electric coupling is based on two electric transducers with common plate between them, though one realization uses biased plates with one plate in each resonator. It allows adjusting stiffness after fabrication at price of more complex system due the wiring for bias voltage and necessary control electronics.

Coupling multiple resonators together has many advantages, such as performance improvements and enabling some applications. Slight differences between individual resonators can also be compensated. Dispersion relation for resonator chain depends from resonator mass and both anchoring and coupling stiffnesses. For linearly coupled undamped oscillators with weak coupling, the passband width is product of oscillator resonance frequency and ratio of coupling stiffness to anchoring stiffness (R), filter quality factor is inversely proportional to R. Nonidentical resonators lead to increased disorder and localization. An 2D-array allows different coupling strengths in vertical and horizontal directions. Strong coupling ($R_s >> R_w$)in one direction reduces sensitivity to disorder though averaging along strongly coupled direction. The passband is now divided into subbands whose width is determined by R for the weak coupling ($R_w << 1$), while R for the strong coupling determines total passband width. It is possible to excite the central mode group and suppress the extraneous bands.

Currently, coupled MEMS-resonator networks are used in RF-technology for signal processing functions, such as mixing, amplification and filtering. MEMS technology enables integration of necessary components of transceiver/receiver to single chip. In delay lines built from chains the group and phase velocities at the center frequency depends from chain period, resonator mass, anchoring stiffness and coupling stiffness. In filter applications nonlinearities causing intermodulation are problematic. Multiple different filter realization have been demonstrated. By replacing individual resonators in with sub-filters consisting of multiple resonators higher order transfer functions are possible.

The mixer can also act as amplifier. One device can provide both mixing and filtering functions by using capacitive mixing transducers to downconvert RF-signal to IF and use coupled MEMS resonators for filtering.

The resonator network is modeled with the electrical equivalent circuit based on voltage controlled current sources. In addition to the network, the system also has capacitive transducers and the external circuit for input, output and biasing. The impact of nonlinearities on the coupling strength is below ten percent if the displacement of the spring is at most a few nanometers.

The numerical data was generated with Aplac simulator and then plotted for

visual analysis. The model was also translated for ngspice and verified. Perl script was written to generate the required netlist files for ngspice and give simulation commands. In this work, Matlab was used for further data analysis.

The time derivatives of the node voltages have direct and indirect dependencies from node voltages and circuit parameters. The circuit has two sources of nonlinearity: transducers and couplings. The amplitude of the steady-state solution to the equation of motion as the function of frequency has bandpass characteristics and the transient part decays exponentially.

The frequency response of the chains approaches that of ideal bandpass filters as chain is lengthened. The rippling present in the response is significant in small chains but is eventually reduced to insignificant levels as the length increases. The magnitude of chains decreases exponentially as M increases at each frequency as relative loss is the same at each resonator and the losses are multiplied with each other. The location of the maximum of the pulse depends linearly on the length of the chain as the delay caused by each resonator is constant.

A 2D network is more interesting case, as it has couplings to multiple directions which can have different strengths. If all couplings have the same strength and are weak the frequency response is so complex due overlapping resonances that the system would be useless.

A MxN network with strong horizontal coupling has N passbands, which are further divided into M subbands. The passband separation increases with horizontal coupling strength and decreases as N increases. The horizontal coupling strength required to fully separate the passbands is order of magnitude larger than in vertical direction when $N = 3$ and increases fast with N. If the passbands are separate then the magnitude decreases exponentially with M. As the network size increases, eventually the signal gets distorted. Increasing Q brings narrow peaks to the frequency response as the subbands become more prominent. The input frequency has a significant impact on the transient response. The delay in the transient response is linearly dependent from the length of the path.

Randomized resonance frequencies cause significant changes in the response due disorder and with only weak couplings responses from different simulation runs have large differences, but their impact can be significantly reduced by using strong couplings in the smaller dimension.

Extra inputs complicate the response and allow adjusting it somewhat. Increasing the number of extra inputs makes the system more sensitive to changes in the amplitudes, phases and locations of the extra inputs. Further investigation is required about both subjects. Multiple outputs lead to higher total output voltage, which is the sum of the voltages on the no6 node and its equivalents in the extra output blocks. Multiple inputs and outputs could be used to implement other signal processing functions than filtering and delay lines.

The chains act as wideband bandpass filters but the signal levels when rippling is low enough are low. Networks often have multiple passbands close to each other. The length of the shortest path of the signal though the network determines the magnitude of the response not the resonator count. The tested system does not have any practical use but it demonstrates what kind of response is expected and how

changes in system parameters and inputs affect the response.

In further investigations, one should look into the equation of motion for different topologies and network sizes and compare the solutions to the one given in Chapter 4.1.3. The goal will be to understand how topology and network size affect the response. Also, why the amount of couplings per resonator has a significant impact on the response and signal delay requires investigation. As the number of topologies is extremely large a way to choose one for specific application should developed.

The response of the system when the impact of the nonlinearities is significant or even dominate should also be looked at. Nonlinear resonators would add another complication that could be interesting. Also the qualitative analysis of the equation of motion with nonlinear couplings and the circuit equations of the system modeled here would be useful.

Additional simulations about systems with randomized resonance frequencies are required along with simulations about the impact of randomized connecting springs. This work was limited to transient and AC small-signal analysis, but other analysis types should also be considered. Also a more realistic model should be developed.

References

[1] Deepak K. Agrawal, Jim Woodhouse, and Ashwin A. Seshia. Synchronization in a coupled architecture of microelectromechanical oscillators. *Journal of Applied Physics*, 115(16):–, 2014.

[2] Ari T Alastalo, Jyrki Kiihamäki, and Heikki Seppä. Microelectromechanical delay lines with slow signal propagation. *Journal of Micromechanics and Microengineering*, 16(9):1854, 2006.

[3] Farrokh Ayazi, Logan Sorenson, and Roozbeh Tabrizian. Energy dissipation in micromechanical resonators. In *Proc. SPIE 8031, Micro- and Nanotechnology Sensors, Systems, and Applications III, 803119*, 2011.

[4] Masoud Baghelani, Afshin Ebrahimi, and HabibBadri Ghavifekr. Design of rf mems based oscillatory neural network for ultra high speed associative memories. *Neural Processing Letters*, 40(1):93–102, 2014.

[5] Masoud Baghelani and HabibBadri Ghavifekr. Ring shape anchored rf mems contour mode disk resonator for uhf communication applications. *Microsystem Technologies*, 16(12):2123–2130, 2010.

[6] Joydeep Basu and TarunKanti Bhattacharyya. Microelectromechanical resonators for radio frequency communication applications. *Microsystem Technologies*, 17(10-11):1557–1580, 2011.

[7] B. Choubey, S. Collins, and M. Ward. On characterizing microelectromechanical processes using coupled resonators. *Microelectromechanical Systems, Journal of*, 21(4):791–800, Aug 2012.

[8] J.R. Clark, Wan-Thai Hsu, M.A Abdelmoneum, and C.T.-C. Nguyen. High-q uhf micromechanical radial-contour mode disk resonators. *Microelectromechanical Systems, Journal of*, 14(6):1298–1310, Dec 2005.

[9] J.R. Clark, Minfan Pai, B. Wissman, Guohong He, and Wan-Thai Hsu. Parallel-coupled square-resonator micromechanical filter arrays. In *International Frequency Control Symposium and Exposition, 2006 IEEE*, pages 485–490, June 2006.

[10] AWR corporation. Aplac 8.5, 2009.

[11] Sepehr Forouzanfar, Raafat Mansour, and Eihab Abdel-Rahman. Lorentz-force transduction for rf micromechanical filters. *Journal of Micromechanics and Microengineering*, 22(3):035018, 2012.

[12] D. Galayko, A. Kaiser, L. Buchaillot, D. Collard, and C. Combi. Electrostatical coupling-spring for micro-mechanical filtering applications. In *Circuits and Systems, 2003. ISCAS '03. Proceedings of the 2003 International Symposium on*, volume 3, pages III–530–III–533 vol.3, May 2003.

[13] D. Galayko, A. Kaiser, L. Buchaillot, D. Collard, and C. Combi. Microelectromechanical variable-bandwidth if frequency filters with tunable electrostatical coupling spring. In *Micro Electro Mechanical Systems, 2003. MEMS-03 Kyoto. IEEE The Sixteenth Annual International Conference on*, pages 153–156, Jan 2003.

[14] Dimitri Galayko, Andreas Kaiser, Bernard Legrand, Lionel Buchaillot, Chantal Combi, and Dominique Collard. Coupled-resonator micromechanical filters with voltage tuneable bandpass characteristic in thick-film polysilicon technology. *Sensors and Actuators A: Physical*, 126(1):227 – 240, 2006.

[15] F.C. Hoppensteadt and E.M. Izhikevich. Synchronization of mems resonators and mechanical neurocomputing. *Circuits and Systems I: Fundamental Theory and Applications, IEEE Transactions on*, 48(2):133–138, Feb 2001.

[16] Li-Wen Hung and C.T.-C. Nguyen. Capacitive-piezoelectric aln resonators with q>12,000. In *Micro Electro Mechanical Systems (MEMS), 2011 IEEE 24th International Conference on*, pages 173–176, Jan 2011.

[17] StatSoft Inc. *Electronic Statistics Textbook*. Tulsa OK: StatSoft, 2013. WEB: http://www.statsoft.com/textbook/.

[18] A. Jaakkola, P. Rosenberg, S. Asmala, A. Nurmela, T. Pensala, T. Riekkinen, J. Dekker, T. Mattila, A. Alastalo, O. Holmgren, and K. Kokkonen. Piezoelectrically transduced single-crystal-silicon plate resonators. In *2008 IEEE Ultrasonics Symposium*, pages 717–720, Nov 2008.

[19] John A. Judge, Brian H. Houston, Douglas M. Photiadis, and Peter C. Herdic. Effects of disorder in one- and two-dimensional micromechanical resonator arrays for filtering. *Journal of Sound and Vibration*, 290(3–5):1119 – 1140, 2006.

[20] Volker Kempe. *Inertial MEMS - Principles and Practice*. Cambridge University Press, 2011.

[21] A Knoll, O Züger, and U Duerig. All mechanical mixing by means of orthogonally coupled cantilevers. *New Journal of Physics*, 10(12):125017, 2008.

[22] Jan G. Korvink and Oliver Paul. *MEMS - A Practical Guide to Design, Analysis, and Applications*. William Andrew Publishing/Noyes, 2006.

[23] Arno Lenk, Rüdiger G Ballas, Roland Werthschützky, and Günther Pfeifer. *Electromechanical Systems in Microtechnology and Mechatronics: Electrical, Mechanical and Acoustic Networks, Their Interactions and Applications*. Springer, 2010.

[24] Sheng-Shian Li, Yu-Wei Lin, Zeying Ren, and C.T.-C. Nguyen. Disk-array design for suppression of unwanted modes in micromechanical composite-array filters. In *Micro Electro Mechanical Systems, 2006. MEMS 2006 Istanbul. 19th IEEE International Conference on*, pages 866–869, 2006.

[25] Sheng-Shian Li, Yu-Wei Lin, Zeying Ren, and C.T.-C. Nguyen. A micromechanical parallel-class disk-array filter. In *Frequency Control Symposium, 2007 Joint with the 21st European Frequency and Time Forum. IEEE International*, pages 1356–1361, May 2007.

[26] Sheng-Shian Li, Yu-Wei Lin, Yuan Xie, Zeying Ren, and C.T.-C. Nguyen. Micromechanical "hollow-disk" ring resonators. In *Micro Electro Mechanical Systems, 2004. 17th IEEE International Conference on. (MEMS)*, pages 821–824, 2004.

[27] Liwei Lin, R.T. Howe, and A.P. Pisano. Microelectromechanical filters for signal processing. *Microelectromechanical Systems, Journal of*, 7(3):286–294, Sep 1998.

[28] Yang Lin, Wei-Chang Li, Bongsang Kim, Yu-Wei Lin, Zeying Ren, and C.T.-C. Nguyen. Enhancement of micromechanical resonator manufacturing precision via mechanically-coupled arraying. In *Frequency Control Symposium, 2009 Joint with the 22nd European Frequency and Time forum. IEEE International*, pages 58–63, April 2009.

[29] Yu-Wei Lin, Sheng-Shian Li, Zeying Ren, and C.T.-C. Nguyen. Low phase noise array-composite micromechanical wine-glass disk oscillator. In *Electron Devices Meeting, 2005. IEDM Technical Digest. IEEE International*, pages 4 pp.–281, Dec 2005.

[30] Mehrnaz Motiee, Raafat R Mansour, and Amir Khajepour. Novel mems filters for on-chip transceiver architecture, modeling and experiments. *Journal of Micromechanics and Microengineering*, 16(2):407, 2006.

[31] T.L. Naing, T. Beyazoglu, Lingqi Wu, M. Akgul, Zeying Ren, T.O. Rocheleau, and C.T.-C. Nguyen. 2.97-ghz cvd diamond ring resonator with q>40,000. In *Frequency Control Symposium (FCS), 2012 IEEE International*, pages 1–6, May 2012.

[32] N Nefedov. Application of coupled nanoscale resonators for spectral sensing. *Journal of Physics: Condensed Matter*, 21(14):144213, 2009.

[33] C.T.-C. Nguyen. Vibrating rf mems technology: fuel for an integrated micromechanical circuit revolution? In *Solid-State Sensors, Actuators and Microsystems, 2005. Digest of Technical Papers. TRANSDUCERS '05. The 13th International Conference on*, volume 1, pages 243–246 Vol. 1, June 2005.

[34] C.T.-C. Nguyen. Mems technology for timing and frequency control. *Ultrasonics, Ferroelectrics, and Frequency Control, IEEE Transactions on*, 54(2):251–270, February 2007.

[35] C.T.-C. Nguyen. Mems-based rf channel selection for true software-defined cognitive radio and low-power sensor communications. *Communications Magazine, IEEE*, 51(4):110–119, April 2013.

[36] C.T.-C. Nguyen. Rf mems for channelizing low-power radios. In *Solid-State Sensors, Actuators and Microsystems (TRANSDUCERS EUROSENSORS XXVII), 2013 Transducers Eurosensors XXVII: The 17th International Conference on*, pages 2455–2460, June 2013.

[37] S. Pourkamali, R. Abdolvand, G.K. Ho, and F. Ayazi. Electrostatically coupled micromechanical beam filters. In *Micro Electro Mechanical Systems, 2004. 17th IEEE International Conference on. (MEMS)*, pages 584–587, 2004.

[38] Siavash Pourkamali and Farrokh Ayazi. Electrically coupled {MEMS} bandpass filters: Part i: With coupling element. *Sensors and Actuators A: Physical*, 122(2):307 – 316, 2005.

[39] Siavash Pourkamali and Farrokh Ayazi. Electrically coupled {MEMS} bandpass filters: Part ii. without coupling element. *Sensors and Actuators A: Physical*, 122(2):317 – 325, 2005.

[40] Christos Stergiou and Dimitrios Siganos. Neural networks. *SURPRISE 96 Journal*, 1996. Retrieved 4.9.2014.

[41] Timo Veijola. Nonlinear circuit simulation of mems components: controlled current source approach. In *Proceedings of the 15th European Conference on Circuit Theory and Design,(Espoo)*, pages 377–380, 2001.

[42] Kun Wang and C.T.-C. Nguyen. High-order medium frequency micromechanical electronic filters. *Microelectromechanical Systems, Journal of*, 8(4):534–556, Dec 1999.

[43] Kun Wang, Ark-Chew Wong, and CT-C Nguyen. Vhf free-free beam high-q micromechanical resonators. *Journal of microelectromechanical systems*, 9(3):347–360, 2000.

[44] Ark-Chew Wong and C.T.-C. Nguyen. Micromechanical mixer-filters ("mixlers"). *Microelectromechanical Systems, Journal of*, 13(1):100–112, Feb 2004.

[45] Darrin J. Young, Christian A. Zorman, and Mehran Mehregany. *Springer Handbook of Nanotechnology*, chapter MEMS/NEMS Devices and Applications, pages 359–387. Springer Berlin Heidelberg, Berlin, Heidelberg, 2010.

[46] Mohammad I Younis. *MEMS Linear and Nonlinear Statics and Dynamics: Mems Linear and Nonlinear Statics and Dynamics*, volume 20. Springer, 2011.

[47] Haoshen Zhu and Joshua E.-Y. Lee. System-level circuit simulation of nonlinearity in micromechanical resonators. *Sensors and Actuators A: Physical*, 186(0):15 – 20, 2012. Selected Papers presented at Eurosensors {XXV} Athens, Greece, 4-7 September 2011.

A Appendix A

The solutions of the equations of motion for one, two and three element chains are given below. One resonator:

$$x1(t) = -\frac{(m\omega^2 - k_r)\sin(\omega t) + \zeta\omega\cos(\omega t)}{m^2\omega^4 + (\zeta^2 - 2k_r m)\omega^2 + k_r^2} + e^{-\frac{\zeta}{2m}t}\,\omega\frac{(2m^2\omega^2 - 2k_r m + \zeta^2)\sin(\frac{\sqrt{4k_r m-\zeta^2}}{2m}t) + \zeta\sqrt{4k_r m - \zeta^2}\,\cos(\frac{\sqrt{4k_r m-\zeta^2}}{2m}t)}{\sqrt{4k_r m - \zeta^2}\,(m^2\omega^4 + (\zeta^2 - 2k_r m)\omega^2 + k_r^2)} \tag{A1}$$

Two resonators:

$$\begin{aligned} x1(t) = &-\frac{\begin{array}{c}[m^3\omega^6 - ((k_r+k_c)3m - \zeta^2)m\omega^4 + ((3k_r^2 + 6k_c k_r + 2k_c^2)m \\ -(k_r+k_c)\zeta^2)\omega^2 - k_r(k_r+k_c)(k_r+2k_c)]\sin(\omega t) \\ + \zeta\omega[m^2\omega^4 - ((k_r+k_c)2m - \zeta^2)\omega^2 + (k_r+k_c)^2 + k_c^2]\cos(\omega t)\end{array}}{((m\omega^2 - k_r)^2 + \zeta^2\omega^2)(m^2\omega^4 - ((k_r+2k_c)2m - \zeta^2)\omega^2 + (k_r+2k_c)^2)} \\ &+ e^{-\frac{\zeta}{2m}t}\omega\frac{(2m^2\omega^2 - 2k_r m + \zeta^2)\sin(\frac{\sqrt{4k_r m-\zeta^2}}{2m}t) + \zeta\sqrt{4k_r m - \zeta^2}\cos(\frac{\sqrt{4k_r m-\zeta^2}}{2m}t)}{\sqrt{(4k_r m - \zeta^2}\,2((m\omega^2 - k_r)^2 + \zeta^2\omega^2)} \\ &+ e^{-\frac{\zeta}{2m}t}\frac{\begin{array}{c}(2m^2\omega^2 - (k_r+2k_c)2m + \zeta^2)\sin(\frac{\sqrt{(4k_r+8k_c)m-\zeta^2}}{2m}t) \\ + \zeta\sqrt{(4k_r+8k_c)m - \zeta^2}\cos(\frac{\sqrt{(4k_r+8k_c)m-\zeta^2}}{2m}t)\end{array}}{\sqrt{(4k_r+8k_c)m - \zeta^2}\,2[m^2\omega^4 - ((k_r+2k_c)2m - \zeta^2)\omega^2 + (k_r+2k_c)^2]} \end{aligned} \tag{A2}$$

$$\begin{aligned} x2(t) = &\,k_c\frac{\begin{array}{c}[m^2\omega^4 - ((k_r+k_c)2m + \zeta^2)\omega^2 + k_r^2 + 2k_c k_r]\sin(\omega t) \\ + [m\omega^2 - (k_r+k_c)]2\zeta\omega\cos(\omega t)\end{array}}{(m\omega^2 - k_r)^2 + \zeta^2\omega^2)(m^2\omega^4 - ((k_r+2k_c)2m - \zeta^2)\omega^2 + (k_r+2k_c)^2)} \\ &+ e^{-\frac{\zeta}{2m}t}\omega\frac{(2m^2\omega^2 - 2k_r m + \zeta^2)\sin(\frac{\sqrt{4k_r m-\zeta^2}}{2m}t) + \zeta\sqrt{4k_r m - \zeta^2}\cos(\frac{\sqrt{4k_r m-\zeta^2}}{2m}t)}{\sqrt{(4k_r m - \zeta^2}\,2((m\omega^2 - k_r)^2 + \zeta^2\omega^2)} \\ &- e^{-\frac{\zeta}{2m}t}\frac{\begin{array}{c}(2m^2\omega^2 - (k_r+2k_c)2m + \zeta^2)\sin(\frac{\sqrt{(4k_r+8k_c)m-\zeta^2}}{2m}t) \\ + \zeta\sqrt{(4k_r+8k_c)m - \zeta^2}\cos(\frac{\sqrt{(4k_r+8k_c)m-\zeta^2}}{2m}t)\end{array}}{\sqrt{(4k_r+8k_c)m - \zeta^2}\,2[m^2\omega^4 - ((k_r+2k_c)2m - \zeta^2)\omega^2 + (k_r+2k_c)^2]} \end{aligned} \tag{A3}$$

Three resonators:

$$
\begin{aligned}
x1(t) = &-[\{m^5\omega^{10} - ((5k_r + 7k_c)m - 2\zeta^2)m^3\omega^8 \\
&+ ((k_r + 2k_c)(5k_r + 4k_c)2m^2 - (3k_r + 4k_c)2\zeta^2 m + \zeta^4)m\omega^6 \\
&+ (-(10k_r^3 + 42k_c k_r^2 + 48k_c^2 k_r + 13k_c^3)m^2 + (3k_r^2 + 8k_c k_r + 6k_c^2)2\zeta^2 m - (k_r + k_c)\zeta^4)\omega^4 \\
&+ ((5k_r^4 + 28k_c k_r^3 + 48k_c^2 k_r^2 + 26k_c^3 k_r + 3k_c^4)m - (2k_r^3 + 8k_c k_r^2 + 12k_c^2 k_r + 5k_c^3)\zeta^2)\omega^2 \\
&- k_r(k_r + k_c)(k_r + 3k_c)(k_r^2 + 3k_c k_r + k_c^2)\} \sin(\omega t) \\
&+ \{m^4\omega^8 - ((2k_r + 3k_c)m - \zeta^2)2m^2\omega^6 + (6(k_r + k_c)(k_r + 2k_c)m^2 \\
&- (2k_r + 3k_c)2\zeta^2 m + \zeta^4)\omega^4 + (-(k_r + 2k_c)^2(2k_r + k_c)2m + (k_r^2 + 3k_c k_r + 4k_c^2)2\zeta^2)\omega^2 \\
&+ k_r^4 + 6k_c k_r^3 + 12k_c^2 k_r^2 + 8k_c^3 k_r + 3k_c^4\}\zeta\omega\cos(\omega t)] \\
&/[(((m\omega^2 - k_r)^2 + \zeta^2\omega^2) * (m^2\omega^4 - ((k_r + 3k_c)2m - \zeta^2)\omega^2 + (k_r + 3k_c)^2) \\
&(m^2\omega^4 - ((k_r + k_c)2m - \zeta^2)\omega^2 + (k_r + k_c)^2))] \\
&+ e^{-\frac{\zeta}{2m}t}\omega \frac{(2m^2\omega^2 - (k_r + 3k_c)2m + \zeta^2)\sin(\frac{\sqrt{(4k_r + 12k_c)m - \zeta^2}t}{2m}) + \zeta\sqrt{(4k_r + 12k_c)m - \zeta^2}\cos(\frac{\sqrt{(4k_r + 12k_c)m - \zeta^2}t}{2m})}{6\sqrt{(4k_r + 12k_c)m - \zeta^2}(m^2\omega^4 - ((k_r + 3k_c)2m - \zeta^2)\omega^2 + (k_r + 3k_c)^2)} \\
&+ e^{-\frac{\zeta}{2m}t}\omega \frac{(2m^2\omega^2 - 2k_r m + \zeta^2)\sin(\frac{\sqrt{4k_r m - \zeta^2}t}{2m}) + \zeta\sqrt{4k_r m - \zeta^2}\cos(\frac{\sqrt{4k_r m - \zeta^2}t}{2m})}{3\sqrt{4k_r m - \zeta^2}(((m\omega^2 - k_r)^2 + \zeta^2\omega^2))} \\
&+ e^{-\frac{\zeta}{2m}t}\omega \frac{((2m^2\omega^2 - 2k_r m - 2k_c m + \zeta^2)\sin(\frac{\sqrt{(4k_r + 4k_c)m - \zeta^2}t}{2m}) + \zeta\sqrt{(4k_r + 4k_c)m - \zeta^2}\cos(\frac{\sqrt{(4k_r + 4k_c)m - \zeta^2}t}{2m})}{2\sqrt{(4k_r + 4k_c)m - \zeta^2}(m^2\omega^4 - ((k_r + k_c)2m - \zeta^2)\omega^2 + (k_r + k_c)^2))}
\end{aligned}
\tag{A4}
$$

$$
\begin{aligned}
x2(t) = k_c &\frac{((m\omega^2 - k_r)^2 - (3k_c m - \zeta^2)\omega^2 + 3k_c k_r)\sin(\omega t) + \zeta\omega(2m\omega^2 - 2k_r - 3k_c)\cos(\omega t)}{((m\omega^2 - k_r)^2 + \zeta^2\omega^2)(m^2\omega^4 - ((k_r + 3k_c)2m - \zeta^2)\omega^2 + (k_r + 3k_c)^2)} \\
&+ e^{-\frac{\zeta}{2m}t}\omega \frac{(2m^2\omega^2 - 2k_r m + \zeta^2)\sin(\frac{\sqrt{4k_r m - \zeta^2}t}{2m}) + \zeta\sqrt{4k_r m - \zeta^2}\cos(\frac{\sqrt{4k_r m - \zeta^2}t}{2m})}{3\sqrt{4k_r m - \zeta^2}((m\omega^2 - k_r)^2 + \zeta^2\omega^2)} \\
&- e^{-\frac{\zeta}{2m}t}\omega \frac{(2m^2\omega^2 - (k_r + 3k_c)2m + \zeta^2)\sin(\frac{\sqrt{(4k_r + 12k_c)m - \zeta^2}t}{2m}) + \zeta\sqrt{(4k_r + 12k_c)m - \zeta^2}\cos(\frac{\sqrt{((4k_r + 12k_c)m - \zeta^2}t}{2m})}{3\sqrt{(4k_r + 12k_c)m - \zeta^2}(m^2\omega^4 - ((k_r + 3k_c)2m - \zeta^2)\omega^2 + (k_r + 3k_c)^2)}
\end{aligned}
\tag{A5}
$$

$$
\begin{aligned}
x3(t) = -kc^2 \frac{\{m^3\omega^6 - ((3k_r + 4k_c)m + 3\zeta^2)m\omega^4 + ((3k_r^2 + 8k_ck_r + 3k_c^2)m \\
+(3k_r + 4k_c)\zeta^2)\omega^2 - k_r(k_r + k_c)(k_r + 3k_c)\}\sin(\omega t) \\
+\zeta\omega\{3m^2\omega^4 - ((3k_r + 4k_c)2m + \zeta^2)\omega^2 \\
+ 3k_r^2 + 8k_ck_r + 3k_c^2\}\cos(\omega t)}{((m\omega^2 - k_r)^2 + \zeta^2\omega^2)(m^2\omega^4 - ((k_r + 3k_c)2m - \zeta^2)\omega^2 + (k_r + 3k_c)^2)} \\
(m^2\omega^4 - ((k_r + k_c)2m - \zeta^2)\omega^2 + (k_r + k_c)^2) \\
+ e^{-\frac{\zeta}{2m}t}\omega \frac{(2m^2\omega^2 - (k_r + 3k_c)2m + \zeta^2)\sin(\frac{\sqrt{((4k_r+12k_c)m-\zeta^2}t}{2m}) + \zeta\sqrt{((4k_r + 12k_c)m - \zeta^2}\cos(\frac{\sqrt{((4k_r+12k_c)m-\zeta^2}t}{2m})}{\sqrt{((4k_r + 12k_c)m - \zeta^2}6(m^2\omega^4 - ((k_r + 3k_c)2m - \zeta^2)\omega^2 + (k_r + 3k_c)^2)} \\
+ e^{-\frac{\zeta}{2m}t}\omega \frac{(2m^2\omega^2 - 2k_rm + \zeta^2)\sin(\frac{\sqrt{4k_rm-\zeta^2}t}{2m}) + \zeta\sqrt{4k_rm - \zeta^2}\cos(\frac{\sqrt{4k_rm-\zeta^2}t}{2m})}{\sqrt{4k_rm - \zeta^2}3(((m\omega^2 - k_r)^2 + \zeta^2\omega^2)} \\
- e^{-\frac{\zeta}{2m}t}\omega \frac{(2m^2\omega^2 - 2k_rm - 2k_cm + \zeta^2)\sin(\frac{\sqrt{(4k_r+4k_c)m-\zeta^2}t}{2m}) + \zeta\sqrt{(4k_r + 4k_c)m - \zeta^2}\cos(\frac{\sqrt{(4k_r+4k_c)m-\zeta^2}t}{2m})}{\sqrt{(4k_r + 4k_c)m - \zeta^2}2(m^2\omega^4 - ((k_r + k_c)2m - \zeta^2)\omega^2 + (k_r + k_c)^2)}
\end{aligned}
\tag{A6}
$$

The solutions of the equations of motion from the beginning of Chapter 4.1.3 for x-direction are following assuming that at t=0 the system is at rest:

$$
\begin{aligned}
&x1(t) = -ax([\omega\zeta(m^4\omega^8 + (\zeta^2 - (2k_r + 5k_c)m)2m^2\omega^6 + (\zeta^4 - (2k_r + 5k_c)2\zeta^2m \\
&+ (3k_r^2 + 15k_ck_r + 14k_c^2)2m^2)\omega^4 + ((12k_c^2 + 5k_ck_r + k_r^2)\zeta^2 - m(2k_r^3 + 15k_ck_r^2 \\
&+ 28k_c^2k_r + 6k_c^3))2\omega^2 + k_r^4 + 10k_ck_r^3 + 28k_c^2k_r^2 + 12k_c^3k_r + 5k_c^4)\cos(\omega t) + (m^5\omega^{10} \\
&+ (2\zeta^2 - (5k_r + 11k_c)m)m^3\omega^8 + (\zeta^4 - 6\zeta^2(k_r + 2k_c)m + 2(5k_r^2 + 22k_ck_r + 18k_c^2)m^2)m\omega^6 \\
&+ (-\zeta^4(k_c + k_r) + \zeta^2 2(3k_r^2 + 12k_ck_r + 16k_c^2)m - (10k_r^3 + 66k_ck_r^2 + 108k_c^2k_r + 31k_c^3)m^2)\omega^4 \\
&+ (-\zeta^2(19k_c^3 + 32k_c^2k_r + 12k_ck_r^2 + 2k_r^3) + (5k_r^4 + 44k_ck_r^3 + 108k_c^2k_r^2 + 62k_c^3k_r + 5k_c^4)m)\omega^2 \\
&- k_r(k_r^4 + 11k_ck_r^3 + 36k_c^2k_r^2 + 31k_c^3k_r + 5k_c^4))\sin(\omega t)] \\
&/[((m\omega^2 - k_r)^2 + \zeta^2\omega^2)((m\omega^2 - (k_r + 5k_c))^2 + \zeta^2\omega^2)((m\omega^2 - (k_r + k_c))^2 + \zeta^2\omega^2)] \\
&+ \omega e^{-(\zeta t)/(2m)}\{[\zeta\sqrt{4(5k_c + k_r)m - \zeta^2}\cos(\sqrt{4(5k_c + k_r)m - \zeta^2}t/(2m)) + (-2(5k_c + k_r)m \\
&+ \zeta^2 + 2m^2\omega^2)\sin(\sqrt{4m(5k_c + k_r) - \zeta^2}t/(2m))]/[20\sqrt{4m(5k_c + k_r) - \zeta^2} \\
&((m\omega^2 - (k_r + 5k_c))^2 + \zeta^2\omega^2)] + [\zeta\sqrt{4k_rm - \zeta^2}\cos(\sqrt{4k_rm - \zeta^2}t/(2m)) \\
&+ (\zeta^2 - 2k_rm + 2m^2\omega^2)\sin(\sqrt{4k_rm - \zeta^2}t/(2m))]/[5\sqrt{4k_rm - \zeta^2}((m\omega^2 - k_r)^2 + \zeta^2\omega^2)] \\
&+ 3[\zeta\sqrt{4(k_c + k_r)m - \zeta^2}\cos(\sqrt{4m(k_c + k_r) - \zeta^2}t/(2m)) + (-2m(k_c + k_r) + \zeta^2 \\
&+ 2m^2\omega^2)\sin(\sqrt{4m(k_c + k_r) - \zeta^2}t/(2m))] \\
&/[4\sqrt{4m(k_c + k_r) - \zeta^2}((m\omega^2 + (k_r + k_c))^2 + \zeta^2\omega^2)]\})
\end{aligned}
\tag{A7}
$$

$$
\begin{aligned}
x2(t) &= ax([k_c(m^2\omega^4 - ((2k_r + 5k_c)m + \zeta^2)\omega^2 + k_r^2 + 5k_ck_r)\sin(\omega t) \\
&+ \zeta k_c\omega(2m\omega^2 - 2k_r - 5k_c)\cos(\omega t)] \\
&/[((m\omega^2 - k_r)^2 + \zeta^2\omega^2)((m\omega^2 - (k_r + 5k_c))^2 + \zeta^2\omega^2)] \\
&+ \omega e^{-(\zeta t)/(2m)}\{[\zeta\sqrt{4k_rm - \zeta^2}\cos(\sqrt{4k_rm - \zeta^2}t/(2m)) \\
&+ (\zeta^2 - 2k_rm + 2m^2\omega^2)\sin(\sqrt{4k_rm - \zeta^2}t/(2m))] \\
&/[5\sqrt{4k_rm - \zeta^2}((m\omega^2 - k_r)^2 + \zeta^2\omega^2)] \\
&- [\zeta\sqrt{4(5k_c + k_r)m - \zeta^2}\cos(\sqrt{4(5k_c + k_r)m - \zeta^2}t/(2m))] \\
&+ [-2(5k_c + k_r)m + \zeta^2 + 2m^2\omega^2]\sin(\sqrt{4(5k_c + k_r)m - \zeta^2}t/(2m))] \\
&/[5\sqrt{4(5k_c + k_r)m - \zeta^2}((m\omega^2 - (k_r + 5k_c))^2 + \zeta^2\omega^2)]\})
\end{aligned}
\tag{A8}
$$

$$
\begin{aligned}
x3(t) &= -ax([k_c^2(m^3\omega^6 - 3m((k_r + 2k_c)m + \zeta^2)\omega^4 + (3\zeta^2(2k_c + k_r) \\
&+ (3k_r^2 + 12k_ck_r + 5k_c^2)m)\omega^2 - k_r(k_r^2 + 6k_ck_r + 5k_c^2))\sin(\omega t) \\
&- \zeta k_c^2\omega(3m^2\omega^4 - (6(k_r + 2k_c)m + \zeta^2)\omega^2 + 3k_r^2 + 12k_ck_r + 5k_c^2)\cos(\omega t)] \\
&/[((m\omega^2 - k_r)^2 + \zeta^2\omega^2)((m\omega^2 - (k_r + 5k_c))^2 + \zeta^2\omega^2)((m\omega^2 - (k_r + k_c))^2 + \zeta^2\omega^2)] \\
&+ \omega e^{-(\zeta t)/(2m)}\{[\zeta\sqrt{4(5k_c + k_r)m - \zeta^2}\cos(\sqrt{4(5k_c + k_r)m - \zeta^2}t/(2m)) \\
&+ (-2(5k_c + k_r)m + \zeta^2 + 2m^2\omega^2)\sin(\sqrt{4(5k_c + k_r)m - \zeta^2}t/(2m))] \\
&/(20\sqrt{4(5k_c + k_r)m - \zeta^2}((m\omega^2 - (k_r + 5k_c))^2 + \zeta^2\omega^2)) \\
&+ [\zeta\sqrt{4k_rm - \zeta^2}\cos(\sqrt{4k_rm - \zeta^2}t/(2m)) \\
&+ (\zeta^2 - 2k_rm + 2m^2\omega^2)\sin(\sqrt{4k_rm - \zeta^2}t/(2m))] \\
&/(5\sqrt{4k_rm - \zeta^2}((m\omega^2 - k_r)^2 + \zeta^2\omega^2)) \\
&- [\zeta\sqrt{4(k_c + k_r)m - \zeta^2}\cos(\sqrt{4(k_c + k_r)m - \zeta^2}t/(2m)) \\
&+ (-2(k_c + k_r)m + \zeta^2 + 2m^2\omega^2)\sin(\sqrt{4(k_c + k_r)m - \zeta^2}t/(2m))] \\
&/[4\sqrt{4(k_c + k_r)m - \zeta^2}((m\omega^2 - (k_r + k_c))^2 + \zeta^2\omega^2)]\})
\end{aligned}
\tag{A9}
$$

B Appendix B

The subcircuit models for ngspice:

```
.SUBCKT NormalTransducer nv+ nv- nz+ nz-  nU+ nU-
PARAMS: l=100e-6 w=20e-6 d=200e-9 a=1e-6
e0=8.854187817e-12
*nv-nodes are where component is attached to resonators

*VCCS/ electrostatic force
BIt nv- nv+ i=l*w*e0*(v(nU+,nU-))^2/(2*(d+v(nz+,nz-)*a)^2)

*voltage controlled capacitor between Nu+,Nu- begins
*C=l*w*e0/(d+a*v(nz+,nz-))

*model from ngspice manual
*Bx: calculate f(input voltage) current though
*nonlinear capacitance=df/dt>nlc*v
Bx 1 0 v=l*w*e0/(d+a*v(nz+,nz-))*v(nU+,nU-)
*Cx: linear capacitance
Cx 2 0 1
*Vx: Ammeter to measure current into the capacitor
Vx 2 1 DC 0
*Drive the current through Cx back into the circuit
Fx nU- nU+ Vx 1
*voltage controlled capacitor ends
.ENDS

.SUBCKT LinearResonator nv+ nv- nz+ nz- PARAMS: K1=1e4
K2=0 K3=0 loss=1e-6 Fr=1e6 m=1e-7 a=1e-6
*VCCS for spring force
Bkr nv- nv+ i=K1*a*(v(nz+,nz-))+K2*(a*v(nz+,nz-))^2
+K3*(a*v(nz+,nz-))^3
*losses
.if (loss>0)
RGr nv+ nv- {1/loss}
.endif
*mass
.if (m>0)
CM nv+ nv- {m}
.endif
*integrator capacitance
CI nz+ nz- {a}
*VCCS of integrator side
BIr nz+ nz- i=v(nv+,nv-)
.ENDS
```

```
.TITLE resonaattorit

.INCLUDE LinearResonator.cir
.INCLUDE NormalTransducer.cir
.INCLUDE NormalTransducerm.cir
*.INCLUDE extra_input.cir
.INCLUDE kytketyt_resonaattorit.cir
.option rshunt=1.0e12
*ensure dc path to ground from every node

*AC source
Vu_AC no1 0 ac 1

*transient source
*sine wave amplitude 1 V, frequency 1.08MHz, phase 0
*Vtran ntran 0 SIN(0 1.00 1.08e6 0 0 0)
*Bin no1 0 v=v(ntran)*(time<=50e-6)

*internal resistance of ac-source
RR_L no1 no2 5e6

*dc separation
CC_cpl no2 no3 100n

RR_bias no3 no4 100e6

*DC bias source
VU_bias no4 0 dc 30

RR_bias2 no4 no5 100e6

*subcircuit containing the resonator network,
*transducers and possible extra inputs and outputs
Xmems_systeemi no3 0 no7 no5 kytketyt_resonaattorit

*dc separation
CC_cpl2 no5 no6 100e-9
RR_L2 no6 0 100e6

*ac-analysis
.ac lin 10000 950e3 1300000
.width=256
.print ac vm(no6) vm(no3)
```

```
*transient analysis
*.tran 2e-08 600e-6
*.width out=256
*.print tran v(no3) v(no6)

.END
```